PERFORMANCE IMPROVEMENT
OF EUTECTOID STEEL

BY

Wenxian Sun

A dissertation submitted in partial fulfillment of the requirements for the

Doctor of Philosophy degree in Department of Engineering Systems

and Technology, Graduate School of Science and Engineering,

Saga University

September 2004

ACKNOWLEDGMENTS

Contents

Chapter 1

Introduction

1.1 Overview of Fatigue Study

1.1.1 A Brief Historical Background of Fatigue Study

In the modern industrial society, despite great advances in innovation and technology in engineering, failures still occur and are often accompanied by great human and economic losses. Among the various failures, fatigue failure is the most common failure pattern in engineering [1]. Although the research on failures and fatigue has been conducted for about 150 years, it is still difficult to precisely predict and prevent them. A brief overview of the history of fatigue study may provide insight in understanding the complexity and nature of this discipline.

In the first half of the nineteenth century, a number of train wrecks occurred as the result of the fatigue failure of railroad car axles. The famous one was the Paris-Versailles train crash. These accidents brought attention to the new failure model and some of the investigations concerning the mechanism of fatigue were initiated [2]. In 1839, Poncelet studied the failure of metals under the repeated load of tension and compression, and used the term of "fatigue". Rankine (1843) observed that the growth process of fatigue cracks in axles. McConnell (1849) claimed that "a change from fibrous to crystalline character" occurred during fatigue. It was speculated that the material of the component that failed had "crystallized", as the material "tired". The so-called crystallized theory of fatigue was continuously explored mainly by railroad engineers [3].

Between 1852-1869, A.Wöhler [4] performed systematic experiments of fatigue failure of railroad car axles and indicated that the cyclic strength of steel axles was much lower than their static strength. He was also the first engineer to carry out extensive fatigue test programs on test specimen rather than practical component, and to use both rotating bending and axial loading test method. Fatigue properties

characterized in term of the relationship between the stress amplitude(S) and the log of the number of cycles to failure (N). At the same time, the concept of "endurance limit" was introduced. The S-N curve has generally been known as "Wöhler curve" in fatigue literatures and is one of the most important fatigue properties of material.

Ewing, Rosenhain and Humfrey [5] published papers and showed that slip bands appeared on most of the multi-crystal materials during the fatigue test and the fatigue crack developed from the slip bands.

Palmgren (1924) [6] and then Miner (1945) [7] developed the "damage accumulation models" for fatigue failure.

Coffin (1954) [8] and Manson (1954) [9] proposed "plastic strain damage theory". It is an empirical relationship between the plastic strain amplitude and the number of cycles. This is so-called "Coffin-Manson relationship" and it has remains the most widely used approach for the strain-based characterization of fatigue.

The linear elastic fracture mechanics (LEFM) methods that model the quantitative relationship of fatigue crack growth rate were firstly introduced by Irwin (1957) [10] and developed by Paris, Gomez, and Anderson (1961) [11]. With these approaches, the fatigue crack growth rates can be expressed mathematically as a function of the scalar quantity between a reversing stress (or strain) field ($\Delta\sigma$ or $\Delta\gamma$), and the crack depth.

In 1960s, the concepts in fracture mechanics were introduced to the study of fatigue failures. Some models were purposed to explain the propagation obstacle of fatigue crack in material (Larid and Smith, 1962; McClintock, 1963; Rice, 1967; Neumann, 1969; Pelloux 1969). [12-16]

Ritchie, Suresh and Moss introduced the concept "crack closure" in 1980[17]. Pearson (1975) was the first scientist to purpose the "short crack problem" [18].

In recently years, more research interests have been concentrated on the fatigue properties of the non-metal material and composite material. The famous researchers include Suresh (1990) and Roebben (1996) on ceramics, Hertzberg and Manson (1980), Hertzberg (1995) on polyatomic materials [19-22]. However, until now, there is no mature theory to explain the complicated fatigue phenomena.

Static fracture
13%

Others
Corrosion
5%

SCC
Delayed
fracture
5%

(Indirect fatigue 10%)

Simple fatigue
58%

Low cycle
fatigue
8%

Total 242 cases. Fatigue failure 87%
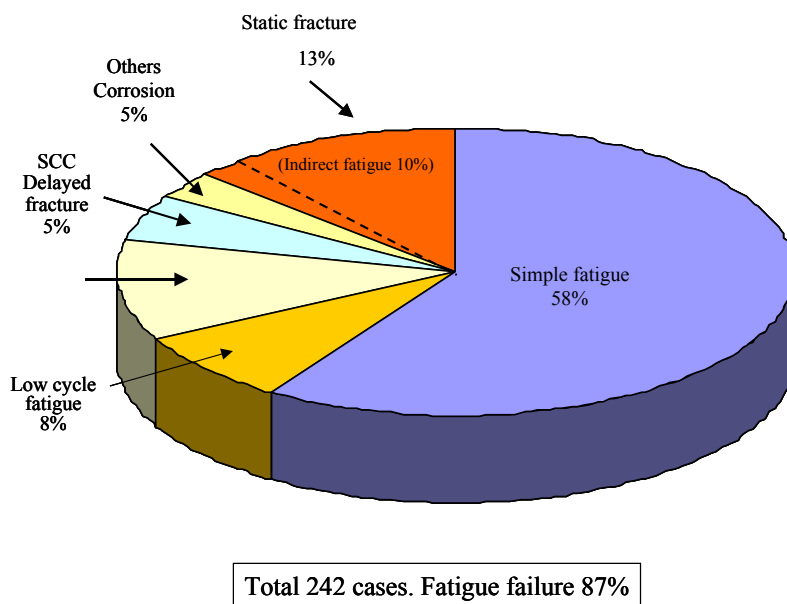
Figure1.1   Classification of failures according to cause (after Nishida).

1.1.2   Basic Conception of Failure and Fatigue

A part of assembly is considered to have failed under one of three conditions: (1) when it becomes completely inoperable (2) when it is still operable but is no longer able to perform its intended function satisfactorily (3) when serious deterioration has made it unreliable or unsafe for continued use, thus necessitating immediate removal from service for repair or replacement [23].

From the viewpoint of fracture mechanics, failure can be classified as fatigue, wear, fretting, creep, corrosion and others. Fatigue is defined as: "The process of progressive localized permanent structural change occurring in a material subjected to conditions which produce fluctuating stresses and strains at some point or point which may culminate in cracks or complete fracture after sufficient number of fluctuation" [23].

According to a systematical study on the cause of engineering failure, more than 80% of failures in steel structures are directly or indirectly caused by fatigue; and more than 90% of failures are initiated at the stress concentrated parts of structural component [24]. A study by Nishida (see figure below) showed that of the 242cases,
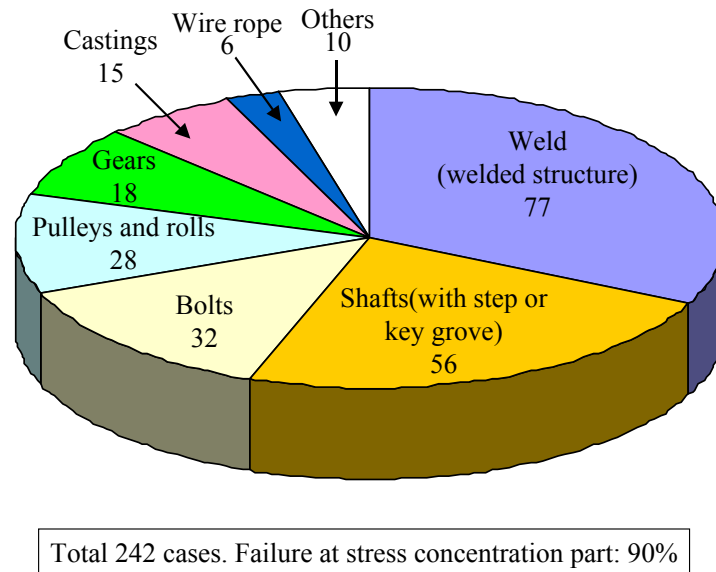
Figure1.2   Classification of failures according to failed components (after Nishida)

Table1.1 Types of failures and macro features (after Nishida)

Type	Frequency of generation	Macroscopic phenomenon	Macroscopic growth	"Safety Level"
Fatigue	1	Invisible	Rapid	Dangerous
Wear	2	Visible	Gradual	Safe
Corrosion	3	Visible	Gradual	Safe
Others(impact load, overload,etc.)	4	Invisible	Rapid	Dangerous

87% of failures were caused by fatigue (including simple fatigue, corrosion fatigue, thermal fatigue. etc.), and other caused are static fracture 13%, which consisted of "indirectly fatigue" (10%) and "pure static fracture" (3%). The greatest numbers of failures were observed in welds, and failures other than weld decreased in the following order: shaft, bolts, pulleys or rolls, gears, wire rope, etc. The classifications of failure by cause and by practical engineering parts are clearly shown in Figs.1.1 and 2.   General aspects for various failures mechanism and the "safe level" in sense of the possibility to cause a catastrophic failure were also introduced in Table1.1 [24].

It is clear that fatigue is the most dangerous type among the failures.

1.1.3   The Importance of Fatigue Research

In practical engineering, preventing fatigue failure is quite difficult because of (a) the scattering nature of fatigue experimental data (b) the difficulty of the prediction (and detection) of both the formation and the behavior of fatigue cracks, which initiate at flaws in metals even if the external load is well below designated level; and (c) errors in estimate of the actual   stresses imposed by mechanical design (notches, stress concentration) or unpredictably varying of external load in service condition. It is the complicity and scattering that makes fatigue a big problem in the engineering and some times resulted in disasters.

Several fatal catastrophe caused by fatigue fracture in history have been documented and studied.

In the early 1950s, the Comet aircraft was the first jet transport introduced into commercial passenger service. The plane was so superior to propeller-driven transport that it was considered the safest plane in the world at that time.   However, not long after coming into service, two planes of the Comet fleet, on climbing to cruise attitude, underwent explosive decompressions of the fuselages, which resulted in the loss of the planes as well as the lives all aboard. Intensive investigation revealed that these crashes were caused by fatigue cracking of the fuselage at the region of high stress adjacent to the corners of more or less square windows [25-26], as shown in Fig.1.3. The failed on launch of the sophisticated H-2 rocket of National Space Development Agency of Japan (NASDA), in November 1999, which cost 24 billions yens, was initiated by metal fatigue of one of the system turbo pumps in the rocket's engine [27].   As a result of this spectacular failure, the progress of H-2 project was heavily set back.
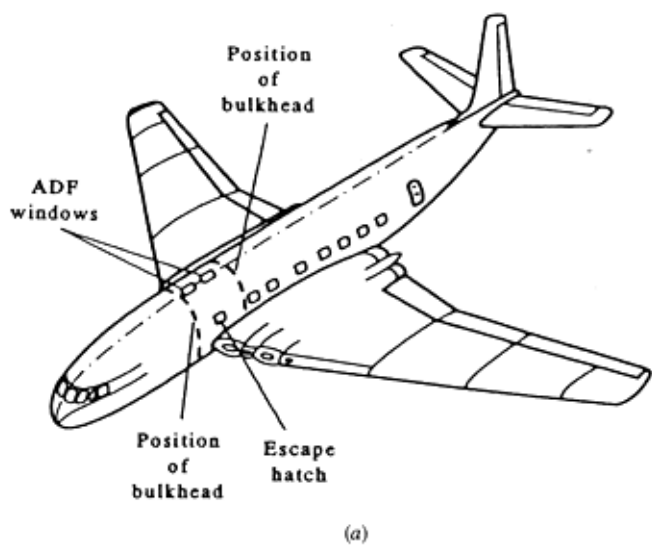
(a)
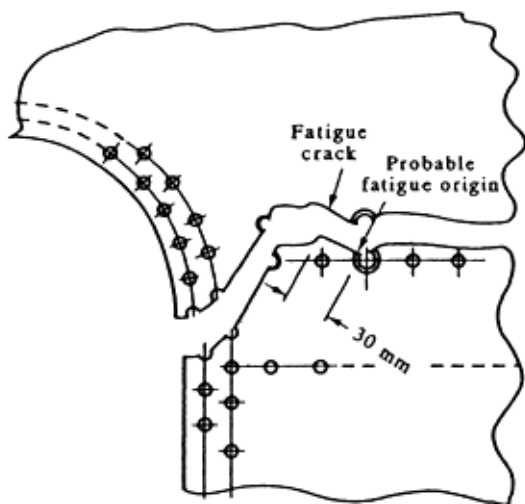
(b)

(a)   The comet aircraft.

(b) The location of fatigue cracking near an aft corner of the ADF (automatic direction finder) windows (After Jones).

Figure 1.3   The location of fatigue cracks of the comet aircraft.

One of the most tragic accidents is the JAL's jumbo jet Boeing 747 plane-crash in Gunma prefecture, Japan, on August 12, 1985. 520 passengers and crews were killed. The investigation concluded that it was the fatigue failure of rear pressure bulkhead of the plane that resulted in this disaster [28].

These facts underline the importance and necessity for a better and through understanding of the mechanism and fatigue properties of the materials. They also demonstrate that why fatigue studies have been and will always be one of the most crucial subjects in engineering.

1.2 Fatigue Design

In order to prevent the fatigue fracture in the engineering, two kinds of design concepts, safe-life (total-life) and fail-safe (damage-tolerance) are used by the engineers.
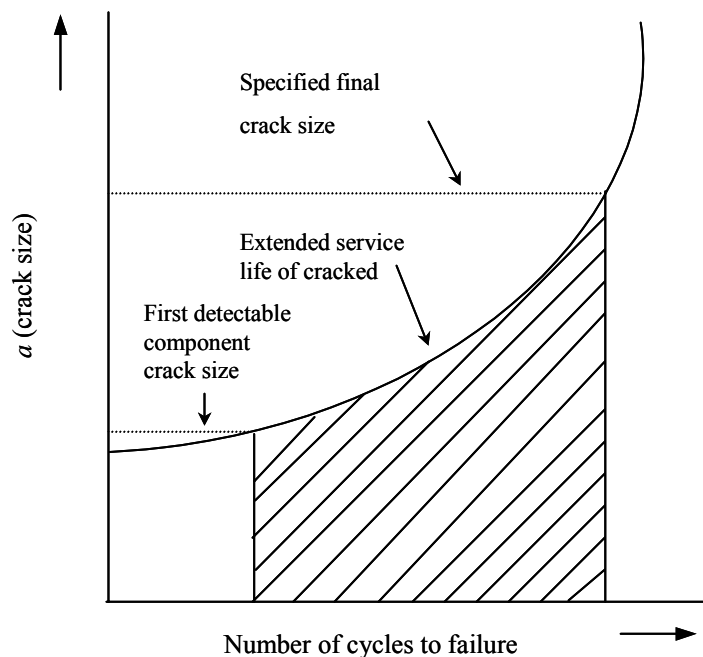
Figure 1.4   Extended service life of a cracked component

The major share of the fatigue life of the component may be taken up in the propagation of crack. By applying fracture mechanics principles, it is possible to predict the number of cycles of a crack spent in growing to some specified length or to final failure.

1.2.1 Safe -life Design

With the safe-life approach, a structure is designed as a statically determinant structure that is intended to last without failure for the design lifetime of the structure. At the end of the targeted safe operation life, the component is automatically retired from service, even if no failure has occurred. To guard against premature failure, the component should be inspected at intervals during its in-service lifetime.

This concept is based on the conservative stress/life relationship (S-N curve), and is considerably uneconomical, particularly when a large margin of safety is set. As noted by Gurney [29], the safe-life approach depends on achieving a specified life without the development of a fatigue cracks so that the emphasis is on the prevention of crack initiation. A schematic of this design concept is shown in Fig.1.4.

1.2.2 Fail-safe design

The fail-safe approach, by contrast, is based on the argument that commercial materials or components always contain flaws, which gives way to fatigue crack initiation and propagation in service. This approach accepts the existence of fatigue cracks in an individual member of a large structure if the remaining parts are sufficient to enable the structure to operate safety until the crack is detected. Periodic inspection is mandated along with the requirement that the crack detection techniques be capable of identifying flaws to enable prompt repairs or replacement.

From the viewpoints of economy and performance, this approach has more advantage than the safe-life one. However, a comprehensive understanding of fatigue initiation and propagation behavior is crucial in this design.

1.2.3 Mechanism of Fatigue

Plastic deformation plays an essential role in the initiation and propagation of fatigue cracks. An important step in understanding the mechanism of fatigue was taken by Ewing and Humphrey [5], who introduced the metallurgical microscope in making their observation. According to the observation to Swedish iron surface during a

fatigue test, they noted that the slip bands were initiated from the surface of the specimen and fatigue cracks originated within them. The latter researcher demonstrated that plastic deformation was essential to fatigue crack initiation.

Usually, the fatigue process can be divided into the following three consecutive and partly overlapping stages [1, 30].

(1) Fatigue hardening and /or softening. This process mainly depends on the original state of the material and the stress or strain amplitude. Fatigue hardening manifests itself by an increase in the stress amplitude necessary to achieve a given strain amplitude. Fatigue softening is typical for hardening materials, and takes place when the obstacles are either removed or at least weakened during cycling.

(2) Micro crack nucleation. It takes place in a small part of the total volume, namely the surface layer. A common denominator of all types of nucleation is the stress concentration in the surface layer. Direct slip observation of the surface show that there are three types of nucleation site.

(a) Fatigue slip bands. Its nature is slip concentration within the grains. Plastic strain amplitude slip-band cracks are generally the most frequent crack nuclei. However, their damaging potential is small due to their low tendency to propagate. This process accelerates cracking process by linking up the crack paths [31].

(b) Grain boundaries. Nucleation at grain boundaries is typical for high stress fatigue, especially at higher temperature. Grain boundary cracks appear to play the most important role at all amplitudes. Because of their high tendency to propagate, their damaging potential is very high.

(c) Surface inclusions. This type of nucleation is typical only in some commercial alloy containing large enough particles.

(3) Crack propagation ending in final failure. The controlling factor of crack propagation is the highly concentrate cyclic plastic deformation within the plastic zone at the crack tip [1].

1.2.4 Fracture Mechanics Approaches to Fatigue Crack Growth

At the present time, three forms of analysis are required to cover the presently known

range of fatigue crack growth.

Linear Elastic Fracture Mechanics (LEFM)

The process of crack propagation can be divided into three stages [28, 30]. Fatigue growth rate, *da/dN,* depends upon numerous factors, in which stress intensity factor range ΔK is the primary variable in metal fatigue. *da/dN* can be expressed by:

$$da/dN=f(\Delta K, K_{max}(or\ R), v\ ,\text{environment, wave form}\ldots) \qquad (1.1)$$

where *R* is the ratio of minimum to maximum applied loads and *v* is the frequency. The crack behavior in Stage I exhibits a low values of ΔK and *da/dN*. An important factor of this region is "fatigue threshold", ΔK_{th}, below which cracks do not propagate under cyclic-stress fluctuations. Stage II represents the fatigue crack propagation behavior above ΔK_{th}, which can be represented by

$$da/dN=C(\Delta K)^{m} \qquad (1.2)$$

where $\Delta K =K_{max}-K_{min} = F(\varDelta\sigma)\sqrt{\pi a}$

Here *C* and *m* are material constants. K_{max} and K_{min} are the maximum and minimum stress intensities at the crack tip. This equation is the famous Paris law [11], it is applicable in linear elastic condition and it is the most widely used form of characterizing crack growth rate for a vast spectrum of material and conditions.

Elastic Plastic Fracture Mechanics (EPFM)

Under elastic-plastic conditions, e.g. strain-controlled low cycle fatigue, EPEM can be employed to characterize fatigue crack growth.

Dowling [32] has proposed a power law characterization of fatigue crack advance under elastic-plastic conditions based on the cyclic J-integral, $\varDelta J(or\ J^{c})$

$$da/dN \propto\partial\,(\varDelta J\,)^{m} \qquad (1.3)$$

where *m* is an exponent analogous to *m* in Eq.(1.2).

The *J*-integral was proposed by Rice [33] to provide a loading parameter for the characterization of monotonic, nonlinear fracture in rate-dependent materials. Considering a cracked body subjected to monotonic load, assuming that the tractions T are independent of crack size and that the crack faces are tractions free, the line integral *J* along any contour Γ which encircles the crack tip is given by:

$$J = \int_{\Gamma} \{\omega dy - T(\partial\mu/\partial x)ds\} \tag{1.4}$$

Where μ is the displacement vector, *y* is the distance along the direction normal to the plane of the crack, *s* is the arc length along the contour, *T* is the traction vector and ω is the strain energy density of the material.

Dowling[34] has found the relationship between Δ and ΔJ can be expressed as:

$$\Delta J \quad (\Delta \quad)^2 / E \tag{1.5}$$

Huntchinson [35], in a review article, pointed out that the use of *J*-integral for characterizing fracture in real ductile materials required ascertaining certain conditions.

Tomkins[36], who equated *da/dN* to crack tip decohesion, proposed the equation:

$$da/dN = B(\Delta\varepsilon_p \sqrt{\pi a})^n - D \tag{1.6}$$

where *D* is the threshold condition, $\Delta\varepsilon_p$ is the strain amplitude and *B* is the scaling factor.

In practical task, the criterion of crack tip opening displacement $\Delta\delta_t$ is also frequently used to characterize fatigue crack growth. A comprehensive understanding of J-integral and $\Delta\delta_t$ can be found in literatures of fracture mechanics.

Micro Fracture Mechanics (MFM)

Though LEFM approach is quite successful in characterizing stable long fatigue crack growth (associated to stage II fatigue), it is inapplicable to characterize the growth of comparatively small cracks (associated to Stage I). To cover the so-called

"anomalous behavior" of small cracks, MFM crack growth model proposed by Navarro and de los Rios [37] led to the laws of the form:

$$da/dN = C_m \, \Delta\gamma^{\beta}(d\text{-}a) \qquad\qquad (1.7)$$

where $\Delta\gamma$ is the shear-strain amplitude, d is a micro structural dimension (for instance, grain size), a is the crack depth, C_m and β is a scaling factor related to materials, loading conditions and temperature.

It is worth noting that MFM indicates the cease of crack growth when a approached to the micro structural dimension, therefore, if the crack continues to grow there should be an overlap between MFM and EPFM or between MFM and LEFM for the transition. Fig 1.5 schematically describes fatigue crack growth behaviors in different regimes. Figure 1.6 illustrates various behaviors of crack ground in the entire fatigue process (Stage I and stage II or small and long crack behaviors and the transition stage between these mechanisms).
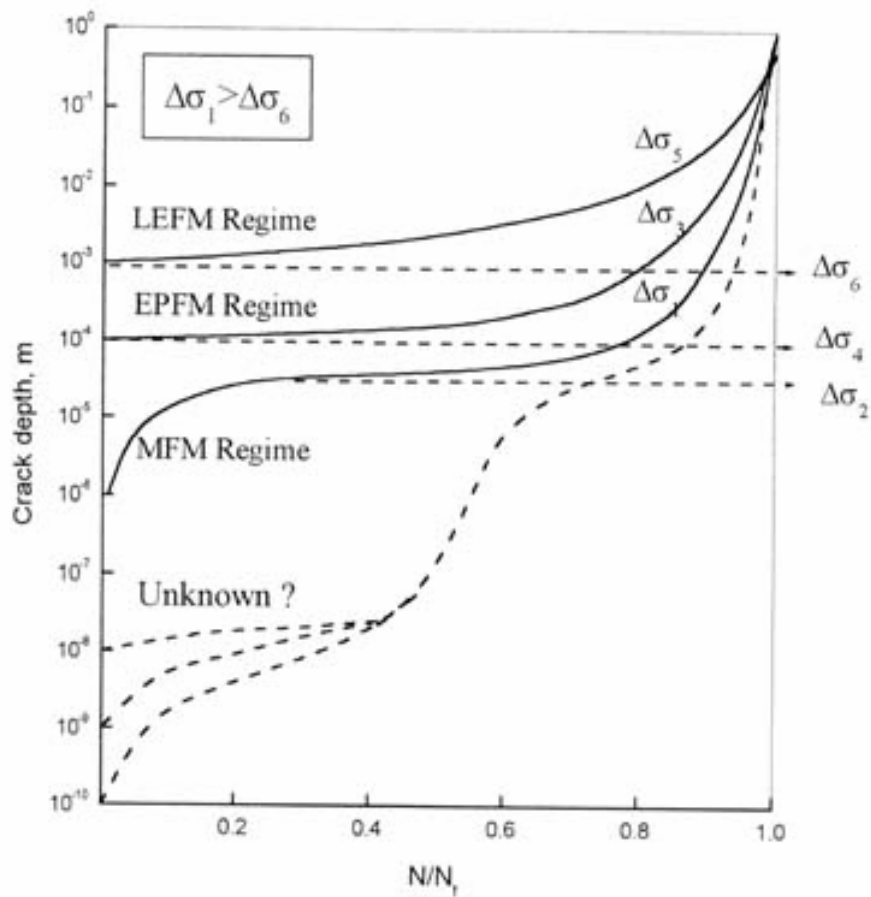
Figure 1.5 The effect of initial crack sizes and three (probably four) fundamental crack growth behaviors in materials (after Miller).
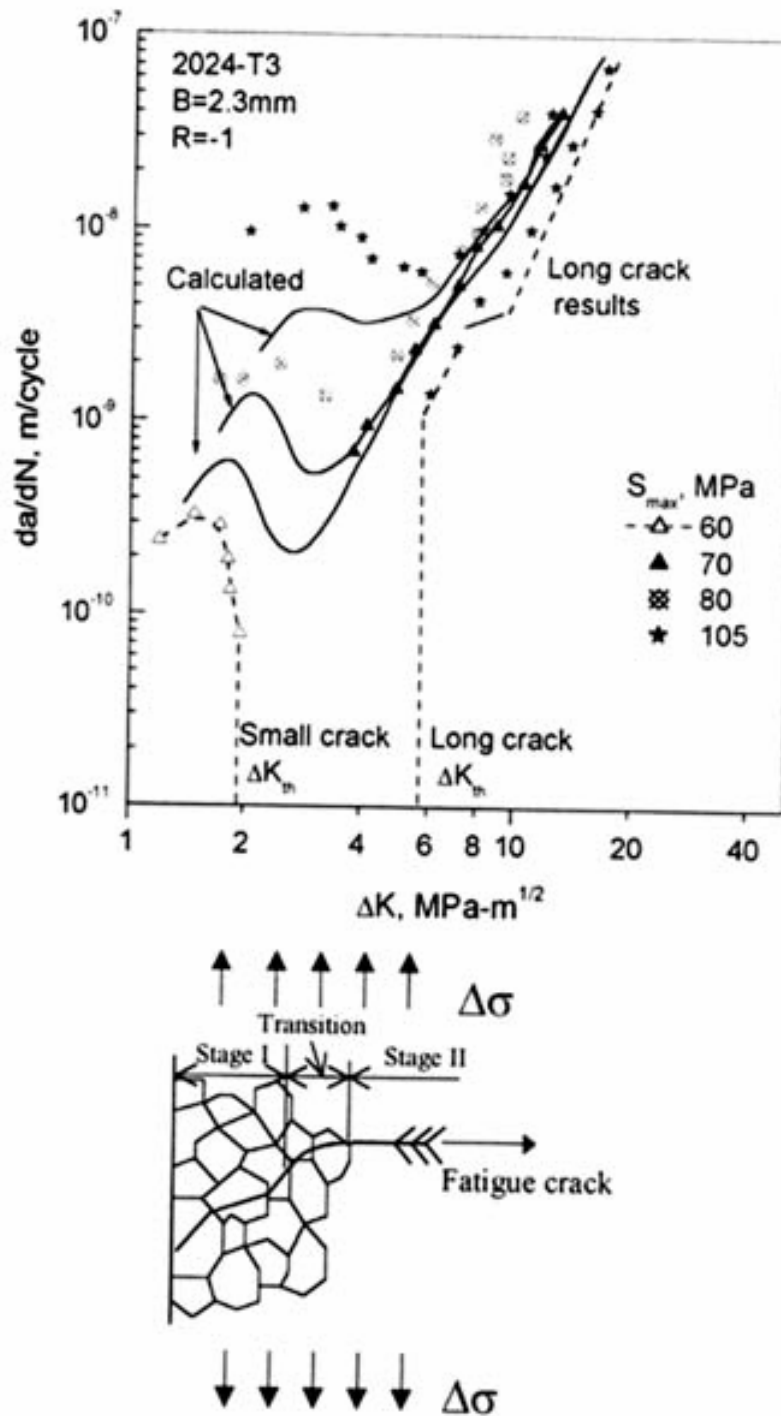
Figure 1.6   Illustration of various behaviors of fatigue crack growth in the entire fatigue process. The (upper) graph shows the experimental data of small and large crack growth in an aluminum alloy 2024-T3 (After Newmann). Behaviors of small (Stage I) and large (Stage II) cracks are schematically described in the lower drawing, respectively.

14

Small (short) Crack and Large (long) Crack Behaviors

Commercial materials always contain flaws or defects from which cracks can initiate and grow. Consequently, the process of crack growth, including micro-small crack and large crack, should be viewed as the major part of the fatigue life cycle in commercial materials. The term "small (short) crack behavior" is generally defined as cracks whose (a) size is small enough, and (b) behavior is not consistently characterized by the form of the Paris law in LEFM. A small crack may grow hundreds times faster than a long one under the same level of Δ and may decelerate then arrest or then decelerate at micro structural barriers. Depending on the mechanism of crack deceleration, small cracks are classified as micro structurally small, physically (or mechanically) small and chemically small cracks [31].

Figure 1.6 illustrates various behaviors of crack growth in the entire fatigue process (Stage I and Stage Π or small and long crack behaviors and the transition stage between these mechanisms).

The fatigue life of structure components is determined by the sum of the elapsed cycles required to initiate a fatigue crack and to propagate the crack from the sub-critical dimensions to the critical size. Ritchie systematically studied fatigue crack propagation in ductile and brittle material [30, 38]. He considered the process of fatigue-crack growth a mutual competition between intrinsic mechanisms of crack advance ahead of the crack tip and extrinsic mechanism of crack-tip shielding behind the tip. The intrinsic mechanism is characterized by alternating crack tip blunting and re-sharpening and it promotes crack growth. The extrinsic mechanism is characterized by crack closure and bridging, which impede crack growth. Take metallic materials, for an example, the intrinsic damage mechanisms involve processes which create micro-cracks by dislocation pile-ups or interface de-cohesion, in the highly stressed region ahead of the tip, leading to classical failure by cleavage, inter-granular cracking or micro-void coalescence; comparable mechanisms under cyclic loads involve the repetitive blunting and resharpening of crack tip. Extrinsic shielding mechanism result from the creation of inelastic zones surrounding the crack
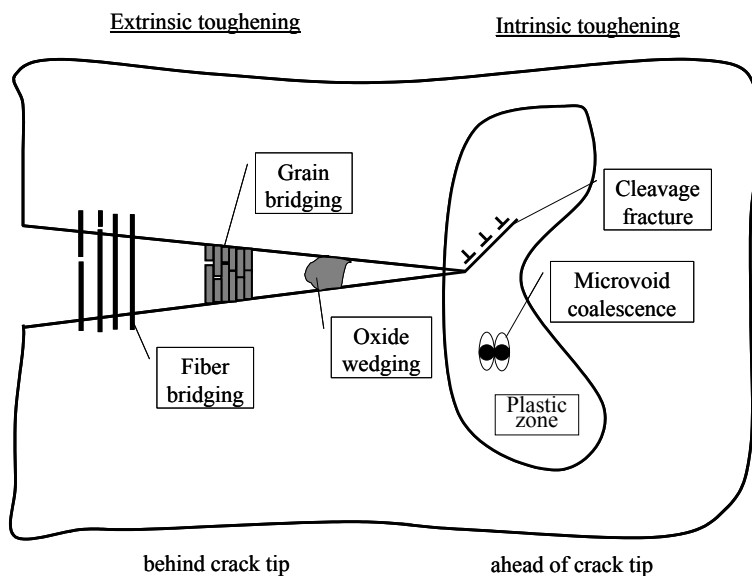
Figure 1.7 Schematic illustration of mutual competition between intrinsic mechanisms and damage/crack advance and extrinsic mechanisms of crack-tip shielding involved in crack growth (after Ritchie).

wake or from physical contact between the crack surfaces via wedging, bridging, sliding or combination thereof. These mechanisms are shown in Fig.1.7 briefly. The intrinsic mechanism is an inherent property of the material, and thus is active irrespective of the length of the crack or the geometry of the test specimen; in other words, these mechanisms are related to initiation of crack. Conversely, extrinsic mechanisms act in the crack wake and are thus critically dependent on crack size and geometry. These mechanisms have no effect on crack initiation (since there are no crack wake), and related to continued crack growth.

Many parameters affect the performance of structure component, including those related to stress (stress ratio, stress range, constant or variable loading, frequency or maximum stress, etc.), geometry and properties of the components (stress or strain raisers, stress concentration level, material properties and heat treatment procedures, etc.) and external environment (temperature and aggressiveness of the environment. etc.)[39]. Of all those factors, the most significant one is the fluctuation in the localized stress or strain. Consequently, the most

effective way to improve the fatigue behavior of structural components is to decrease the severity of stress concentration. This is the main subject of this thesis it will be addressed in Chapter 3 and 4.

1.3 Application of Eutectoid Steel in Engineering

Eutectoid steel is a material that has been widely used in various industrial fields, such as rail, wheel, wire rope, crankshafts, rod, piano wire, tire, spring and axles etc, for their high strength and low cost. The tensile strength of the eutectoid steel falls between 800MPa to 2343MPa. Rail and mechanical components are the two fields where eutectoid steel is used the most and it is reported that the most common failure in rail is also fatigue fracture [40]. In recent years, the speed of passenger trains and the load of the freight trains have been increased to raise the efficiency of railway transport. As a result, an increase in fatigue failures in rails has also been observed. (Besuner, 1978, Sugino., 1991)[41]. Therefore, the research on fatigue properties of eutectoids steel is very importance to the safety of the transportation.

1.4 Objectives and Scope of The Present Study

The objectives of the present study are to evaluate the effect of plastic deformation and different of surface treatments on practical properties of eutectoid steel, and to determine the optimal parameter for improving the stress concentrated components.

In chapter 1, the general history of fatigue research was reviewed, basic mechanisms of the fatigue were introduced, and the importance of the fatigue research was emphasized.

Chapter 2 is concentrated on the effect of plastic pre-strain on fatigue properties of eutectoid steel. The influence of pre-strain on fatigue strength, crack initiation, propagation behavior and the microscopic behavior during the pre-strain are also investigated, observed, and discussed.

Chapter 3 presents the effect of roller working on notched eutectoid steel. The purpose of this study are to (1) examine and quantify the effect of roller working on fatigue strength of notched eutectoid steel; (2) discuss the fundamental mechanism

for improving fatigue properties; (3) study crack initiation and propagation behaviors.

Chapter 4 focuses on the influence of ion nitriding treatment on practical properties of eutectoid steel. Two different treatment temperatures are applied to investigate the effect on smooth and notched specimens. The mechanisms for this improvement and effect of parameters are analyzed.

Chapter 5 is a general summary of the present study. The effect of pre-strain and two different surface treatments on fatigue properties of the test material are compared. The advantages and limitations of each are discussed. Some recommendations for future research are provided.

References

[1] M. Klesnil and P. Lukas: *Fracture of Metallic Materials*, United States: Elsevier Science Publishing Company, 1980.

[2] R.A. Smith, The Versailles railway accident on 1842 and the first research into metal fatigue, in Fatigue 90 (Eds. H. Kitagawa & Tanaka), Berminghan: *Materials and Component Engineering Publications,* vol.4, pp 2033-2041.

[3] A.J. McEvily, Metal failures: mechanisms, analysis, prevention. *Willey Interscience publication,* U.S.A   pp.181

[4] A . Wöhler, *Abstract in English, in Engineering,* 1871, Vol.11, pp 199.

[5] J.A Ewing and J. C. Humfrey, *The fracture of metals under rapid alterations of stress, in Philosophical Transactions of the Royal Society*, London, A200, pp.241-250.

[6] A. Palmgren, *Die Lebendauer von Kugellagern, Zeitschrift des Vereins Deutscher Enginieure*, 68,1924, pp. 339-341.

[7] M. A. Miner, Cumulative damage in fatigue, *Journal of Applied Mechanics,* No.12, 1945, pp. 159-164.

[8] L. F. Coffin, A study of the effect of cyclic thermal stresses on a ductile metal, *Transactions of the American Society of Mechanical Engineers*, 1954, 76, pp. 931-950.

[9] S. S. Manson, Behavior of materials under conditions of thermal stress, National Advisory Commission on Aernautics, Cleveland: *Lewis Flight Propulsion Lab*., Report 1170, 1954.

[10] G. R. Irwin, Analysis of stresses and strains near the end of a crack traversing plate, *Journal of   Applied Mechanics,* 1957, 24, pp.361-364.

[11] P. C. Paris, M. P. Gomez & W. P. Anderson, A rational analytic theory of fatigue, *The Trend in Engineering,* 1961, 13, pp. 9-14.

[12] C. Larid and G. C. Smith, Crack propagation in high stress fatigue. *Philosophical Magnize*, 8, pp. 847-857.

[13] F. A. McClintock, On the plasticity of the growth of fatigue cracks. *Fracture of Solids,* Vol.20, pp. 65-102, New York: Wiley.

[14] J. R. Rice, Mechanics of crack tip deformation and extension by fatigue, In fatigue crack propagation, *Special Technical Publication* 415, pp. 247-309. Philadephia: American Society for Testing and Materials.

[15] P. Newman, Coarse slip model of fatigue, *Acta Metallurgica* 17, pp.1219-1225.

[16] R.M. N, Pelloux, Mechanism of formation of ductile fatigue striation, *Transactions of the American Society for Metals*, 62, pp.281-285.

[17] R.O. Ritchie, S. Suresh and C.M. Moss, Near–threshold fatigue crack closure at near threshold stress intensities due to fracture surface morphology, *Metallurgical Transactions* 13A, pp.293-299.

[18] S. Pearson, Initiation of fatigue cracks in commercial aluminum alloy and the subsequent propagation of very short cracks, *Engineering Fracture Mechanics* 7, pp235-247.

[19] S. Suresh, C. F. Shih, A. Morrone and N.P. O'Dowd, Mixed-mode fracture toughness of ceramic material, *Journal of American ceramic society* 73, 1257-1267.

[20] G. Roebben, M. Steen, J. Bressers, O. Van der Biest, Mechanical fatigue in monolithic non-transforming ceramic. *Progress in Material Science* 40, 265-331.

[21] R. W. Hertzerg and J.A. Manson, Micromechanisms of fatigue crack advance in PVC. J*ournal of Material Science* 8, 1554-1558.

[22] R. W. Hertzerg, Deformation and fracture mechanism of engineering materials, 4th edition. New York: Wiley.

[23] Metals Handbook 8th Edition, Vol.10, *Failure Analysis and Prevention, American Society for Metals,* 1975, pp.1.

[24] S. Nishida, Failure Analysis in Engineering Application, Butterworth Heinemann Ltd., 1992, pp1-5.

[25] D.D. Dempster, the Tale of the Come., New York, N. Y: David McKay.

[26] H. Petroski, Invention by design: How Engineers Get from Thought to Thing. Cmbridge, MA: Harvard University Press.

[27] NASA Report, Investigation into the cause of H-II lauch vehicle No.8 failure

progressing, No.94, April 2000.

[28] H. Kobayashi, Y. Arai, H. Nakamura, Fatigue failure analysis of the rear pressure bulkhead of the crashed Boeing jumbo jet plane (In Japanese), *Journal of the Society of Material Science* Japan, 36, pp.1084-1089.

[29] T.R. Gurney, Fatigue of Welded Structure, Cambridge University Press, 1968.

[30] R. O. Ritchie, Mechanisms of Fatigue-Crack Propagation in Ductile and Brittle Solid, *Inter. J. Fatigue,* 100(1999), pp.55-83.

[31] A.J. McEvily, The Growth of Short Fatigue Cracks: A review, *Mater. Sci. Resear. Inter.,* 4(1998), pp.3-11.

[32] N.E. Dowling and J .A. Begley, Fatigue crack growth during gross plasticity and the J-integral, in mechanics of crack growth, *American Society for Testing and Material,* 1976,pp.82-103.

[33] J. R. A path independent integral and the approximate anaysis os strain concentration by notches and cracks, *Journal of Applied Mecnanics,* 1968,35,pp.379-386.

[34] N. Dowling and J.A. Beley, in Mechanics of crack growth, ASTM STP590, 1976, pp.82-103.

[35] J. W. Hutchinson, Fundsmental of the phenomenological theory of nonlinear fracture mechanics, *Journal of Applied Physics,* 1983,50,pp.1042-1051.

[36] B. Tomkins, Philosophical Magazine, 1968,155,pp.1041-1066.

[37] A. Navarro and E.R. de los Rios, F*atigue of Engineering Materials and Structures,* 1987, 17,pp.169-186.

[38] R.O. Ritchie, C.J. Gilbert and J.M. McNaney, "Mechnics and Mechanisms of Fatigue Damage and Crack Growth in Advanced Matrials", *Inter. J. Soli. Struc.,* 37(2000), pp.311-329.

[39] J. M. Barsom and S.T. Rofle, Fracture and Fatigue Control in Structures, United States: Prentice-Hall, Inc., 1987.

[40] Kato, Rail, The rail association of Japan, 1978.

[41] C. Urashima and S. Nishida, F*atigue Crack Initiation and Propagation Behavior in Pearlite Structure, *Proc. of Fatigue 96*(1996), pp.319-324.

Chapter 2

Effect of Pre-strain

on Fatigue Properties of Eutectoid Steel

2.1 Introduction

Eutectoid steel is a commonly used industrial material due to its high strength and low cost. Rail and mechanical components are the two fields where eutectoid steel is used the most. It is well known that the most popular failure patterns in rail and component are fatigue fractures [1, 2]. In recent years, the speed of passenger trains and the load of the freight trains have been increased to raise the efficiency of railway transport. Fatigue failures to rails as a result of such increases have been observed (Besuner, 1978, Sugino, 1991) [3]. In practical structural component, many of the parts are pre-strained before use or during machining process. For example, rail is rolling straightened before use and the plastic pre-strain ratio is about 2~5%. From the standpoint of material safety, a comprehensive understanding of the effect of pre-strain on fatigue properties of eutectoid steel is essential.

In the past 30 years, there have been extensive research efforts on eutectoid steel. Nishida and Urashima have had important impact on the research of rail [3-6]. They proposed that fatigue crack initiate at the interface in rail steel with pro-eutectoid ferrite; in rail steel without pro-eutectoid ferrite, fatigue cracks occur at the inter-lamellar of pearlite due to slip. Initiated fatigue crack is arrested by the pearlite block boundary. Therefore, in order to obtain higher fatigue strength and fatigue limit ratio, it is desirable to reduce the lamella spacing and block size of pearlite. The fatigue crack preferentially propagates along the inter-lamellar of pearlite in the early stage. As it grows, however, it propagates perpendicularly to the stress axis by changing its direction at every pearlite block.

Fatigue crack propagation behavior can be summarized as follows:

(1) Chemical composition, pearlite block size and mechanical properties have little effect on the fatigue crack propagation rate if the stress ratio is held constant.

(2) The fatigue crack propagation rate can be expressed as

$$\frac{dl}{dN} = C\,(\Delta k_{eq})^{m}, \qquad\qquad (2.1)$$

where $\Delta k_{eq} = \sqrt{\Delta k \times k_{max}}$

It can be well represented by a linear relation irrespective of the stress ratio. In addition, the values of C and m can be evaluated immediately from the case of zero stress ratios.

(3) The variation of the crack propagation ratio at the constant stress ratio disappears by the annealing (520°C, 30 min, furnace cooling). This is mainly attributed to the relief of residual stress in the specimens.

The main conclusions about the influence of segregation on fatigue strength are:

(1) Carbon, manganese and phosphorous are segregated positively in the segregation band, where the proof stress, tensile strength and hardness become higher but the elongation and reduction of area become lower than the other position.

(2) The rotating bending fatigue strength vary little irrespective of the presence of segregation and the degree of segregation or the orientation of test specimen in the rail.

(3) The fatigue crack initiate in the position where there is no segregation, and its originating place exhibits a flat surface, which seems to be parallel along a pearlite lamellar.

(4) The reason that the segregation has no influence on the fatigue strength is due to the high resistance for slip in the segregation band.

The effect of micro structure includes the surface decarburizing layer, martensite volume and pro-eutectoid cementite. Fatigue strength of rail decreases with the increase of decarburized layer; when the martensite volume in the pearlite increases, the fatigue strength of rail improves. The pre-cementite in the pearlite has almost no effect on fatigue limit. This may be because the pre-cementite is harder than the segregation, fatigue crack is difficult to generate in this place.

Study on contact rolling fatigue (RCF) test [7-11] is another important aspect in rail. Nishida [7-8] performed this test with a special high-speed rail-testing machine, which was designed to imitate the condition of Shinkansen. Especially, the running surface layer of actual rail was investigated in detail. The main results

obtained are as follows: (1) Defect in running surface; cracks were initiated at the surface, being remarkably propagated in the wheel direction and a little in the opposite direction. In this test, the white phase was observed in the surface layer and the crack run through the white phase. (2) Many cracks were observed at the corner with the similar pitch and angle to wheel direction. (3)The possibility of crack propagation could be calculated from fracture mechanics, and would be very small for the shorter crack duck has 0.5mm in length due to the friction of cracked surface. The conclusions from other researchers [9-11] about RCF showed that there appeared no single solution to the rolling contact fatigue problem, a combination of developments and actions were more likely to be required; because of the very high axle load in the present traffic situation, the local wheel-rail contact loads governed the fatigue life to crack initiation.

The basic property of high strength rail is that it has better wear resistance and anti-failure and higher strength [11]. One of the very effective methods is given induction hardening to the head of the rail to get fine pearlite microstructure. New head hard rail (NHH) is one of the products to meet this demand. Comparing to the normal carbon steel, it has fine pearlite microstructure and better mechanical properties than the former. The surface hardness is between HV340-350, which is much higher than that of the conventional rail (HV270-280). The test result showed that this kind of rail also had better wear resistance and anti-failures.

Although all rails suffer rolling straighten and the plastic pre-strain is about 2%~5% in this process, it is very difficult to find the research about the effect of plastic pre-strain on its fatigue properties. A paper studied the effect of residual stress formation during the straightening process, but it did not evaluate the effect of plastic deformation on its practical properties [12]. Considering the NHH rail is mostly used in place like tunnels and mining area where the environment conditions are harsh. In order to improve the safety of the railways and strengthen their durability, it is essential to have a through understanding of the fatigue behavior of this material.

The objectives of this study are to: (1) clarify the effect of pre-strain on fatigue strength and detailed microscopic behavior; (2) investigate its microscopic behavior during plastic pre-strain and fatigue experiment; (3) study fatigue crack initiation and propagation behavior.

2.2 Material and Procedure

2.2.1 Material

The material used in this test is NHH rail. The detailed chemical composition and mechanical properties are listed in Table 2.1 and 2.2, respectively. Compared to the conventional rail, NHH rail has finer pearlite grain size and higher surface hardness. Since the effect depth of induction hardening is about 20mm for NHH rail, specimens used in this experiment were taken from the upper part of the rail head in the longitudinal direction, as shown in Fig.2.1.

Figure 2.2 shows the shape and dimensions of the specimens for tensile test. The specimen for pre-strain and fatigue test are shown in Fig.2.3. In this figure, solid lines describe the pre-strained specimen and dotted lines describe the fatigue specimen. A shallow notch was made to ensure the fatigue crack would be initiated in this part and it is certified this kind of notch does not affect the fatigue limit of the test material.

2.2.2 Experiment Procedure

All of the specimens were annealed in vacuum at 520°C for 30 minute and then electro-polished to the depth of 50μm in diameter to relief the residual stress and remove the work hardened layer. The electrolyte used in this study and electro polishing condition are listed in Table 2.3. The setting of the specimen and the arrangement of equipments are shown in Fig.2.4. Tensile properties of the material in consideration were tested before fatigue test. Tensile specimen was tested on a universal testing machine (SHIMAZU EHF-10) with a loading speed of 20mm/min. The pre-strain was also done with this machine. The microstructure of the specimen was observed by successively taken replica samples. The length of cracks was measured with an optical microscope equipped with a digital measurement system (KEYENCE VH-6300 digital microscope). The fatigue test was performed with an Ono-type rotating and bending fatigue testing machine and the hardness was tested with a Vickers hardness tester. A SEM and an optical microscope were used to observe the fatigue cracks initiation, propagation behavior and fracture surface.

Table 2.1   Chemical composition.   mass%

C	Si	Mn	P	S	Cr	T-Al
0.78	0.21	0.89	0.023	0.08	0.03	0.002

Table 2.2   Mechanical properties.

$\sigma_{0.2}$, MPa	σ_B, MPa	RA, %	El, %
823	1260	34.0	15.7
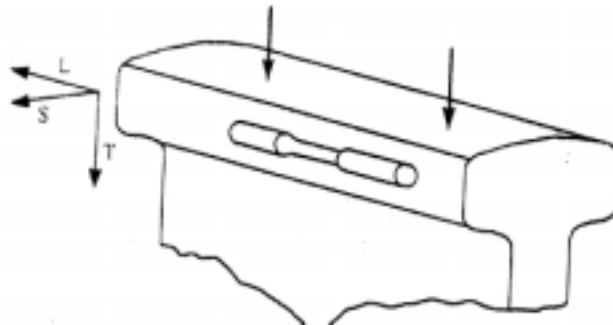
Figure 2.1   Schematic representation of specimen extracted from rail.
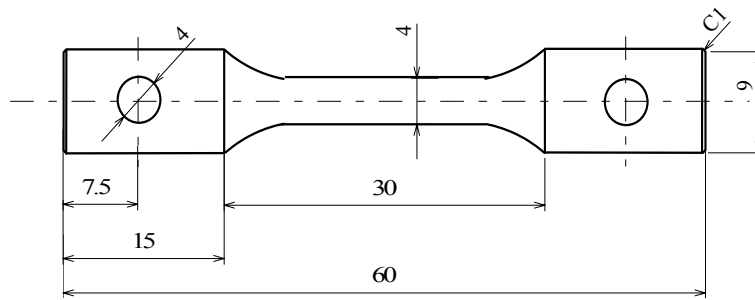
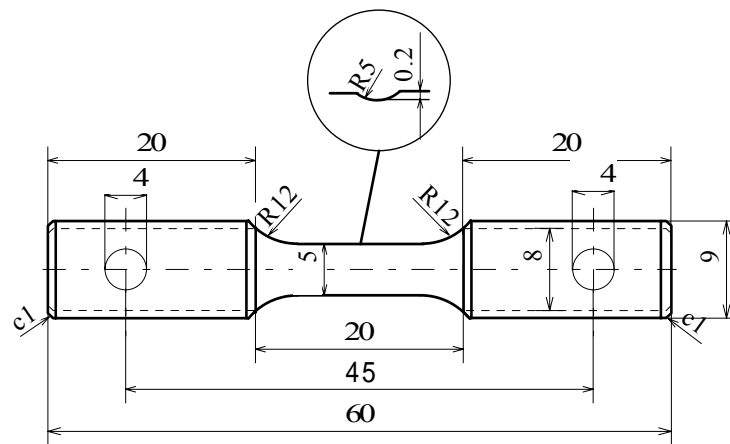Figure 2.2   Shape and dimensions of the specimen for tensile test.

Figure 2.3   Shape and dimensions of the specimen for pre-strain and fatigue test.

Table 2.3   Electrolyte for electro polishing of eutectoid steel.

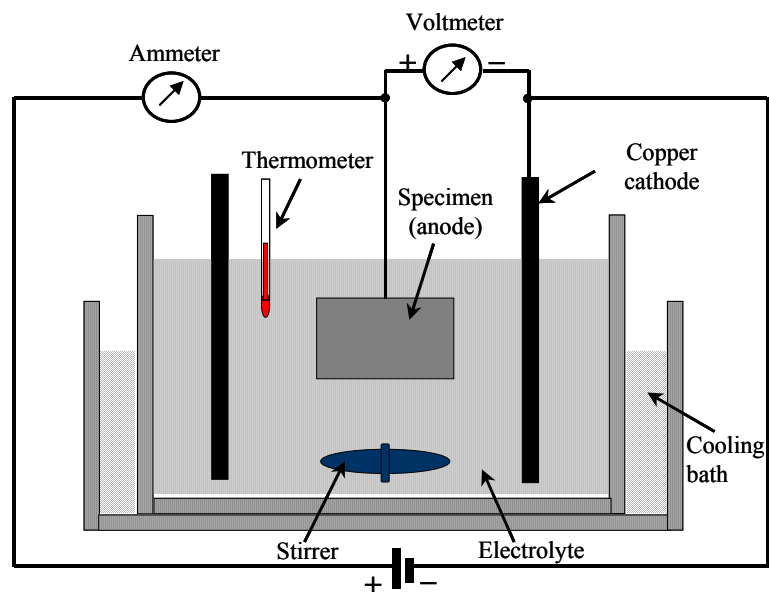| Electrolyte	Current (A)	Time (Sec)
Phosphoric acid (1000g) Nitric acid (20g) Gelatin (20g) Distilled water(250g)	6+2	120+15

Figure 2.4   Electrical circuits and arrangement of equipment for electro-polishing.

2.2.3 Rotating Bending Fatigue Test

A four-point rotating bending fatigue test was conducted using an Ono-type fatigue test machine (14.7Nm,3000rpm) on a load control with the stress ratio R = -1.   The moment model of the fatigue test machine and the maximum normal stress applied on specimen, σ_{max}, is calculated as follows:

$$\sigma_{max} = \frac{M_{max}}{W} \tag{2.2}$$

where M_{max} is the maximum bending moment, and in the case of four-point bending,

$$M_{max} = \frac{Fa}{2} \quad (Nm) \tag{2.3}$$

W is the bending strength area coefficient of material, and for a round bar specimen with a minimum diameter.

$$W = \frac{\pi d^3}{32} \tag{2.4}$$

For Ono-type fatigue test machine using in this study, a is 100mm, therefore,

$$\sigma_{max} = \frac{M}{W} = \frac{16Fa}{\pi d^3} \tag{2.5}$$

from this equation, the maximum normal stress applied to specimens can be calculated using the applied load, F.   The Moment model of Ono-type fatigue testing machine is shown in Fig.2.5.
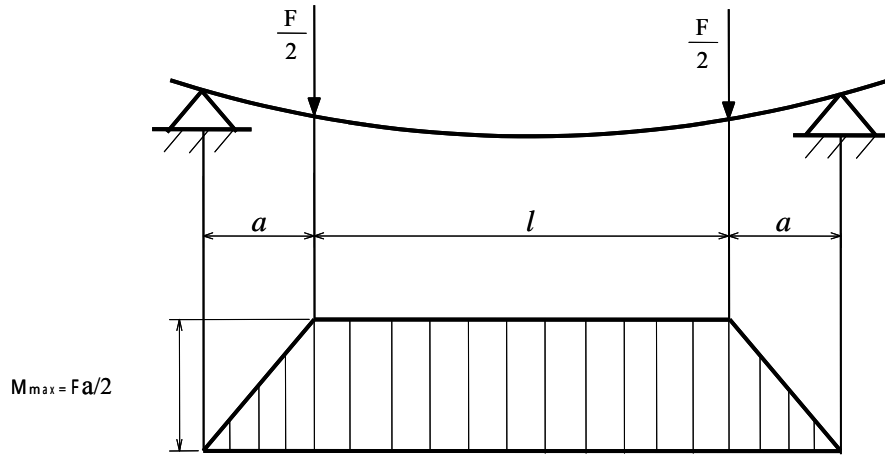
Figure 2.5   Moment model of Ono-type fatigue testing machine.

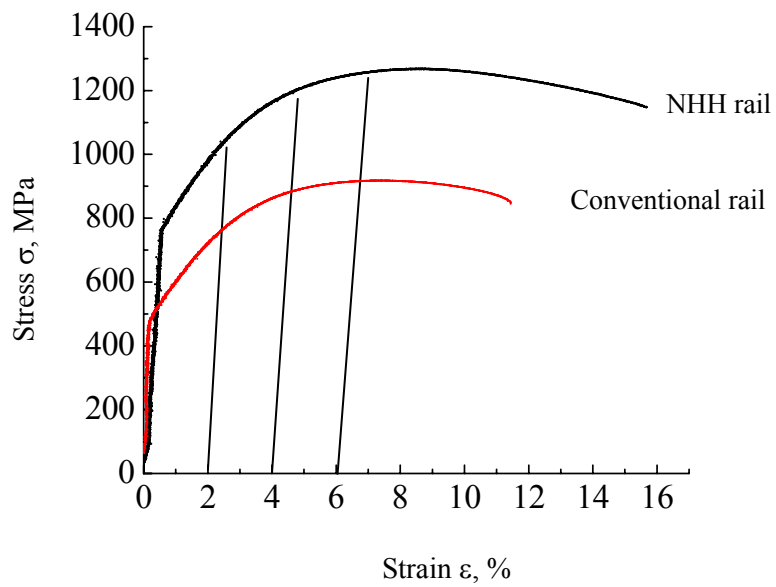

Figure 2.6   Stress-strain curves.

2.3 Test Results

2.3.1 Tensile test

Figure2.6 shows the stress-strain curves of conventional rail and NHH rail. NHH rail is superior to the conventional rail in every aspect. There is no obvious yield point for eutectoid steel. The tensile strength, yield strength, reduction of area and elongation ratio is 1260MPa, 823MPa, 34% and 15.7%, respectively. Compared to the conventional rail, the tensile strength of the latter is 37% higher.

Figure 2.7 shows the surface of the specimens during the pre-strain test. From these photos, slip line or microscopic crack occurred in the surface of the tensile specimen. Figure 2.8 shows the detail observation results of pre-strain ratio at ε_p= 2%, it is clear that the slip line and micro cracks are initiated in the pearlite block by crossing the lamellar.

2.3.2 Fatigue Test

Fatigue strength

Figure 2.9 shows the S-N curves of NHH rail and conventional rail. The fatigue limits of specimens at ε_p=0%, 2%, 4% and 6% are 425MPa, 385MPa, 390MPa and 385MPa, respectively. The fatigue limit of conventional rail without pre-strain, on the other hand, is only 285MPa, which is far lower than those of NHH rail with and without pre-strain. In other words, induction hardening process is a very effective way to improve the fatigue strength of rail.

All of the fatigue limits of pre-strained specimens were lower than that of the specimen without pre-strain (ε_p=0%). The fatigue limit of NHH rail decreased nearly 10% at ε_p= 2% and has no obvious change until ε_p= 6%, as shown in Fig.2.10. The increase in plastic pre-strain ratio did not cause apparent variation in the fatigue limits.

Hardness

The surface hardness values of the specimens without and with different plastic deformation ratio are HV350, HV 353, HV357 and HV357 for pre-strain ratios of 0%, 2%, 4% and 6%, respectively. The net increase in hardness is only about HV7. It means the effect of work hardening on fatigue strength is very limited.
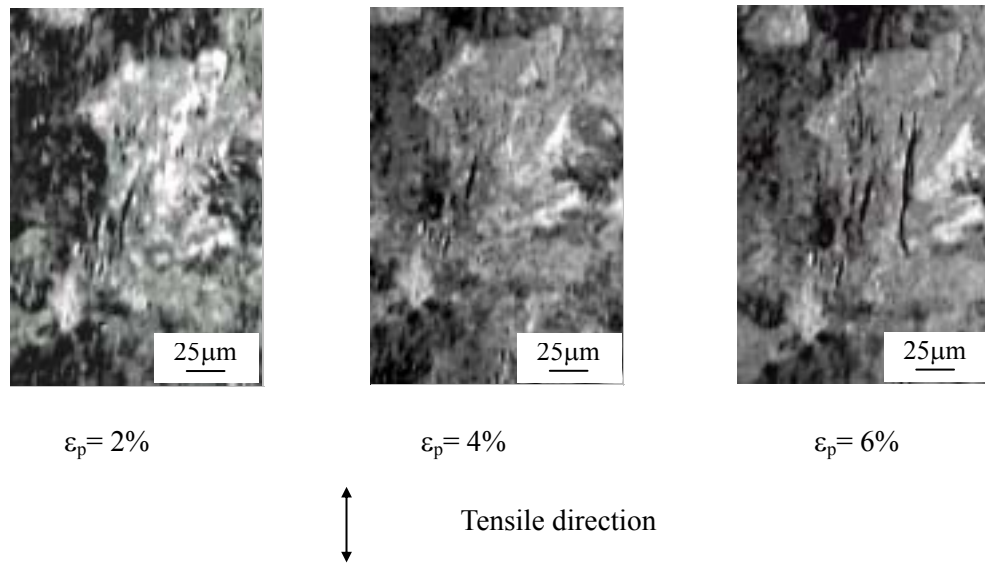
$\varepsilon_p = 2\%$ $\qquad\qquad$ $\varepsilon_p = 4\%$ $\qquad\qquad$ $\varepsilon_p = 6\%$

Tensile direction

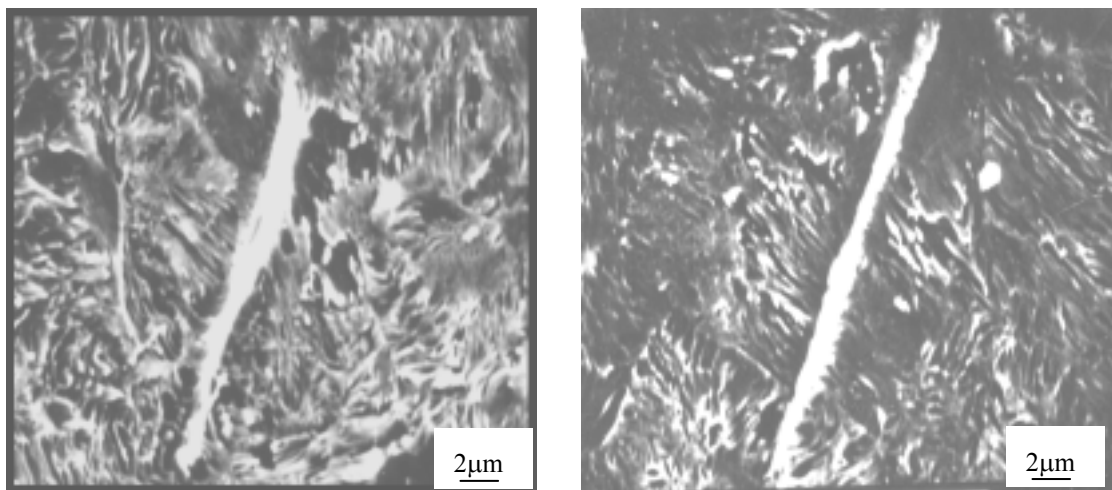Figure 2.7   Successive observation of surface under pre-strain.

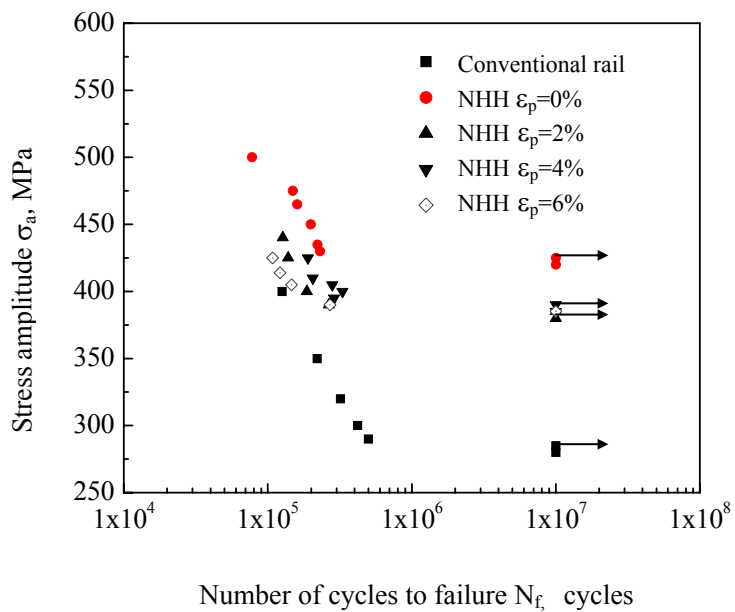Figure 2.8   Magnified micro-crack generated during the pre-strain process, $\varepsilon_p = 2\%$

Figure 2.9   S-N curves of eutectoid steel.

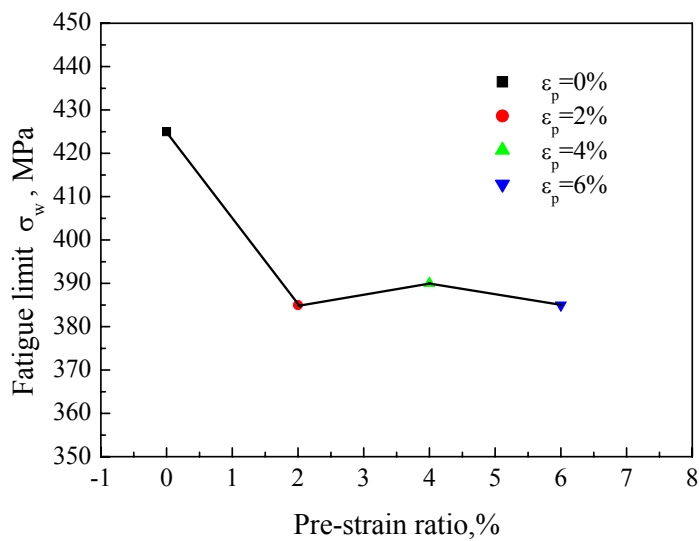
Figure 2.10   Relationship of fatigue limit and pre-strain ratio.

Fatigue crack initiation and propagation behavior

The results of the test showed that the fatigue cracks were initiated in the surface of the specimen. In this study, for non-pre-strained specimen, the crack initiated at 1~4% of the whole fatigue life [4], and propagated along the direction that perpendicularly to the load axis, as shown in Fig 2.11. The images from the SEM revealed that the fatigue cracks were initiated at the boundary of the pearlite blocks (Fig.2.12). The fatigue cracks could also occur at the inter-lamellar of the pearlite [4].

From Fig.2.12, it is clear that the fatigue micro crack was initiated along the boundary of pearlite block at point A, and the crack propagated along the inter-lamellar at B and crossed the inter-lamellar at point C. The other specimens showed almost the same result. That is: the fatigue cracks initiated in the boundary or inter-lamellar of the pearlite due to slip and the direction of the crack occurred was about 20° to 45° from the loading axis, as it grew; the cracks turned their direction to perpendicularly to loading axis.

For pre-strained specimens, the fatigue cracks occurred in the slip lines and micro cracks that were generated in the process of the plastic strain and propagated along this slip lines or cracks. Fig.2.13 shows the successive observation of pre-strained specimen (ε_p=2%). The magnification of the crack initiation is shown in Fig.2.14. It is evident that micro crack were generated in the pearlite block by crossing the inter-lamellar. Figs 2.14 and 2.15 show the micro cracks in the surface of specimen under pre-strain ε_p=4% and 6%, respectively. The slip lines and fatigue cracks preferentially initiated in crossing the lamellar (Figs2.14 and 2.16) or along the inter-lamellar in the pearlite (Fig 2.15). The micro cracks are about 20° to 45° from the tensile stress direction; this direction is nearly coincident with that of the maximum shear stress. It is also clear that the slip lines and micro cracks were generated in the process of the pre-strain. The micro crack generated in pre-strain at 6% and propagation behavior in the following fatigue test is shown in Fig.2.16. According to this figure, the crack propagated perpendicularly to the loading axis by crossing the inter-lamellar at A, along the inter-lamellar at B or along the boundary at C.
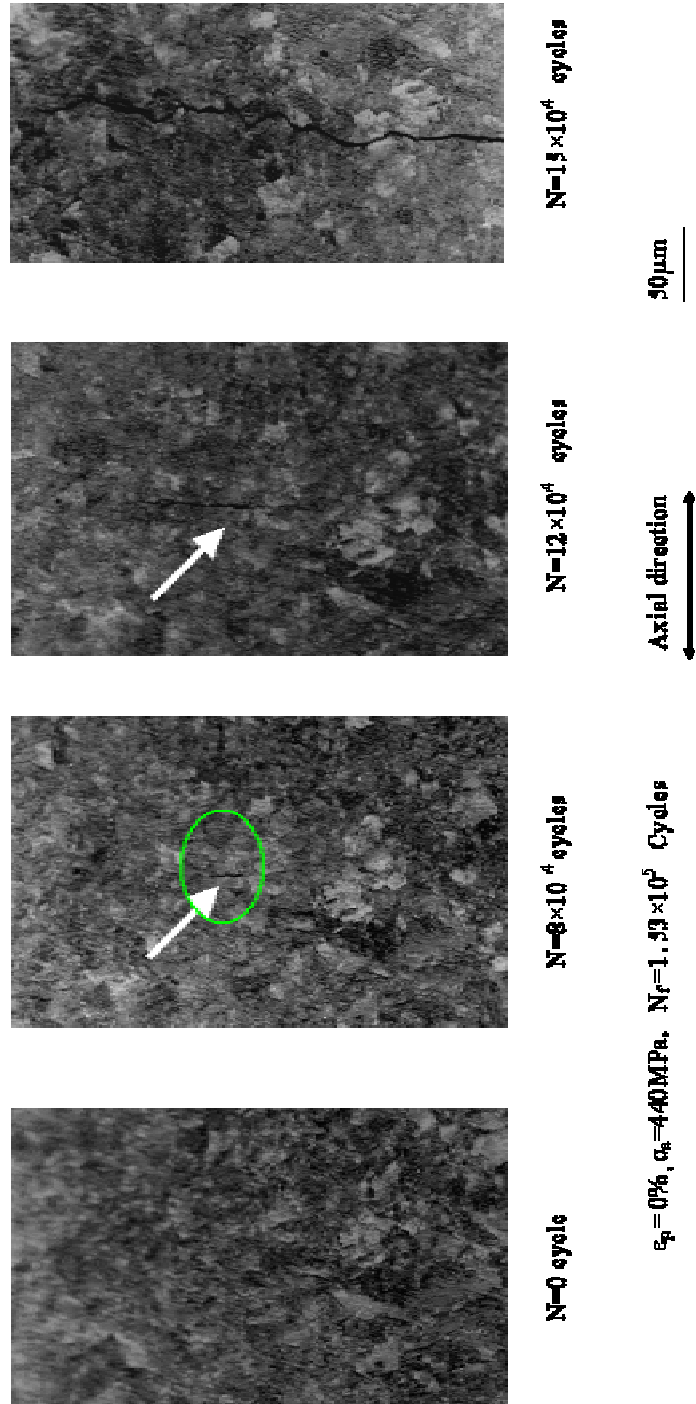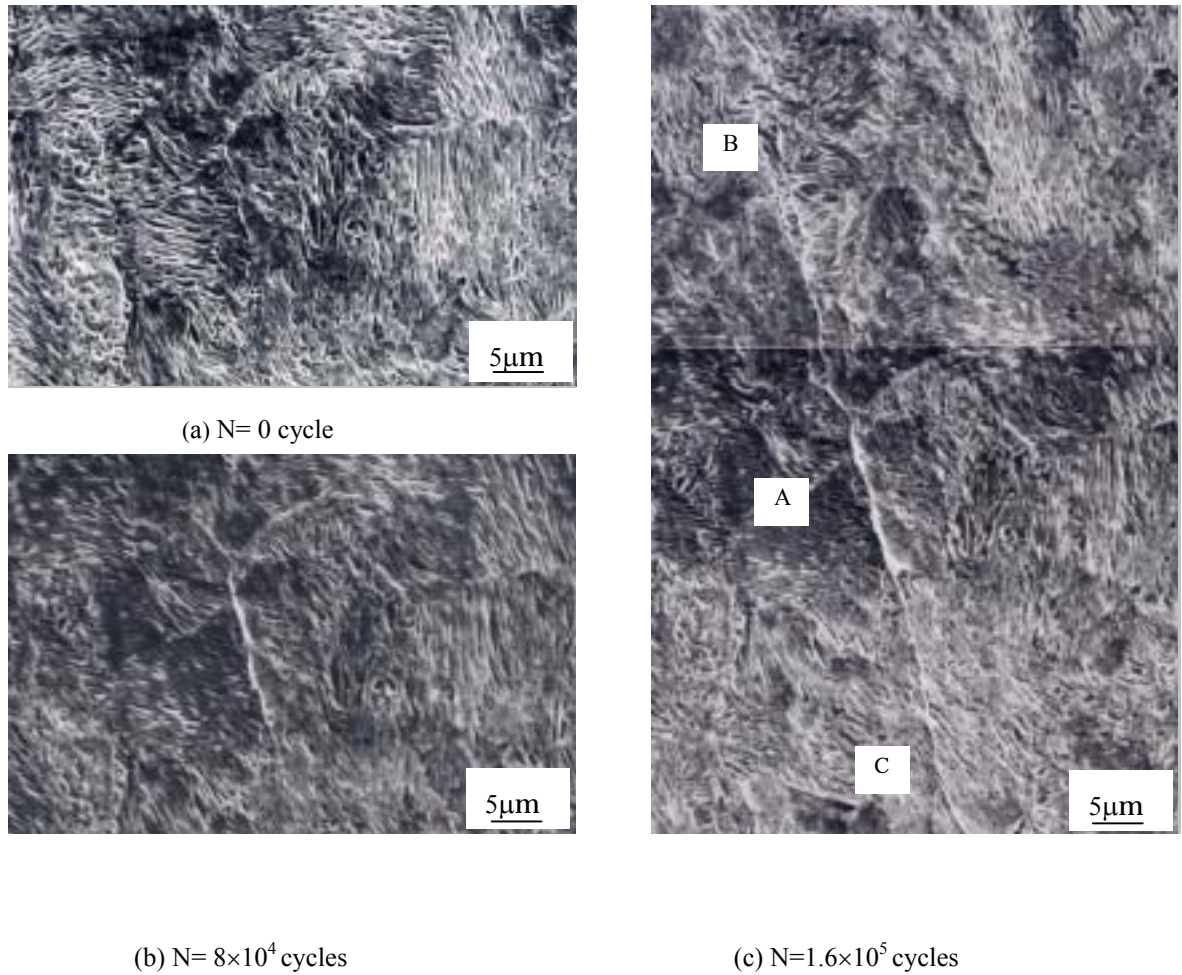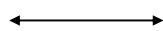
$\varepsilon_p = 0\%$, $\sigma_a = 440 \text{MPa}$, $N_f = 1.53 \times 10^5$ Cycles

Figure 2.11   Successive observation of fatigue crack initiation and propagation behavior;

(a) N= 0 cycle

(b) N= 8×10^4 cycles   (c) N=1.6×10^5 cycles

ε_p =0%, σ_a =440 MPa, N_f=1.65×10^5 cycles

Axial direction

A: initiation of the fatigue crack   B: Crack propagation by crossing the inter-lamellar

C: Crack propagation along the inter-lamellar

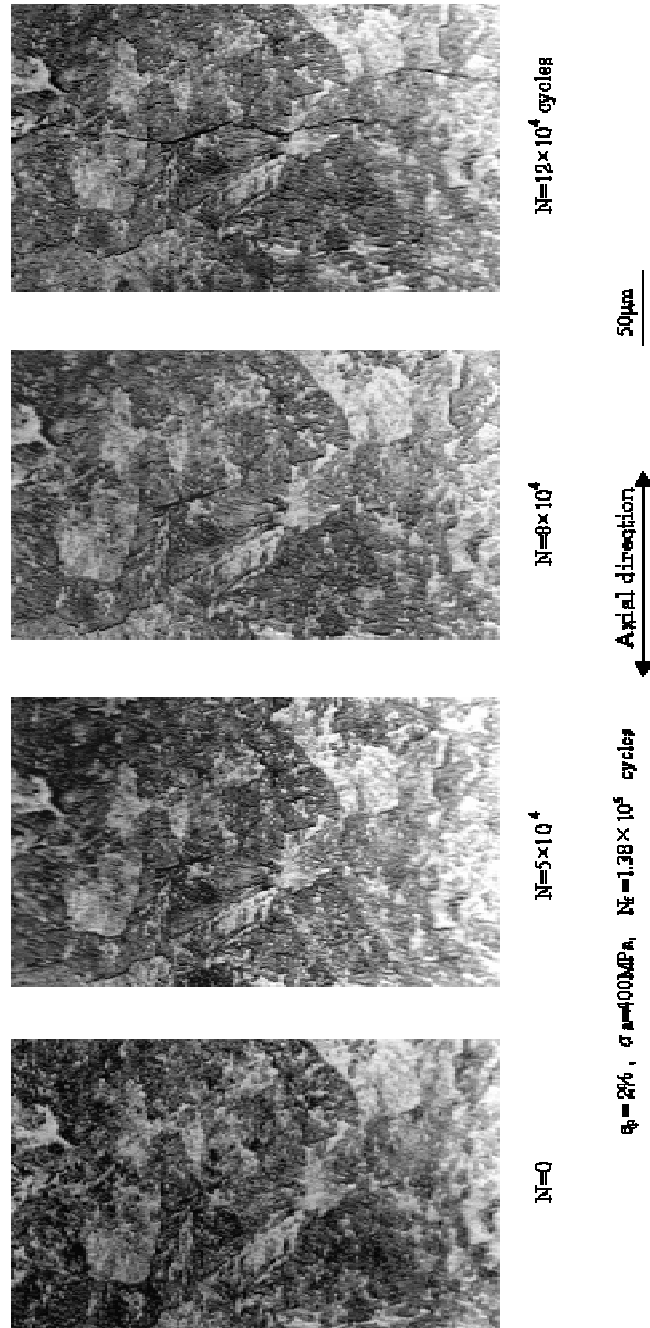Fig.2.12   An example of fatigue crack initiation and propagation behavior

Figure 2.13 Successive observation of fatigue crack initiation and propagation behavior.
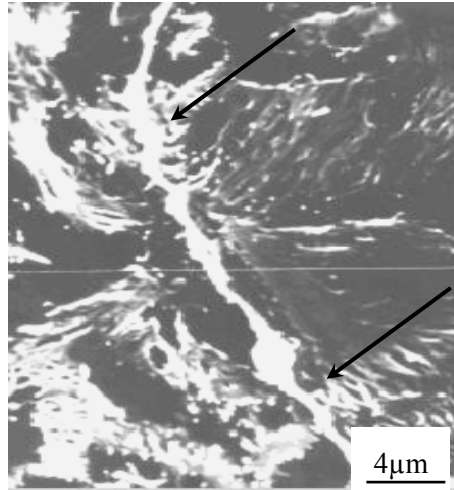
Figure 2.14   Magnified crack initiation of Fig.2.13 ($N_f = 5 \times 10^4$).
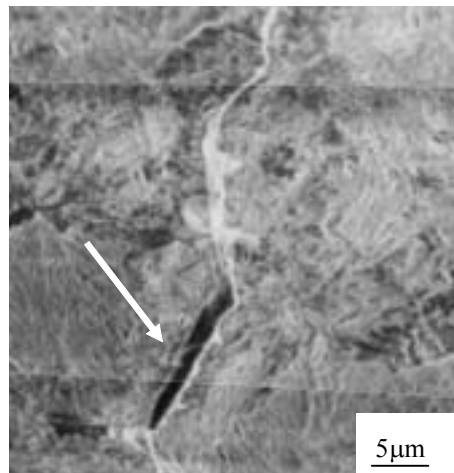
$\varepsilon_p = 4\%$, $\sigma_a = 440$ MPa, $N_f = 1.9 \times 10^5$ cycles.

Figure 2.15   An example of fatigue crack initiation site
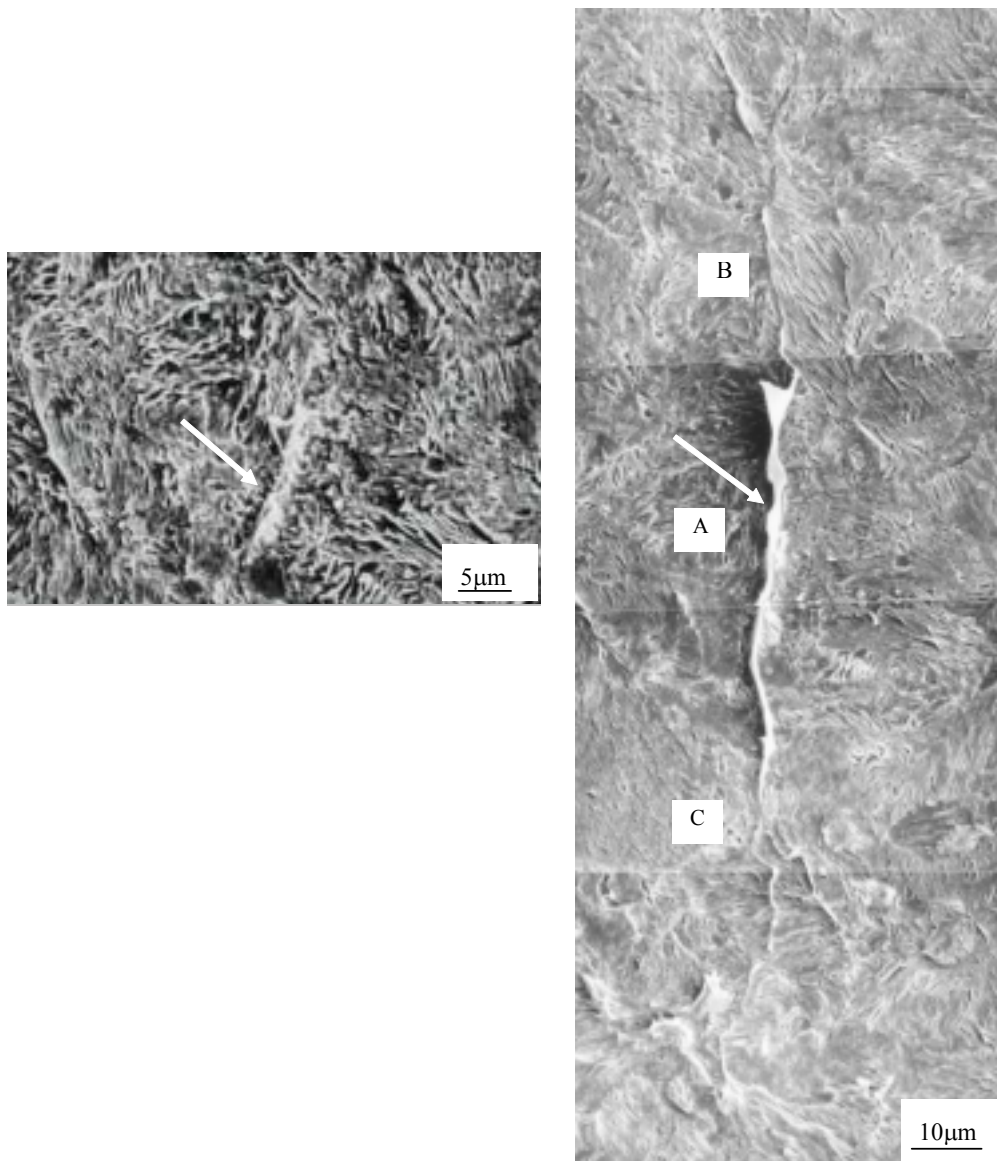
⟵⟶ Axial direction   (b) ε_p=6%, σ_a =425MPa, N=2.08×10⁵cycles

Crack propagated by crossing the inter-lamellar

Crack propagated along the inter-lamellar

C.   Crack propagated along the boundary of the pearlite.

Figure 2.16   Crack propagation behavior of pre-strained specimen.

Figure 2.17 Relationship between the main crack length and cyclic ratio.

Table 2.4   Relationship of ε_p, Hv and σ_{w0}.

$\varepsilon_{p,}$ %	0	2	4	6
HV	350	353	357	357
$\sigma_{w0,}$ MPa	425	385	390	385

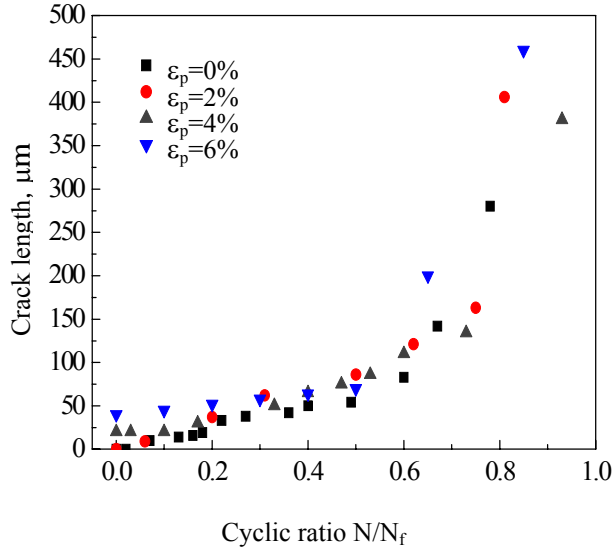Figure 2.17 shows the fatigue crack propagating behavior of four kinds of specimens with different pre-strain ratios. The stress amplitude applied is 15MPa higher than its own fatigue limit, respectively. It seems there is no obvious difference among the propagating rates of fatigue cracks of different plastic strain ratios. In other words, the effect of pre-strain rate on the fatigue crack propagation properties is very limited.

2.4 Discussion

Table 2.4 shows the test results of eutectoid steel after pre-strain. All of the specimens under pre-strained treatment have lower fatigue limits than that without pre-strain. The fatigue limit of eutectoid steel decreased nearly 10% at $\varepsilon_p = 2\%$ and have no obvious change until $\varepsilon_p=6\%$. This phenomenon is in contrast to other

structural carbon steels from S15C to S45C [13], as shown in Fig.2.18.

For low and medium carbon steel from S15C to S45C, even though the fatigue strength of pre-strained specimen decreased at small pre-strain ratio (ε_p=2%), the fatigue limit ratios increased with the plastic pre-strain ratios, and the fatigue limit ratios could be higher than their original ones (S15C, S25C and S35C) or be equal to the original one (S45C). On the other hand, for eutectoid steel, fatigue limit ratios under different pre-strain ratios decreased but hardly change between ε_p= 2% to 6%. The reason for this difference can be explained by their different microstructure and the degree of work hardening. Slip line, micro crack, density of dislocation and work hardening have direct effect on fatigue limits. Slip line and crack reduced the fatigue strength; on the other hand, fatigue limits increased with the density of dislocation and work hardening. The result was the cooperation effect of them. For low and medium carbon steels, when a small pre-strain were given, the original equilibrium was broken and the effect of work hardening was not evident, this may be the reason for the decrease of fatigue limit. With the increase in pre-strain ratio, the density of dislocation increased too. At the same time, materials were strengthened due to work hardening. Both processes may improve the fatigue limits of test materials. This may explain why the fatigue limits increased with the increase of pre-strain ratio.
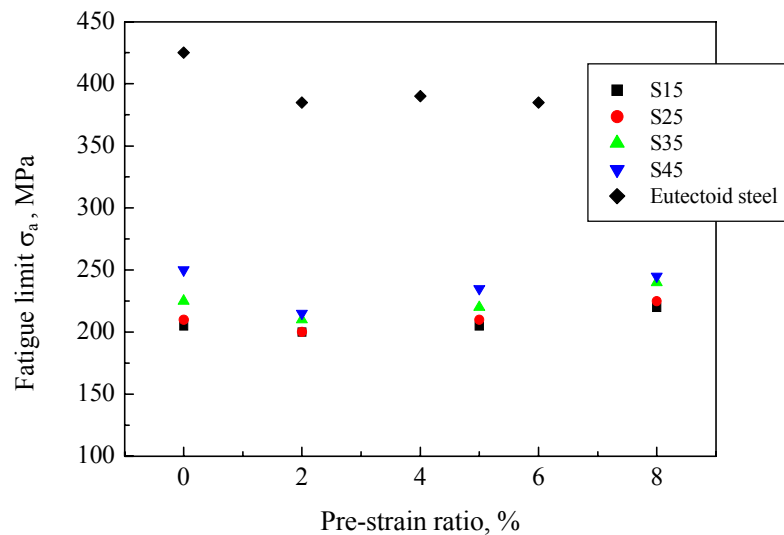

Figure 2.18   Relationship of fatigue limits and pre-strain ratios of carbon steel.

Work hardening is directly related to carbon content. With the increase of carbon content, the volume ratio of pearlite became bigger and that of ferrite became smaller at the same time. The main factor for the improvement in the fatigue limit ratio is the work hardening, and it depends on the weak ferrite structure that can be easily work-hardened. The higher ferrite volume ratios are the easier this material can be work hardened. In other word, S15C that has the highest volume ratio of ferrite structure is the most remarkable one that can be work-hardened.

For eutectoid steel, all of the microscopic structure consisted of fine pearlite. Since pearlite is very hard and has much high strength, the effect of work hardening is not expected to improve the fatigue strength significantly.

Comparing the net increase of surface hardness (HV25-30 for S15C to S45C), the net increase value for eutectoid steel is only HV7 after pre-strain. In other word, the influence of work hardening of eutectoid steel is very limited. This may be the reason why all of the fatigue limits of eutectoid steel were lower than that of the original one.

Comparing the fatigue limit ratio of carbon steel and eutectoid steel may provide some insight into understanding the difference of them, as shown in figure 2.19. For carbon steel (S15C to S45C), the fatigue limit ratios decreased with the carbon content at the same pre-strain ratio. This may be explained by the main effect factors of tensile strength and fatigue limit. Tensile strength is mainly determined by average strength of the grains; on the other hand, fatigue limit depends on the microscopic strength of the weakest grains. Table 2.5 lists the mechanical properties and fatigue limit from low carbon steel S15C to high carbon eutectoid steel. With the increase of the carbon content, the average strength increased significantly. The tensile strength increased from 442MPa to 1260 MPa; however, the microscopic strength in the weakest point (ferrite grains in this case) had no apparent increase from S15C to S45C. The fatigue limit just increased from 205MPa to 250MPa. For eutectoid steel, although the microscopic strength was remarkably increased because of its pure pearlite structure, the increase on fatigue limit is smaller than that in tensile strength. Consequently, the fatigue limit ratio at the same pre-strain ratio decreased with the increase in carbon content.

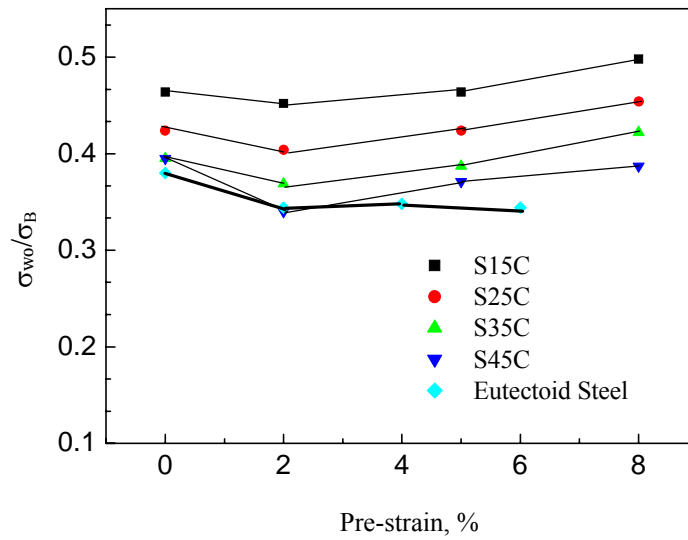Figure 2.19   Relationship of fatigue limit and pre-strain ratio.

Table 2.5   Mechanical properties including fatigue limits of carbon steels.

	$\sigma_{Y, MPa}$	$\sigma_{B, MPa}$	$\sigma_{wo, MPa}$
S15C	284	442	205
S25C	298	495	210
S35C	314	569	225
S45C	360	633	250
Eutectoid steel	823	1260	425

$\sigma_{wo:}$ fatigue limit of plain specimen.

2.5 Conclusions

The main results obtained in this test are as follows:

(1) Induction hardening is a very effective method to improve the practical properties including fatigue strength in addition to the wear resistance and mechanical properties.

(2) Plastic pre-strain decreases the fatigue limit of eutectoid steel. All fatigue limits of specimens with different pre-strain ratio are lower than that of specimens without pre-strain (ε_p=0%).

(3) The fatigue limits of pre-strained eutectoid steel become deteriorated and have no obvious change in the range of ε_p=2% to ε_p=6%.

(4) For non-pre-strained specimen, fatigue cracks preferentially initiate from boundary of the pearlite blocks or inter-lamellar of the pearlite; but for pre-strained specimens, fatigue cracks occur in slip lines, or microscopic cracks that were generated in the process of plastic pre-straining. The fatigue cracks initiate by crossing or along the inter-lamellar of the pearlite and their direction are about 20° to 45° with the loading axis in the early stage. As it grows, however, the cracks change their direction and propagate perpendicularly to the stress axis by crossing the lamellar or along the boundary or the inter-lamellar.

References

[1] Kato,   *Rail*, The rail association of Japan, 1978.

[2] M. Klesnil and P. Lukas: *Fracture of Metallic Materials*, United States: Elsevier Science Publishing Company, 1980.

[3] C,Urashima and S. Nishida, Fatigue crack initiation and propagation behavior in pearlite structure, *International conference Fatigue'96*.pp.319-324.

[4] C,Urashima and S. Nishida, Fatigue crack initiation and propagation behavior of fracture surface of eutectoid steels*, Material,* Japan, Vol.43, No. 488, pp.515-521, May 1994(In Japanese).

[5] S. Nishida, C, Urashima, H. Masumoto, *Influence of residual stress on fatigue crack propagation of rail steel, Material,*Japan,Vol.32,No.352(1982),pp.57-63(In Japanese).

[6] C,Urashima and S. Nishida, Influence of segregation on fatigue strength of rails, *Material,* Japan,   Vol.38,No.428(1988).pp.69-74(In Japanese).

[7] S. Nishida, K. Sugino, C, Urashima, H. Masumoto, Study on contact rolling fatigue of rails, Development of high speed rail testing machine, *Journal of mechanical society, Japan, Series A.*Vol.**51**. No.461(1985), pp.291-295 (In Japanese).

[8] C, Urashima and S. Nishida, Study on contact rolling fatigue of rails, A result by high speed rail testing machine, *Journal of mechanical society,* Japan, Series A.Vol.51.No.461(1985) ,pp.296-301(In Japanese).

[9] W.R. Tyfour, J.H.Beynon, A. Kapoor, Deterioration of rolling contact fatigue life of pearlite steel due to dry–wet rolling–sliding line contact, *Wear*, 197(1996), pp.255-265.

[10] D.F. Cannon, H. Pradier, Rail rolling contact fatigue research by the European rail research institute, *Wear,*191(1996),pp.1-13.

[11] J. W. Ringaberg, T. Lindback*,* Rolling contact fatigue analysis of rails including numberical simulations of the rail manufacturing process and repeated wheel-rail contact loads, *Int. J. Fatigue*, 25(2003),pp547-558.

[12] K. Suzuo, H. Masumoto, S. Nishida, C. Urashima, M. Hattori, The basic properties of rial with high strength and development of new rail, *Steel Research.* No.303(1980),pp.23-38(In Japanese)..

[13] G. Schleinzer F. Fischer, Residual stress formation during the roller

straightening of railway rails, *International journal of Mechanical Science* 43(2001), pp.2281-2295.

[14] D. Miao, S. Nishida and N. Hattori, Effect of carbon content on fatigue properties of pre-strained carbon steel, *Proceeding of International conference of fatigue,* Fatigue 99(1999),pp.619.

Chapter 3

Evaluation of Cold Rolling

on Fatigue Properties of Eutectoid Steel

3.1 Introduction of Surface Modification

The term of surface modification encompasses a wide field of technologies. The common denominator of these technologies is the formation of modified surface layer in which the microstructure and /or the mechanical properties are different from the initial material. Potential improvements in the characteristics of engineering materials that may be expected included [1-2]:

• Improved corrosion and erosion resistance

• Enhanced hardness and improved wear resistance

• Improved strength, toughness and fatigue properties

It is well known that fatigue failure usually initiates on the surface of a component. Therefore, surface modification is an important and cost-effective method to improve fatigue properties of components without alerting the bulk mechanical properties of components. Surface modification includes wide range of techniques, which can be briefly grouped into three categories: plastic deformation, heat treatment and surface treatment method [3]. Surface treatment can be further divided into two principle methods based on the reaction occurred on the surface of substrate. One is that the surface layer on the substrate is modified so that the compositions or microstructures are changed through chemical, thermal–chemical, thermal or mechanical actions. The other is that a new surface layer is created on the substrate surface through coating with chemical or physical vapor deposition, plating, spraying, electro-chemical metallizing and so on [4]. Generally, the effects of surface modification on fatigue behavior are regarded as (1) surface roughness (2) surface strengthened layer and (3) surface compressive residual stress. In the following sections, some important methods are introduced.

3.1.1 Shot Peening

Shot peening (SP) is a well established industrial process that is used extensively to improve fatigue performance and to prevent stress corrosion cracking. The effects introduced by SP are believed to include structure change within the surface layer, the formation of a residual stress field and the change of surface roughness. Numerous researchers demonstrated that SP can significantly improved fatigue strength [5-8].   Wang and co-workers conducted a quantitative and systematic study of the fatigue behavior of surface-strengthened metals [9-10]. They found that proper SP introduces compressive residual stress (CRS) within the surface layer, pushes the crack source into the tensile residual stress (TRS) region under the surface hardened layer, and leads to optimum strengthening effects. For any steel, after suitable surface-strengthening treatment like SP, as long as the fatigue crack source is located within the TRS zone, no matter how great the strengthening intensity is (i.e. the depth of the CRS field), and no matter what kind of TRS field is formed, the critical stress to fatigue fracture is approximately equal. Let σ_{wi} be the "internal fatigue limit", and σ_{ws} the surface fatigue strength, the following equation describes their relationship, i.e., the fatigue strength of the un-peened material:

$$\sigma_{wi} = 1.35\ \sigma_{ws} \tag{3.1}$$

And two empirical equations are deduced to express the relationship of CRS at the surface, σ_{s}^{rs}, and the maximum CRS, σ_{max}^{rs}, with the yield strength, $\sigma_{0.2}$, and the ultimate tensile strength, σ_B.

$$\sigma_{s}^{rs} = 120 + 0.5\sigma_{0.2}(\pm 30)(\text{MPa}) \tag{3.2}$$

$$\sigma_{max}^{rs} = 70 + 0.667\sigma_B \quad (\sigma_B < 1000\text{MPa}) \tag{3.3}$$

or

$$\sigma_{max}^{rs} = 430 + 0.323\sigma_B \quad (\sigma_B \geq 1000\text{MPa}) \tag{3.4}$$

Based on shot peening, the other surface strengthening method, hard shot peening (HSP) or laser shot peening (LSP) for instance, are developed [11-12]. Compared to conventional SP treatment, LSP can develop an almost equal residual stress (RS) level in the first $100\mu m$ and the stress field induced by LSP is shown to extend two to five times deeper than what is typical for SP. But generally,

shot-peened specimens display much higher RS level than laser-shocked material, mainly in the first 100-200μm of depth. SP induces double surface hardness increase generated by LSP. This may be attributed to differences in the pressure duration, which result in higher dislocation generation and motion, and to the number of slip planes activated by multi-axial surface loading such as SP. In terms of the surface geometry modifications, LSP is proven to be able to provide a partially unchanged surface while SP generates a detrimental roughened surface. The beneficial effects of LSP originate from the large affected depth and surface state quality, which are expected to influence favorably the initiation and crack stages [12].

3.1.2 High Energy Surface Modification Method

High-energy processes are relatively new surface treatment methods. They can alter the properties of surfaces without changing the dimension of the surface. Common high-energy process includes electron beam treatment, ion implantation and laser beam treatment. Electron beam treatment alters the surface properties by rapid heating and cooling in a very shallow region, 100μm in depth, near the surface. Ion implantation uses electron beam or plasma to impinge gas atoms to ions with sufficient energy, and embed these ions into atomic lattice of the substrate, accelerated by magnetic coils in a vacuum chamber. The mismatch between ion implant and the surface of a metal creates atomic defect that harden the surface. Laser beam treatment is similar to electron beam treatment, i.e., it alters the surface properties by rapid heating and cooling in a very shallow region near the surface.

Plasma-enhanced ion beam treatment is a new method based on conventional ion beam treatment [2]. This technology combines the material surface preparation/cleaning and modification stages in single–step process. The interaction of microsecond plasma flow, followed by a plasma-enhanced nanosecond high power ion beam with the material's surface provides surface preparation (heating, degassing and cleaning), rapid melting and cooling, and ion mixing in the surface layer. Surface morphology and microstructure of the surface layer of the ion-treated region are much different from that of the untreated region. Melting of surface is accompanied by pronounced changes in the surface layer microstructure. This technology can be potentially applied for improving corrosion and erosion resistance; enhancing hardness and wear resistance and improving strength, toughness and fatigue properties of material.

Induction hardening is also a widely used surface hardening method, which applied energy directly to materials that require a hard surface. Bertini investigated fatigue behavior of induction-hardened components [13], and discovered that the surface layer after treatment constituted by very hard martensite with uniform microstructure, whereas the core maintains the initial tempered martensite microstructure. The residual stress field is mainly due to the volume expansion associated with the martensite transformation. Consequently, fatigue properties of the treated specimen exhibited remarkable improvement. The NHH rail used in Chapter 2 underwent this kind of heat treatment and possessed very hard surface hardness.

3.1.3 Surface Modification by Chemical Reaction

For surface hardening of various metals, nitriding, i.e. the diffusion introduction of nitrogen atoms into subsurface layers with a thickness between approximately $10 \mu m$ to $1mm$, is appropriate [14]. This method is widely used as a processing tool to increase the fatigue and wear resistance of machine parts of carbon or alloy steels. The effect of ion-nitriding on practical properties will be discussed in the next chapter.

3.1.4 Cold Rolling

Cold rolling is a method that is usually applied to fillets or circumferential notches in part with rotational symmetry, e.g. crankshafts, axles, cylinder or rod.   This makes it possible to use a relatively low strength and low cost material and to raise the fatigue strength locally where it needs the most.   Most of above components are made of eutectoid steel. Therefore, the focus of this Chapter is to evaluate the influence of cold rolling on practical performance of eutectoid steel.

The improvement in fatigue strength after cold rolling in the high cycle region of the S-N curve is typical 30% and more, compared with the fatigue strength of the untreated component [15]. The important process parameters in this method are:
   (1) Rolling force (for a given roller geometry)
   (2) Number of passes(number of cycles of rolling at full load)
   (3) Roller geometry as compared with notch geometry.
The combination of roller force and number of passes is important because it controls the amount of cold working that the material is subjected to. On the other hand, there

is a limitation to the benefits of cold working since an excessive amount of plastic deformation will introduce low cycle fatigue damage, and the benefits of cold work will saturate. There is an optimal number of passes after which the fatigue strength starts to deteriorate. Also the geometry of the roller tip radius relative to the notch geometry influences fatigue strength; an oversize roller appears to be better than an undersize roller. Last but not least, the surface roughness after rolling appears to have a small or no influence on the effectiveness for heavily cold rolled notched components, particularly in the high cycle part of the S-N diagram.

In practical structural components, notches or steps are often necessary due to structural requirements. However, the fatigue strength of these components is significantly weakened due to high stress concentration placed on them. It is reported that more than 80~90% of failures in steel structural components are directly or indirectly caused by fatigue and 90% of the failures are initiated from the stress concentrated parts [16]. How to improve the fatigue strength of these stress concentrated parts has been a major research subject in mechanical engineering.

Few studies, however, have been carried out in this area on eutectoid steel. One study on the effect of pre-strain on fatigue property of eutectoid steel [17] showed that pre-strain decreased the fatigue strength and affected the initiation of fatigue crack. Studies on other materials [18, 19] demonstrated that the cold rolling was very effective in improving the fatigue properties.

The objectives of this study were to: (1) evaluate and quantify the effect of cold rolling on fatigue strength of notched eutectoid steel; (2) discuss the fundamental mechanism for the improvement in fatigue properties; (3) study crack initiation and propagation behaviors.

3.2 Material and Experiment Procedure

3.2.1 Material and Preparation

Tables 3.1 and 2 list the chemical composition and mechanical properties of the test material. A smooth specimen (SS) and five notched specimens were used in the study. Figure 3.1 shows the shape and dimensions of the fatigue specimen and Table 3.3 lists the cold rolling conditions. Here, Δt represents the plastic deformation value by cold rolling. Five types of notched specimens, denoted by R00, R05, R10, R15 and R25, respectively, were used in the test. The material of rolling disc was

SKD-11 and its hardness was HRC60-65. Specimens without cold rolling (SS, R00) were first polished with emery paper (#400-#3000) and then with diamond paste (the grain size from 0.1μm to 0.03μm). After that the specimens were annealed at 520°C for 30 minute in a vacuum furnace to relieve the residual stress. In order to remove the work hardened layer, the specimens were also electro-polished over 50μm in diameter size. Finally, they were etched (5% HNO_3 and 95% Ethanol) to observe the microstructure of the specimens. The cold rolled specimens were similarly treated except that they were not annealed and electro-polished in order to maintain the influence of plastic deformation.

The fatigue test was performed with an Ono type of rotating and bending machine (14.7Nm, 3000rpm) under the stress ratio of $\sigma_{max}/\sigma_{min} = -1$. The fracture surface was observed with a scanning electron microscope (SEM) to observe the initiation and propagation of the fatigue crack. The hardness was tested with a Vickers hardness tester and the residual stress was measured by the X-ray method. Replicated samples were successively taken to monitor the fatigue crack initiation and propagation behavior. The detail information for cold rolling method and residual stress measurement are introduced in the following text.

3.2.2 Cold Rolling Treatment

Cold rolling is plastic working method, in which materials are set between two rotating rollers and rolled to predetermined dimensions. In the present study, fatigue specimens were first machined on lathe into a round bar with a V-notch in the center of the specimens. The shapes of rollers and the setting of specimens are shown in Figure 3.2. In cold rolling, both of the fixing roller and the moving roller as well as the specimens rotate around their own axis. Meanwhile, the moving roller moves towards the specimen and the fixing roller and they contact with predetermined pressure. The contact of rollers with the specimen keep for a period of time until the desired area reduction is obtained. In this study, the pressure was 3 tons and treatment time was 6 seconds.

Table 3.1 Chemical composition, mass%

C	Si	Mn	P	S
0.73	0.27	0.75	0.018	0.014

Table 3.2　　Mechanical properties

$\sigma_{0.2}$MPa	σ_B,MPa	ϕ, %	EL, %
527	918	26.8	11.4

Table 3.3　　Specimen symbols and dimensions of notched part before/after cold rolling, mm

	Before cold-rolling			After cold-rolling			
	d	ρ	t_1	d	ρ	t_2	**Δt**
R00	5	1	0.5	5	1	0.5	0
R05	5.1	1	0.45	5	1	0.5	0.05
R10	5.2	1	0.4	5	1	0.5	0.1
R15	5.3	1	0.35	5	1	0.5	0.15
R25	5.5	1	0.25	5	1	0.5	0.25
SS	5	0	0	5	0	0.5	0

d: Minimum diameter;　　ρ: Notch radius　　t: Notch depth

$\Delta t = t_2 - t_1$: Cold rolling value;　　SS: Smooth specimen.
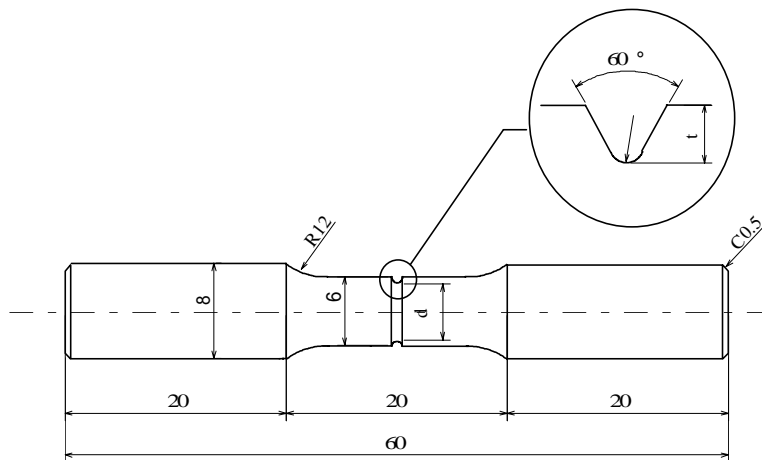
Figure 3.1   Shape and dimensions of specimen.

Fixed roller   Specimen   Moving roller
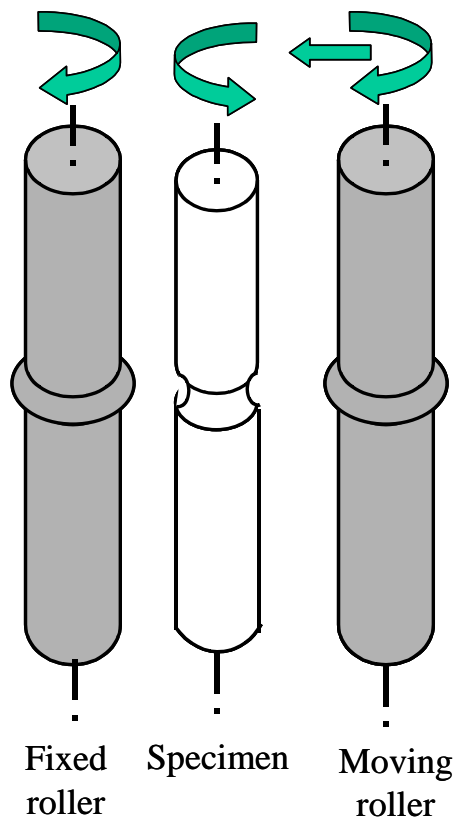
Figure 3.2   Schematic illustration showing the configuration of the specimen
and rollers in cold–rolling treatment.

Table 3.4   X-ray   diffraction analysis condition

Characteristic X-ray	Cr
Tube voltage, KV	40
Tube current, $\mathbf{A}\cdot m^{-3}$	300
Irradiated area	$\phi 0.1$

3.2.3   Residual Stress Measurement

The residual stresses introduced by hard rolling in the axial direction of the specimens were measured by X-ray diffraction method (SHIMADZU *X-ray stress measurement equipment DX-10*). The X-ray diffraction conditions for measurement residual stress are listed in Table 3.4.

  The advantages of X-ray diffraction method are [20]:

1. It is a non-destructive testing method that can be used directly to equipments, components or products.

2. In this method, residual stress is estimated by the variation in lattice spacing causing by elastic stress.

3. X-ray beam can strike only a small area on a specimen with the spot size only several millimeters. Therefore, the measurement of stress on a local region or the variation of surface stress as well as the measurement of stress in given direction on surface is possible.

4. Measurement can be finished quickly.

5.   Stress variation with the depth of components can be tested using surface removal by electro-polishing techniques.

3.3   Experiment Results

3.3.1   Fatigue Strength

Figure 3.3 shows the S-N curves of the eutectoid steel. For all specimens, the fatigue strength is enhanced significantly after cold rolling. Compared to the specimen without cold rolling (R00), the fatigue limits for R05, R10, R15 and R25 increased to 175%, 210%, 235% and 255%, respectively. The fatigue limits of the

specimens with cold rolling treatment were also much higher than that of the smooth specimen (SS) with the same diameter; whose fatigue limit was 285MPa.   Table 3.5 lists the fatigue limit, the ratio of the fatigue limit improvement, the stress concentration factor, the residual stress and Vickers hardness. The relationship of the fatigue limit and deformation value is graphically depicted in Fig.3.4. It is evident that the fatigue limits increased with the deformation values.

3.3.2 Hardness

Figure 3.5 shows the Vickers hardness distribution patterns from the surface of the specimen to its interior in the smallest section of the notch part for each of the five specimens. The Vickers hardness was measured under 0.98N load.   After cold rolling, the hardness increased by about 30HV for R05 and 50HV for R10, R15 and R25. At the same time, the depths of work hardening layer of R05, R10, R15 and R25 were about 200μm, 280μm, 360μm and 400μm, respectively. Clearly, the work hardening layer increased with the plastic deformation value. As it is well known, the increase in hardness directly affects the fatigue strength of the materials.

3.3.3 Microstructure

Figure 3.6 shows the fibered microstructure at the root of the notch under cold rolling with different cold rolling value 0.1 and 0.25*mm,* respectively. The results showed that the depth of deformation layer increased with the increasing of deformation value and the pearlite blocks at the notched part were elongated in axial direction. It is considered that the fibered structure may have prevented the crack initiation and resisted the propagation of fatigue crack into the interior region during the following fatigue test.

3.3.4 Residual Stress

The residual stress can be another factor that affects the fatigue strength. Under cold rolling, a compressive residual stress is introduced to the root of the notch. In this test, the longitudinal residual stress was measured by the side-inclination method. The residual stresses was determined using a relationship of 2θ-$\sin^2\psi$, where ψ was 0°, 18.5°, 26.5°, 33°, 39°and 45°, and 2θ was the diffraction angle determined from the half value breadth method.
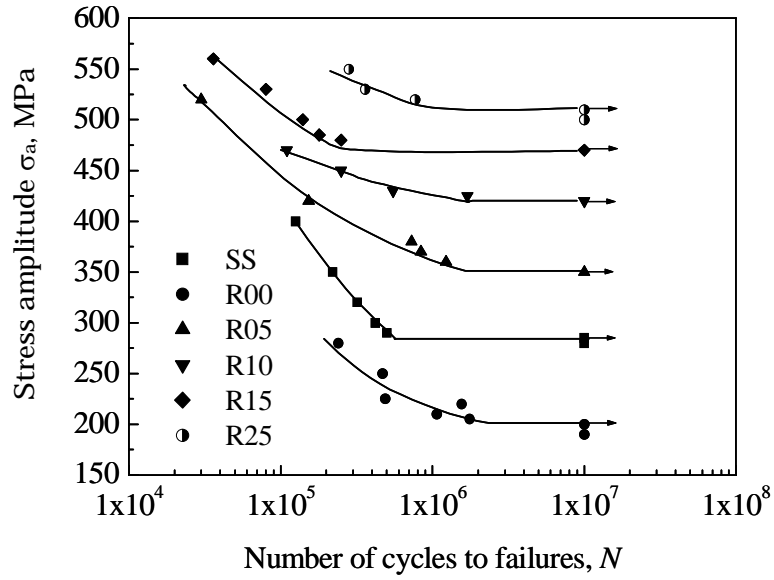
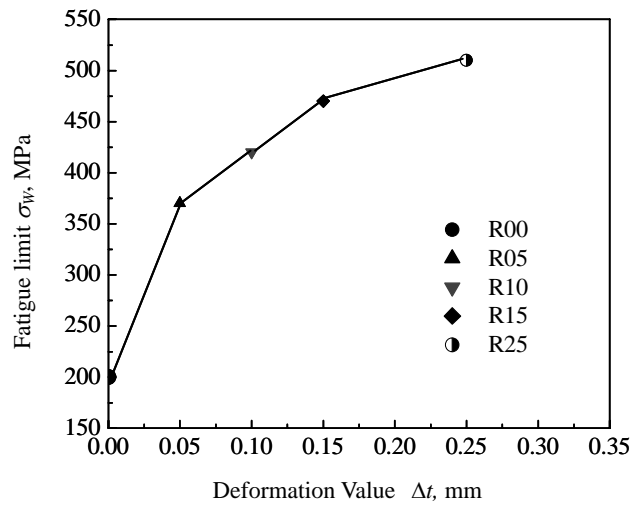Figure 3.3   S-N curves of eutectoid steel.

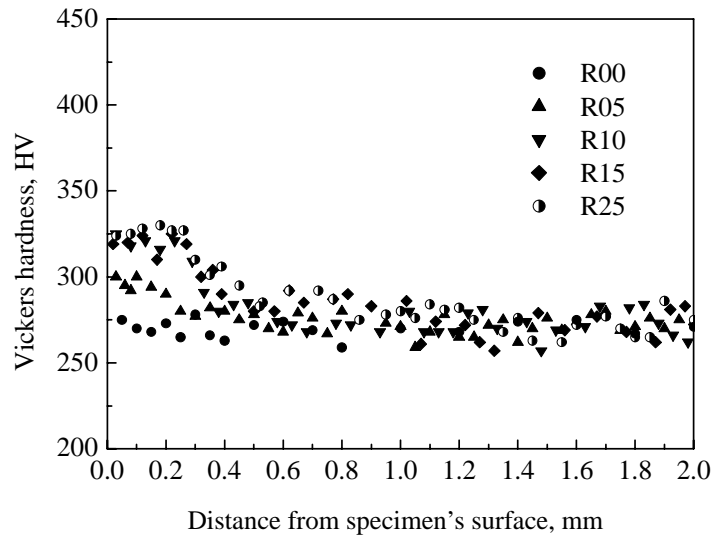Figure 3.4   Relationship of fatigue limit and plastic deformation value.

Figure 3.5 Hardness distributions from the notch root to the interior region.

Table 3.5   Test results of S25C after cold rolling.

	R00	R05	R10	R15	R25	SS
σ_w, MPa	200	350	420	470	510	285
σ_w*, %	100	175	210	235	255	142
K_t	1.43	1.43	1.43	1.43	1.43	-
σ_{RS}, MPa	-	-411	-482	-558	-639	-
HV	271	300	320	325	325	-

σ_w: Fatigue limit, σ_w*:   Ratio of fatigue limit improvement

K_t: Stress concentration factor, σ_{RS} Residual stress

R10   R25

Fibered microstructure at the notch part

⟷ Axial direction
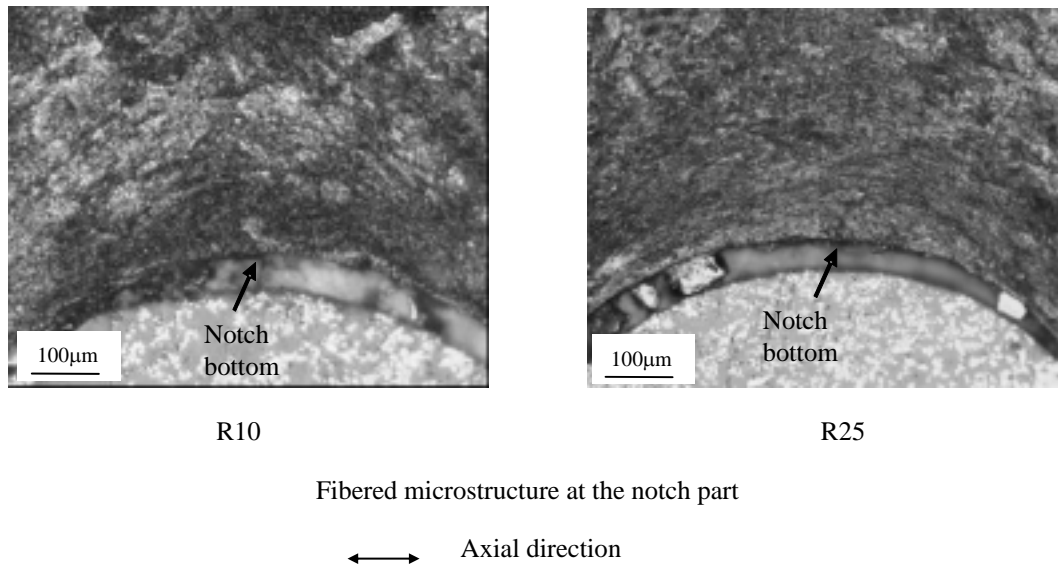
Figure 3.6   Observation of transverse section.

$$\sigma_{RS} = -1135 \, \Delta t - 366$$
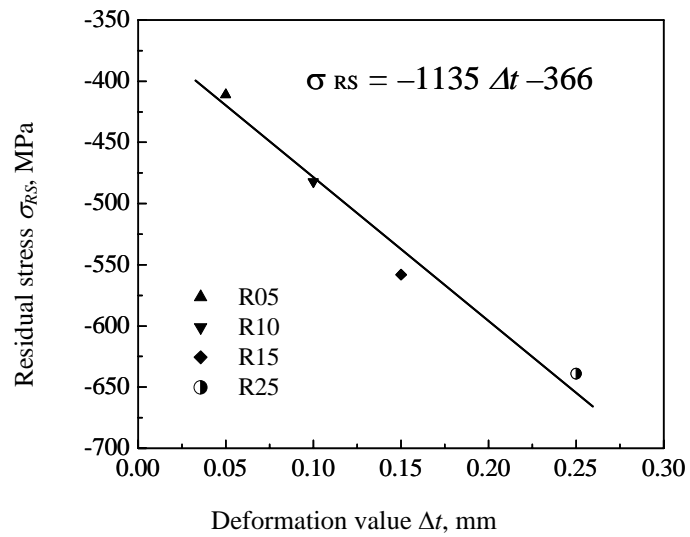
Figure 3.7   Relationship of residual stress and plastic deformation value.

Figure 3.7 illustrates the relationship between compressive residual stress (σ_{RS}) and deformation value (Δt). It is evident that the absolute value of σ_{RS} increased almost linearly with Δt. The relationship between σ_{RS} and Δt can be expressed by the following equation:

$$\sigma_{RS} = -1135\Delta t - 366 \tag{3.5}$$

3.3.5 Non-propagating Crack

In the fatigue test, non-propagating cracks were observed on the surfaces of all kinds of the cold rolled specimens, as shown in Fig.3.8.   In order to measure the depths of the non-propagation crack, the specimens were broken with impact load after they were kept in liquid nitrogen (about -200°C) for a few seconds. Figure 3.9 shows the depths of the non-propagation cracks after the specimens were applied their own fatigue limit stress and the number of cycles was over 10^7 cycles, the depths of the cracks for R05, R10, R15 and R25 were 180µm, 254µm, 292µm and 370µm, respectively. The depths of non-propagating crack increased with the increase of deformation value. However, these depths were smaller than the work hardened layer shown in Figure 3.5.   On the other hand, no non-propagation crack was observed on the surface of the specimen without cold rolling.

## 3.3.6   Crack Initiation and Propagation Behavior

According to the fatigue test, fatigue crack initiated at the surface of the specimen. Figure 3.10 is the detailed observation of the samples under SEM. It is evident that the crack initiated in pearlite block along the inter-lamellar, just like smooth specimen [21]. The specimen with different deformation value showed the similar results. That is, the fatigue crack preferentially initiated and propagated along the inter-lamellar of pearlite. In other word, the cold rolling did not affect the initiation of the fatigue crack initiation like pre-strain [17].
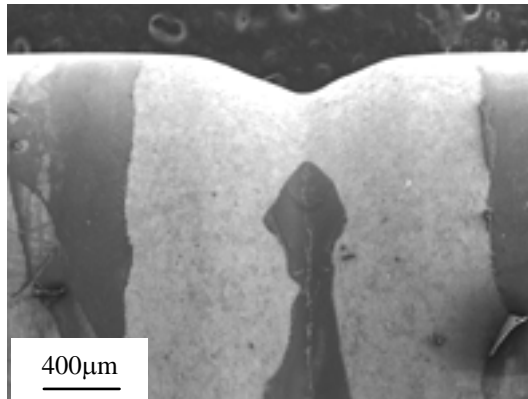
R10
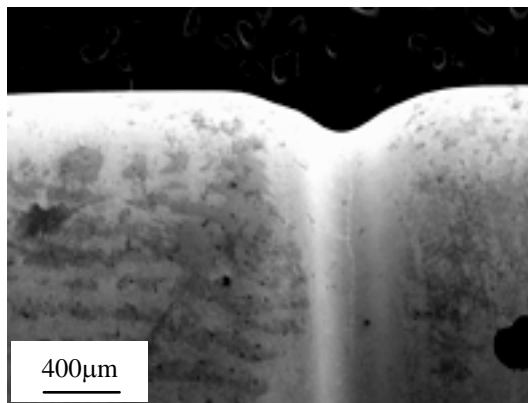
R15
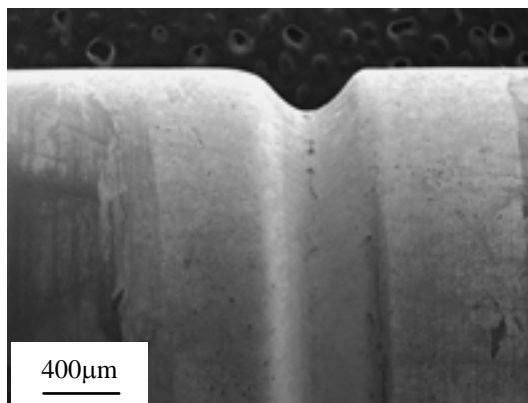
R25

Axial direction

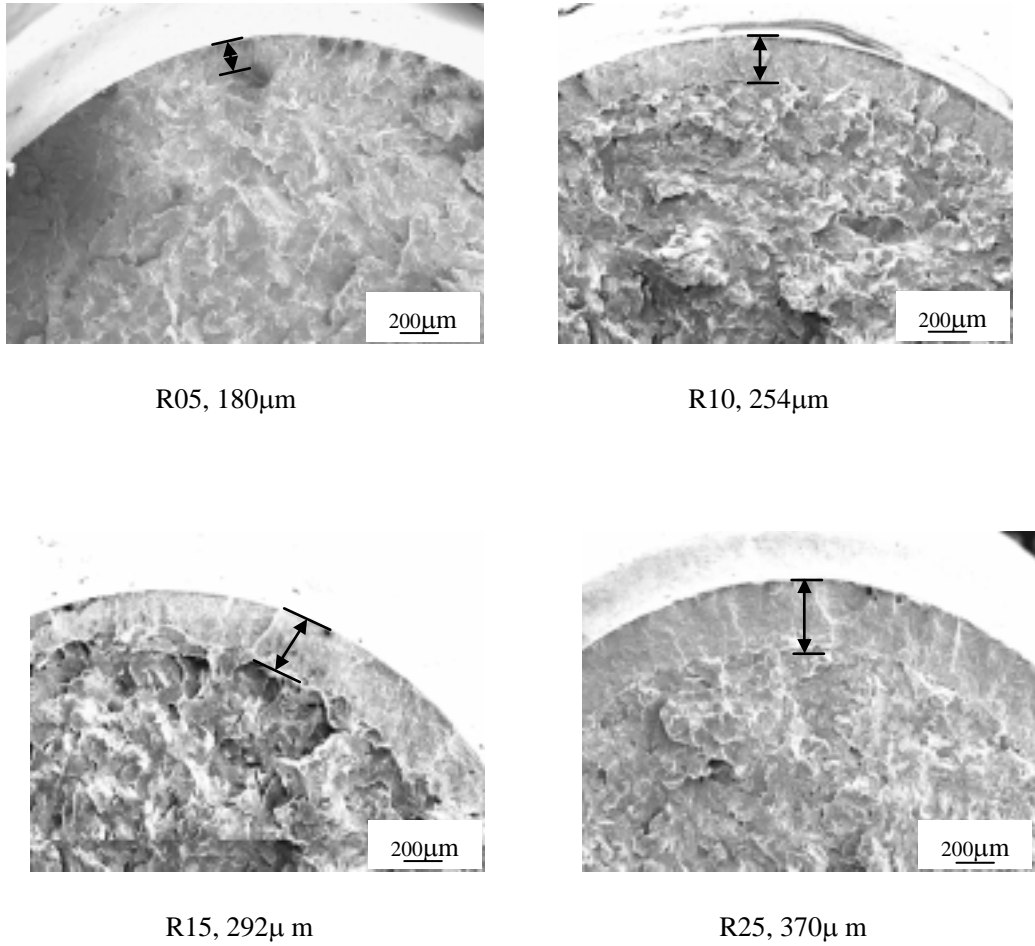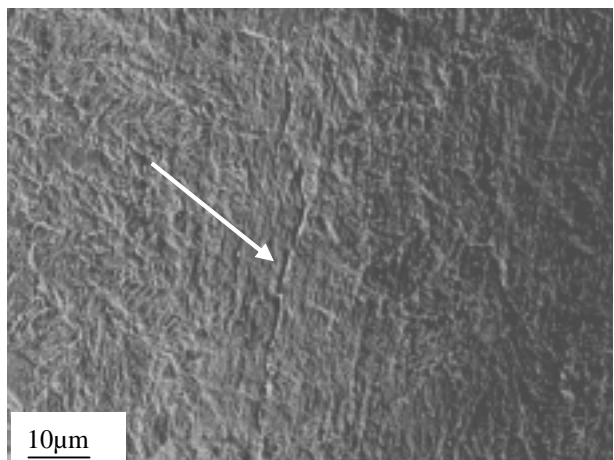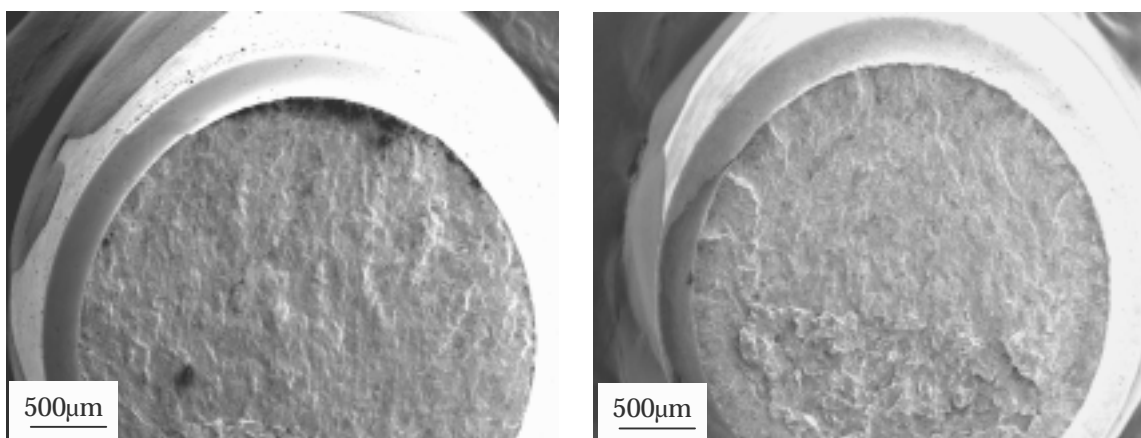Figure 3.8 Non-propagating cracks in the specimen surfaces after fatigue test.

R05, 180μm

R10, 254μm

R15, 292μ m

R25, 370μ m

Figure 3.9   Depths of non-propagating cracks.

R10, σ_a=485MPa, N_f=11×10^4 cycles

Figure 3.10   Magnification of fatigue crack initiation(n= 2×10^4 cycles).

R00

σ_a =210MPa

N_f=1.2×10^6 cycles

R25

σ_a =520MPa

N_f=2.7×10^5 cycles

Figure 3.11   Fracture surfaces of specimens.
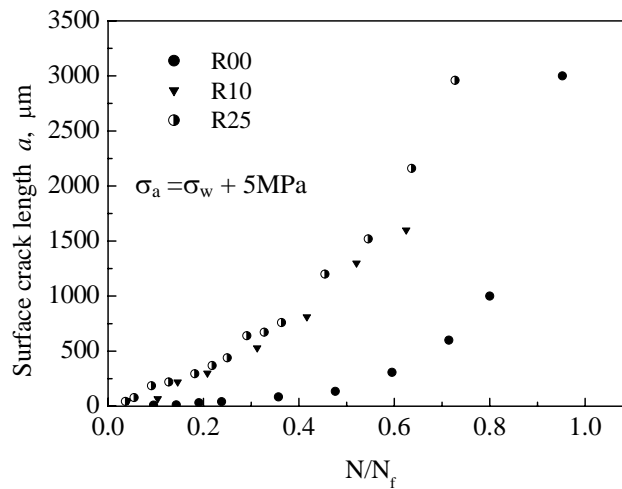
Figure 3.12   Fatigue crack propagation behavior.

Figure 3.11 shows the surface fractures of the specimens with and without cold rolling. Fatigue cracks initiated from the surface on both types of specimens. For the specimen without cold rolling, the fatigue cracks initiated from one or two points and propagated to the opposite side of the surface.   For the cold rolled specimen, however, cracks initiated from many points around the circumference and propagated to the core of the specimen.

Figure 3.12 shows the fatigue crack propagation behavior for the three specimens, R00, R10 and R25, respectively.   Because of their significant differences in fatigue limits, an equivalent stress amplitude was applied   to these specimens. In other word, the applied load stress was 5MPa higher than its own fatigue limit value, respectively. The lengths of the surface cracks were obtained with replicated sampling under a digital microscope (VH-6300, KENENCE, Japan). It is clear that the fatigue crack in the cold rolled specimen occurred earlier and propagated much faster than that in the non-cold rolled one. However, at the same time, the fatigue limit of the former was much higher than that of the latter.

3.4 Discussion

3.4.1 Mechanisms of Fatigue Strength Improvement.

The mechanism for the improvement in fatigue strength after cold rolling is relatively complex. The modification in fatigue strength may be attributed to the

fiberized microstructure, work hardening and residual stress introduced by cold rolling.

Fibered Microstructure: Figure 3.6 shows the fibered microstructure at the root of the notch under cold rolling. The results showed the pearlite blocks at the notched part were elongated in axial direction and the depth of deformation layer increased with the deformation value. The fibered structure may have prevented the crack initiation and resisted the propagation of fatigue crack into the interior region during the fatigue test. Consequently, fatigue strength was improved.

Hardness Increase: After cold rolling, the hardness increased by about HV30 for R05 and HV50 for R10, R15 and R25. At the same time, the depths of work hardening layer of R05, R10, R15 and R25 were about 200μm, 280μm, 360μm and 400μm, respectively. Clearly, the work hardening layer increased with the increase of plastic deformation value. As it is well known, the increase in hardness usually improves the fatigue strength of the materials.

Residual Stress Field: the residual stress can be another factor that affects the fatigue strength. Under cold rolling, a compressive residual stress was introduced to the root of the notch. In the fatigue test, parts of the applied stress may have been offset by the residual stress. This is another factor for the improvement of the fatigue strength.

While the increase in hardness was significant after cold rolling in R05 and R10 (HV29~49), the hardness improvement in R15 and R25 occurred to a much less extent (no more than HV5), as shown in Table 3.5. When the residual stress absolute value increased from 482MPa to 639MPa, the fatigue limits were improved from 420MPa to 510MPa. It may be concluded that the compressive residual stress exerted the most important effect in the improvement of the fatigue strength.

A comparison of the effect of cold rolling on the fatigue properties of low carbon steel (JIS S25C) and eutectoid steel may provide insight into the role of work hardening and residual stress in the modification of fatigue properties. Table 3.6 lists the test results of S25C after cold rolling. Figs 3.13 and 3.14 show the relationship of hardness and residual stress of S25C and eutectoid steel with different plastic deformation ratios of diameter at the notch root ($\Delta t/d_{before}$).

Although cold rolling is very effective in improving the fatigue properties of the two materials, the relative significance of work hardening and residual stress is distinctively different. As indicated in Fig.3.13, the hardness for S25C at different

plastic deformation ranged from HV155 to HV267; the net increase in Vickers hardness was over HV100. In the case of eutectoid steel, however, a much smaller range was observed (from HV271 to HV325). The net increase in hardness was less than HV55. The residual stresses of the two materials, on the other hand, exhibited very different behavior. The residual stresses of the eutectoid steel were much greater than those of S25C. At plastic deformation ratio of 9%, the residual stress for S25C was more than three times greater than that of eutectoid steel. These results suggest that the residual stress played a bigger role in eutectoid steel than that in S25C. Conversely, the work hardening contributed more in improving fatigue strength of S25C than that in eutectoid steel.

The above difference can be explained by the microstructure of the two materials.   S25C has higher volume ratio of ferrite than that of eutectoid steel. The soft ferrite is easily work hardened by cold rolling.   Eutectoid steel, on the other hand, is mainly composed of hard pearlite. The lamellar–like pearlite is difficult to be work hardened.   Based on the results of the residual stress and Vickers hardness, it may be concluded that for the carbon steel, the effect of residual stress increases with the increasing of carbon content. The effect of work hardening, on the other hand, decreases with the increasing of carbon content.

Table 3.6   Test results of S25C after cold rolling

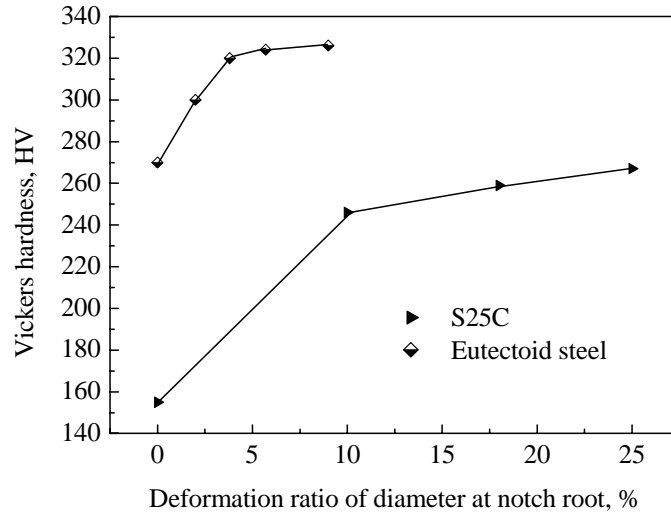|	ND	SS	D05	D10	D15
σ_w, MPa	170	210	370	320	325
σ_w*, %	100	124	218	188	191
Kt	1.51	-	1.51	1.51	1.51
σ_{RS}, MPa	-	-	-189	-238	-297
HV	155	-	246	259	267

Figure 3.13 Relationship of deformation ratio of diameter
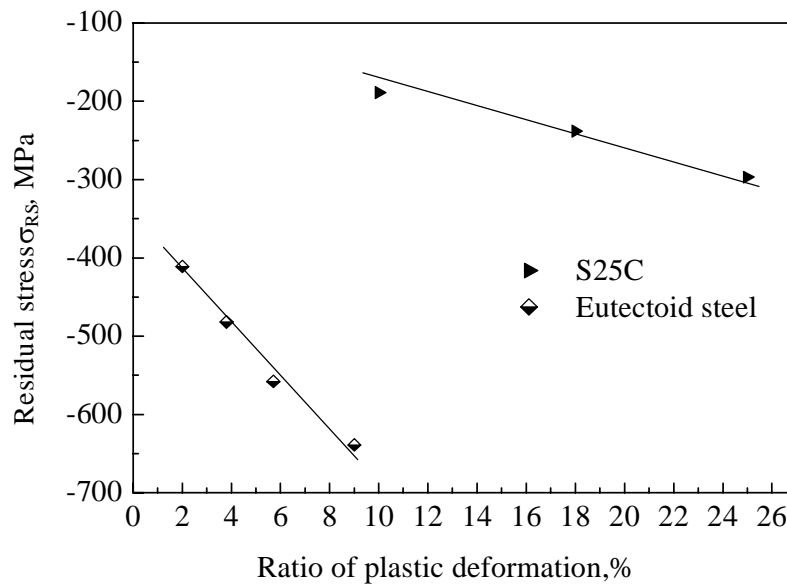and surface hardness at notch part.

Figure 3.14   Relationship of deformation ratio of diameter and
residual stress value at notch part.

3.4.2 Optimum Deformation Value

In practical engineering material, there is a limitation to the beneficial effect of cold working. There exists an optimum value by roller working for improving the fatigue strength. In order to ascertain the optimum deformation value in this test, R30 and R35 (deformation in diameter is 0.3 and 0.35mm is used in the fatigue test). The result of the fatigue test shows that fatigue limits of R30 and R35 are 530MPa and 500 MPa, respectively. The relationship of fatigue limit and deformation value is shown in Fig.3.15.

The reason for the optimum deformation value can be explained by residual stress and surface state. With the increase of deformation values, the plastic deformation layer will also increase. When compressive residual stress exists in the plastic deformation layer, tensile residual stress will be generated in the non-deformed area at the center of the specimen, to balance the stress distribution. Therefore, with the increase of the plastic deformation layer, the volume fraction of the non-deformed area will decrease and tensile stress will increase at the same time. With the increase of deformation value, the beneficial effect of cold work will saturate. The test results of the compressive stress of R30 and R35 were -637MPa and -600MPa. There was no obvious difference between R25 and R30.
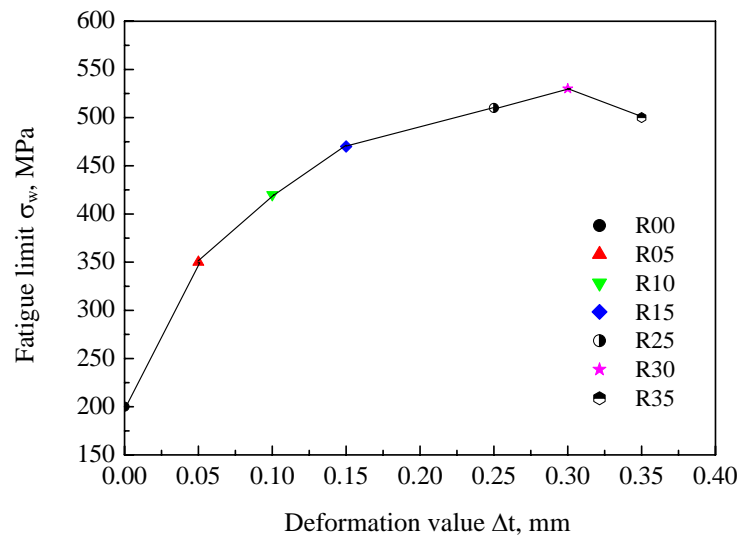

Figure 3.15   Relationship between fatigue limit of roller worked specimen
and plastic deformation value.

On the other hand, when an excessive amount of plastic deformation is given to the specimens, low cycles fatigue damage may be introduced. Therefore, the fatigue limit is lower than the optimum one. In this test, the ideal deformation value is 0.3*mm.* In other word, deformation ratio is about 10% for eutectoid steel.

3.4.3   Crack Propagation Rate and Depth of Non-propagating Crack

Figure 3.12 shows the fatigue crack propagation behavior for the three specimens, R00, R10 and R25, respectively.   Because of their significant differences in fatigue limits, equivalent stress amplitude was applied to these specimens. In other word, the applied load stress was 5MPa higher than its own fatigue limit value, respectively. It is clear that the fatigue crack in the cold rolled specimen occurred earlier and propagated much faster than that in the non-cold rolled one. However, at the same time, the fatigue limit of the former is much higher than that of the latter.

Figure 3.11 shows the surface fractures of the specimens with and without cold rolling. Fatigue cracks initiated from the surface on both types of specimens. For the specimen without cold rolling, the fatigue cracks initiated from one or two points and propagated to the opposite side of the surface.   For the cold rolled specimen, however, cracks initiated at many points around the circumference and propagated to the core of the specimen.

The above phenomena can be explained by the effect of cold rolling. Since the applied stress amplitudes of specimens with cold rolling were much higher (the applied stress of R25 was about 1.5 times higher than that of R00), this stress amplitude remarkably exceeded the stress amplitude that will result in the initiation of the fatigue crack. As a result, the crack of the cold rolled specimen initiated at many points and propagated faster than that in the non-cold rolled ones.

On the other hand, the cold rolled specimens also had greater resistance to delay the crack propagation into the core part. It is the compressive residual stress and fiberized microstructure that retarded the fatigue crack propagation into the interior region of the specimen, the fatigue limit of the cold rolled specimen was improved significantly, even if the crack in them initiated earlier and propagated faster in the former than that in the latter. The existence of non-propagating crack is another certificate for this explanation.
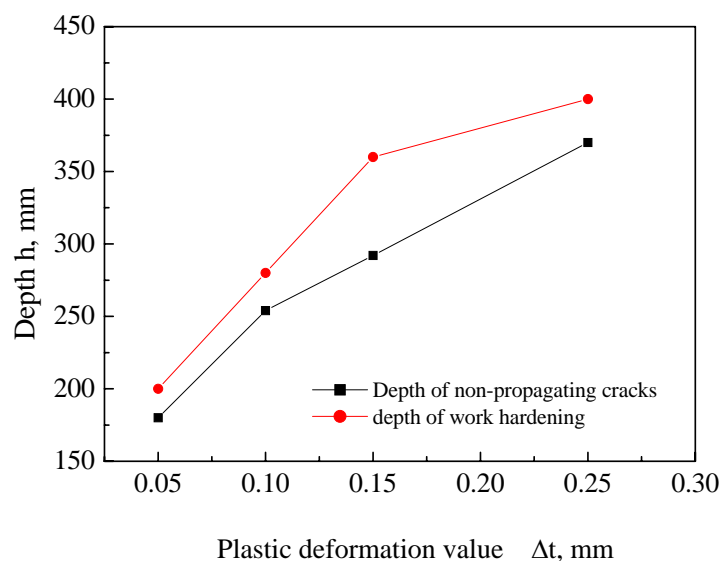
Figure 3.16   Relationship of deformation value, depth of non-propagating   crack
and work hardening.

In the fatigue test, non-propagating cracks were observed on the surfaces of all
cold rolled specimens. Fig.3.10 shows the relationship of deformation value, depths
of the non-propagation cracks and depths of work hardening layers, after the
specimens were applied their own fatigue limit stress and the number of cycles was
over 10^7 cycles, the depths of the cracks for R05, R10, R15 and R25 were 180μm,
254μm, 292μm and 370μm, respectively. However, the depths were smaller than the
work hardened layer shown in Figure 3.5. The values of them were 200, 280, 360
and 400μm respectively. In other word, the non-propagating cracks were within the
work hardened layer. On the other hand, no non-propagating crack was observed on
the surface of the specimen without cold rolling. The existence of non-propagating
crack on the cold rolled specimen may be attributed to the compressive residual
stress. In other words, it was the residual stress that determinate the propagation of
the fatigue crack, although it had no strong effect on the fatigue crack initiation [15].

A good understanding of the distribution of residual stress on the cross section
of the specimen can provide valuable insights into the relationship among the
non-propagating crack, applied stress and residual stress. Ideally, the distribution of
residual stress should be measured non-destructively with synchrotron or thermal
neutron method. The maximum test depth of this method can get to 85mm for Fe

[22]. On the other hand, the residual stress varies with the number of applied load cycles, fatigue crack's initiation and propagation. It is almost impossible to quantify the relationship among the applied stress, residual stress and depth of non-propagating crack.

Assuming there is no obvious variation of residual stress value from the surface of notch root to the depth where the non-propagation crack terminated, and the initiation and propagation of fatigue crack have no great effect to the existed residual stress field. The following equation may be used to explain why the depth of non-propagating crack increases with the plastic deformation value:

$$K_{th} = \Phi \sigma_a \sqrt{\pi l} \qquad \text{or} \qquad \sqrt{\pi l} = \frac{K_{th}}{\Phi \sigma_a} \qquad\qquad (3.6)$$

Where K_{th} is the threshold stress intensity factor of the fatigue crack,

Φ is a modified factor that is decided by the shape, dimension of the specimen and the way the stress is applied,

σ_a is the stress amplitude applied to the specimen;

l is the depth of the non-propagation crack.

Under the given test conditions, K_{th} and Φ are constant. Therefore, the crack depth l is only related to σ_a and it increases with the decreases of σ_a. During the fatigue test, when the load was applied to the cold rolled specimen, the practical symmetrical stress amplitude was changed. The tensile stress amplitude was decreased and the compressive stress amplitude was increased due to the compressive residual stress. However, the compressive stress resisted the crack propagation, only the tensile stress amplitude was effective for crack propagation. In this test, with the increase of cold rolled values, the compressive residual stress increased lineally and the absolute value increase in the residual stress is larger than that in applied stress, as shown in Fig.3.3 and Fig.3.7. In other word, it may be concluded that the effective tensile stress decreased with the increase of cold rolling value. Therefore the depth of non-propagation cracks increased with increasing the cold rolled value.

3.5   Conclusions

The main results obtained in the present study are as follows:

1). Cold rolling is an effective method for improving the fatigue strength of notched eutectoid steel. After cold rolling, the fatigue limits of specimens increased from 175% to 265%.

2). Compressive residual stresses, work hardening and fiberized microstructure are the three main factors for the improvement of fatigue properties. The residual stress is the most effective factor in improving the fatigue limit.

3). Non-propagating cracks are found at the notch bottom surfaces of all three cold rolled specimens, and the depths of these cracks increase with the increasing of plastic deformation value.

4). There is a limitation to the beneficial effect of cold working since an excessive amount of plastic deformation will introduce low cycles fatigue damage, and the beneficial effect of cold work will saturate. The optimum deformation value in which the fatigue limit is the highest is R30.

References

[1] Material Science Society of Japan: *Surface Treatment in Material,* Tokyo: Shokabo,1996.(in Japanese)

[2] X. D. Peng, A. Kharlov, V. Bystriski, E. Garate and E. J. Lavernia, "Characteristics of Material Surface Modified Using Plasma-Enhanced Ion Beams", *Mater. Sci. Eng.*, A251(1998), pp.142-149.

[3] Material Science Society of Japan, *Handbook of Fatigue Design*, Tokyo: Yogento, 1995 (in Japanse).

[4] K. Shiozawa, "Effect of Coating Thin Film on Fatigue Strength of Material", *Proceedings of the 7th Inter. Fatigue Congress, Beijing, 3*(1999), pp.1913-1920.

[5] K. J. Kang, J. H. Song and Y. Y. Earmme, "Fatigue Crack Growth Fatigue Behavior through a Compressive Residual Stress Field", *Fat. Fact. Eng. Mater. Struct.,* **13**(1990), pp.1-13.

[6] T. Hirsch, H. Wohfahrt and E. Marcherauch, "Fatigue Strength of Case Hardened Shot Peening Gears", *Proc. Third Int. Conf. on Shot Peening*, (1987), pp.547-560.

[7] Y. M. Chen and R. Z. Wang, "Investigation on the Effect of Shot Peening on the Elevated Temperature Fatigue Behavior of Superalloy", *Proc. Third Int. Conf. on Shot Peening,* (1987), pp.253-260.

[8] R. Z. Wang, X. B. Li and H. Wu, "Relationship between Shot Peening Surface Strain Layer and the Fatigue Strength of High –Strength   Alumimun Alloy", *Proc. Third Int. Conf. on Shot Peening,* (1987), pp.417-422.

[9] S. Wang, Y. Li, M. Yao and R. Wang, "Fatigue Limits of Shot-Peened materials", *J. Mater. Process.Tech.*,73(1998), pp.57-63.

[10] S. Wang, Y. Li, M. Yao and R. Wang, "Compressive Residual Stress Introduced by Shot Peening", *J. Mater. Process.Tech.*,73(1998), pp.64-73.

[11] K. Masaki, Y. Ochi and A. Ishii, "Fatigue Properties of Hard Shot-Peened SUS316L",*Mater. Sci. Resear. Inter.*,14(1998), pp.200-205.

[12] P. Peyre, R. Fabbro, P. Merrien and H. P. Lieurade, "Laser Shock Peening of Aluminum Alloys. Application to High Cycle Fatigue Behavior", *Mater. Sci. Eng.*, A210(1996),pp.102-113.

[13] L. Bertini, and V. Fontanari,"Fatigue Behavior of Induction Hardended Notched Component", *Inter. J. Fatigue*,21(1999),pp.661-667.

[14] W. Moller, S. Parascandola, T. Telbizova, R. Gunael and E. Richter, "Surface Processes and Diffusion Mechanism of Ion Nitriding of Stainless Steel and Aluminum", *Surf. Coat. Technol.*, 136(2001),pp.73-79.

[15] P.J. Haagensen,"Residual Stress Technique for Fatigue Life Improvement", *Proceedings of the 8th Inter. Fatigue Congress*, Sweden, **1**(2002), pp.1-114.

[16] S. Nishida, *Failure Analysis in Engineering Application*, Butterworth Heinemann Ltd., 1992, pp1-5.

[17] Sun .W. X. Nishida. S. and Hattori N: " Fatigue Properties of Pre-strained eutectoid steel: *Mater. Sci. Resear.Int***. 2003.9(3).pp.210-215.

[18] Ding J, Nishida S, Hattori N, Zhang D and Sun W X: Application of roller-working on improving the fatigue strength of notched austenitic stainless steel. *Proceeding of The Fifth International Conference on Fracture and Strength of Solid. 2003,* pp.189.

[19] Wang S W, Nishida S, Hattori N, Tamasaki H, Nakamura N: Improvement of fatigue strength of notched specimen by roller working. *J Soc.Mech.Eng*. Japan. Series A 64 (1998).156-161.

[20] C.S. Barrett, and T.B. Massalski: *Structure of Metals: crystallographic Methods, Principles and Data,* New York: McGraw-Hill Inc.,1996.

[21] Urashima C and Nishida S. Fatigue crack initiation and behavior and fracture surface of eutectoid steel. J. *Soc. Mat. Sci*; Japan. 1993: 43: 515-521.

[22] Tanaka K T. Diffraction measurements of residual micro and macro stresses. ATEM'03: *Proceeding of international conference on advanced technology in experimental mechanics 2003.* Sep.10-12, Nagoya,Japan.

Chapter 4

Effect of Ion-nitriding on

Fatigue Properties of Eutectoid Steel

4.1 Introduction

Ion-nitriding, also known as plasma nitriding, is one of the most widely used thermal-chemical methods to improve the mechanical properties of traditional and new materials. This treatment produces strong and shallow case with high compressive residual stresses on the surface of steel components such as gears, crankshafts, dies and tools [1-2]. Ion-nitriding process is being preferred recently in most surface hardening application of machine parts, to the conventional techniques such as gas or liquid nitriding, because the process has the characteristics of faster nitrogen penetration, simplicity in application, cleanliness and low cost, as well as its ease of control of the compound and diffusion layer formation. The requirement of lower process temperature, shorter process period and suppressed compound layer formation are reported to be the other advantage of ion nitriding [2]. The ion-nitriding process has been described in earlier reports [3-5], and some mechanisms for the penetration of nitrogen have been proposed: bombardment of NH^+ and NH_2^+ ion [3], thermodynamic diffusion, and gas absorption. However, there is still some disagreement with respect to the role of nitrogen during nitriding process [6,7]. A discussion on mechanisms and identification of nitrogen reactant species has been given by Michel et.al [8].

The prior investigations on nitrided steels have revealed that fatigue limit increase with increasing case depth of nitrided layers, emphasizing the effectiveness of case depth or case area in the cross section of specimen by the use of dimensionless parameter defining relative case depth [9-12]. Some models predicting the fatigue strength of nitrided steels have been proposed by relating the strength and residual stress distribution in the cross-section of specimen. It has been reported that the increase in fatigue strength by ion nitriding was roughly 25% higher than conventional gas nitriding [3]. It has also been documented the subsurface crack

formation is the dominant failure initiation mechanism in the conventional one [13], and the ion nitrided steel excluding low cycle fatigue regime [9, 14-16]. It has been reported that the increase in fatigue performance of notched specimen is higher than that of the smooth specimen, due to the geometry of the former [17]. However, the effect of nitriding on fatigue properties of eutectoid steel is still not well understood, let alone the attempt to evaluate the effect of treatment condition and stress concentration on it. The objectives of this part are to: (1) evaluate the effect of ion-nitriding on fatigue properties of eutectoid steel with smooth and notched specimens; (2) investigate the influence of temperature on practical performance and (3) fatigue characteristic of eutectoid steel under nitriding treatment.

The schematic representation of ion nitriding equipment is given in Fig.4.1. The stainless steel was employed as the anode, while the fatigue specimens were cathode. The ratio of the gas mixture of N2:H2: Xe: Ar is 4:1:2:1 and the pressure is 200 Torr. The ion nitriding temperatures are 550°C and 500° C and the process is showed in Fig.4.2.
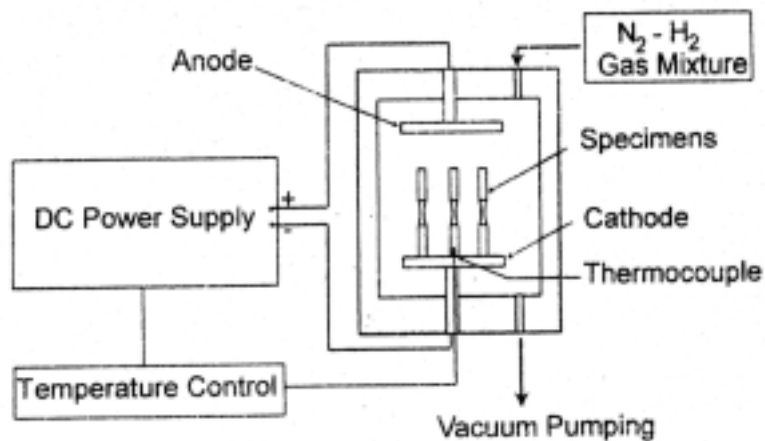
Figure 4.1   Schematic illustration of ion nitriding equipment.
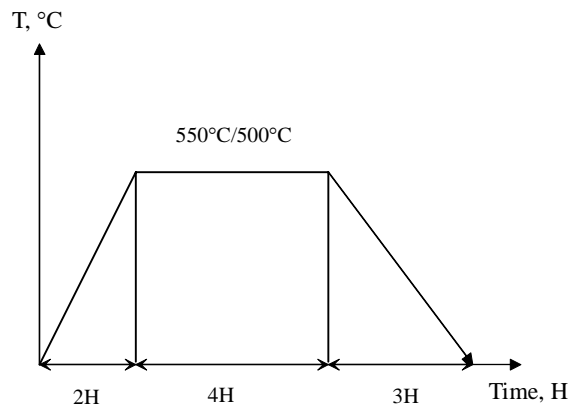
Figure 4.2   The process of ion nitriding treatment.

4.2 Material and Method

4.2.1 Material and Experimental Procedure

Table 4.1 lists symbol and temperature of ion-nitriding treatment. Three kinds of specimens, denoted as (S1, N1), S1* and (S2, N2) are smooth and notched specimens treated at 550°C and 500°C, respectively. Table 4.2 and 4.3 list the chemical composition and mechanical properties of the test material. Tensile specimens, smooth specimens and notched specimens were used for fatigue test in the study. Figs 4.3-4.5 show the shape and dimensions of specimen for tension, smooth and notched one for fatigue test, respectively. Specimens were firstly polished with emery paper (#400-#3000) and then with diamond paste (the grain size from $0.1 \mu m$ to $0.03 \mu m$). After that the specimens were annealed at 520°C for 30 minute in a vacuum furnace to relieve the residual stress. Finally, they were nitrided on two temperature level 550°C (S1, S1* and N1) and 500°C (S2 and N2).

The tensile test was performed with a universal testing machine. The fatigue test was performed with an Ono type of rotating and bending machine (14.7Nm, 3000rpm) under the stress ratio of $\sigma_{max}/\sigma_{min}= -1$.   A scanning electron microscope (SEM) was employed to investigate the initiation and propagation behavior of the fatigue crack by observing the fracture surfaces. Hardness was tested with a Vickers hardness tester. Replicated samples were successively taken to monitor the crack initiation and propagation behavior in the tensile and fatigue test.

77

Table 4. 1   Symbol and temperature of ion-nitriding treatment.

Symbol	Temperature, °C	Depth of Compound Layer, µm
S1, N1	550	17-20
S1*	550	8-10
S2, N2	500	17-20

Table 4.2   Chemical composition, mass%

C	Si	Mn	P	S
0.73	0.27	0.75	0.018	0.014

Table 4.3   Mechanical properties

$\sigma_{0.2,}$MPa	σ_{B},MPa	RA, %	EL, %
527	918	26.8	11.4

$\sigma_{0.2,}$:   Yield stress, σ_{B} : Ultimate strength

RA: Reduction of area,   EL: Elongation ratio
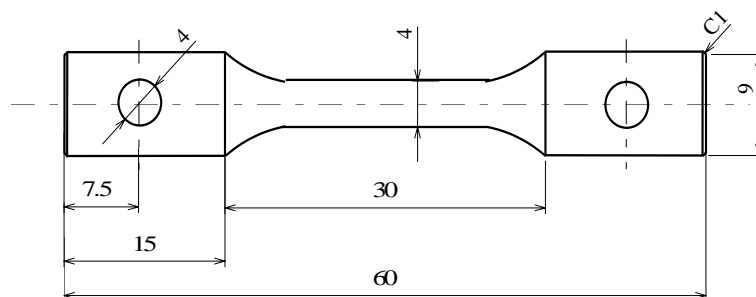
Figure 4.3   Shape and dimensions of the specimen for tensile test.
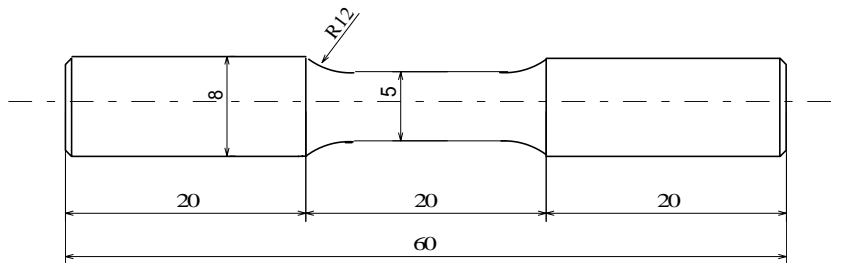
Figure 4.4 Shape and dimensions of smooth specimen for fatigue test.
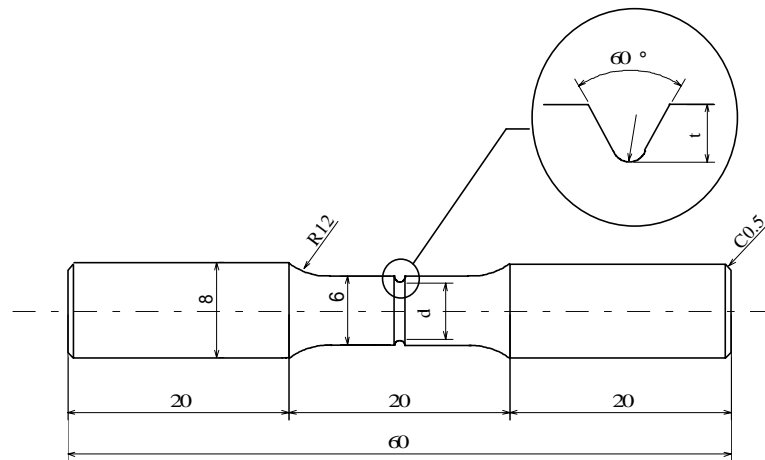
d = 5mm,   t = 0.5mm, ρ = 1mm

Figure 4.5 Shape and dimensions of notched specimen for fatigue test.

Table 4.4   X-ray diffraction analysis condition

Characteristic X-ray	Cr
Tube voltage, KV	40
Tube current, $A \cdot m^{-3}$	300
Irradiated area	$\phi 0.1$

4.2.2 Residual Stress Measurement

The residual stresses introduced by nitriding treatment were measured by X-ray diffraction method (SHIMADZU *X-ray stress measurement equipment DX-10*). The X-ray diffraction conditions for measurement of residual stress are listed in Table 4.4.

4.2.3 EPMA analysis

In order to clarify the composition of the surface compound layer and its depth, EMPA (JXA-8900) was used to measure the ion-nitrided specimens. The voltage used in this test was 15KV and the current was 2×10^{-8}A.

4.3 Experiment Results and Discussion

4.3.1 Tensile test

Table 4.5 lists the mechanical properties of eutectoid steels before and after nitriding. The change of microstructure of the surface layers improves the properties of fatigue resistance and surface hardness. The compound layer provides the material with good physical properties against wear and corrosion. However, after nitriding, the mechanical properties of this material become deteriorate in tensile strength, yield stress, elongation ratio and reduction of area.

In order to investigate the reason for this appearance, replica samples were taken successively to monitor the surface variation during the tensile test, as shown in Figure 4.6. It is clear the circle crack was generated in the surface of the specimen. It is the brittle compound layer that resulted in the crack in the tensile test and that weakened the main mechanical properties.

4.3.2 Surface Microstructure and EMPA Analysis.

Figure 4.7 shows the surface microstructures of the specimen before and after ion-nitriding. Comparing the surface of the two kinds of specimens, the grain sizes of the treated samples are greatly refined. It is well known that the refined grain is very effective in resisting the initiation of the crack and in improving the fatigue strength. Based on the results of EMPA, two kinds of ion-nitrided specimens consisted of Fe_3N compound and the depth of compound layer is about 20μm. The results are shown in Figure 4.8. The depth of smooth and notched specimen is similar. This indicates that the ion-nitriding treatment temperature has no great effect on the depth of compound layer. However, the case depth is different between the smooth and notched specimens.   Fig.4.8 (a) is the Fe and N distribution in *N2* taken by X-ray and (b) is that of *S2*. The detail information about this test is listed in the following pages.

Table 4.5 Mechanical properties of eutectoid steel before and after nitriding treatment

	$\sigma_{0.2}$	σ_B	EL	RA
Ion-Nitriding Ⅰ	180 MPa	747 MPa	< 5%	< 3%
Ion-Nitriding Ⅱ	171 MPa	654 MPa	< 5%	< 3%
Non-Nitriding	527 MPa	918 MPa	11.4%	26.8%

$\varepsilon_p = 0\%$ $\varepsilon_p = 1.5\%$

Ion-nitriding 550°C

$\varepsilon_p = 0\%$ $\varepsilon_p = 1.5\%$

Ion-nitriding (500°C)

——— 200µm,   ↕   Tensile direction
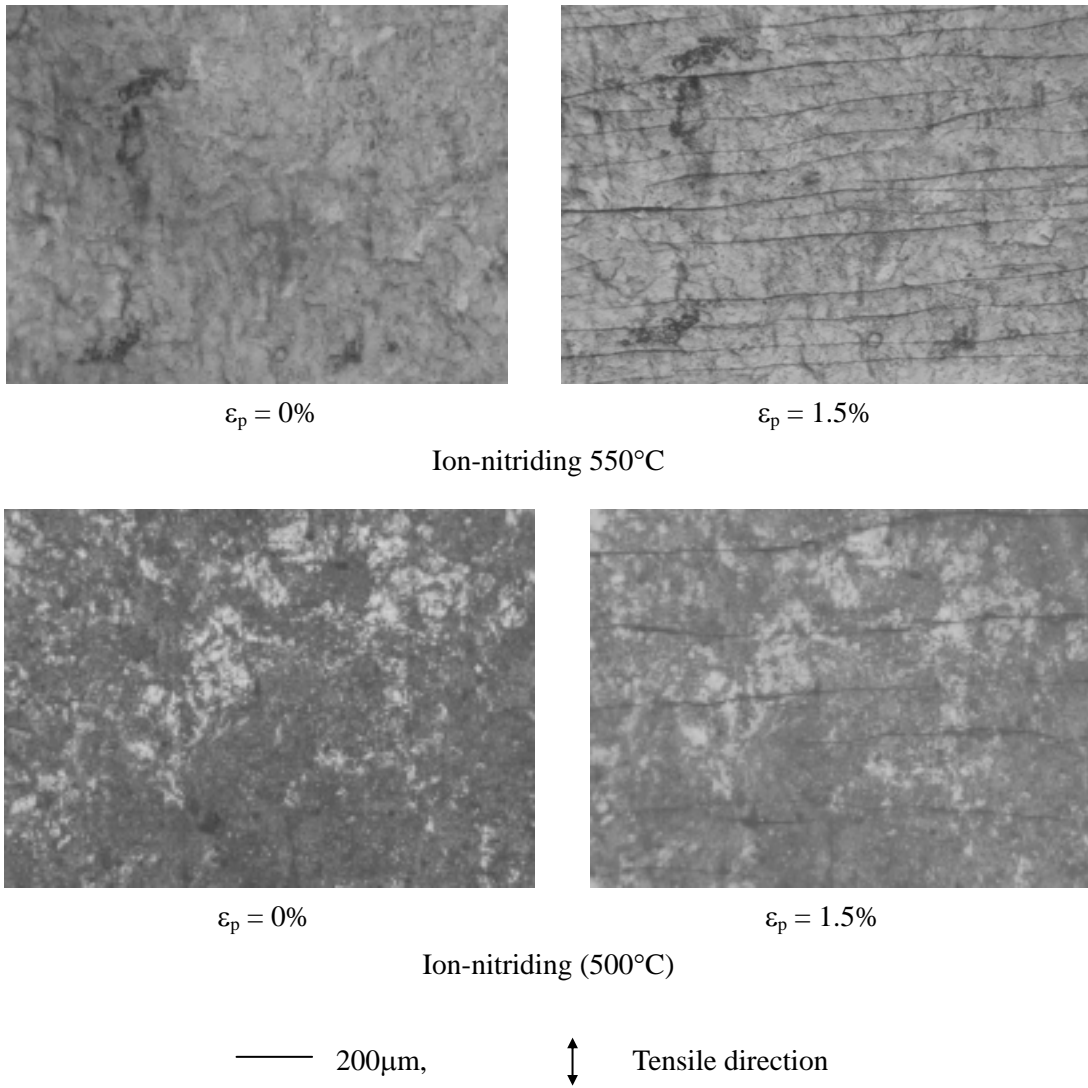
Figure 4.6   Surface observation in tensile test.

(a)   (b)
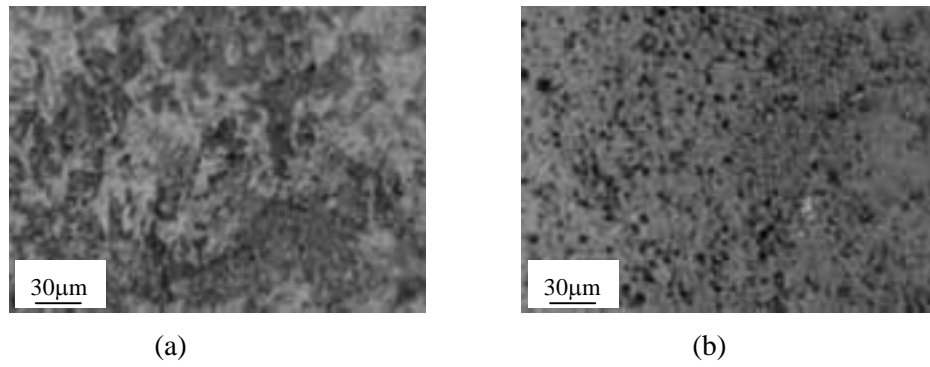
Figure 4.7   Surface observations before (a) and after (b) ion nitriding treatment.

Fe-X ray, N2   Fe-X ray, S2

(a)   (b)

N-X ray, N2   N-X ray, S2

(a)   (b)
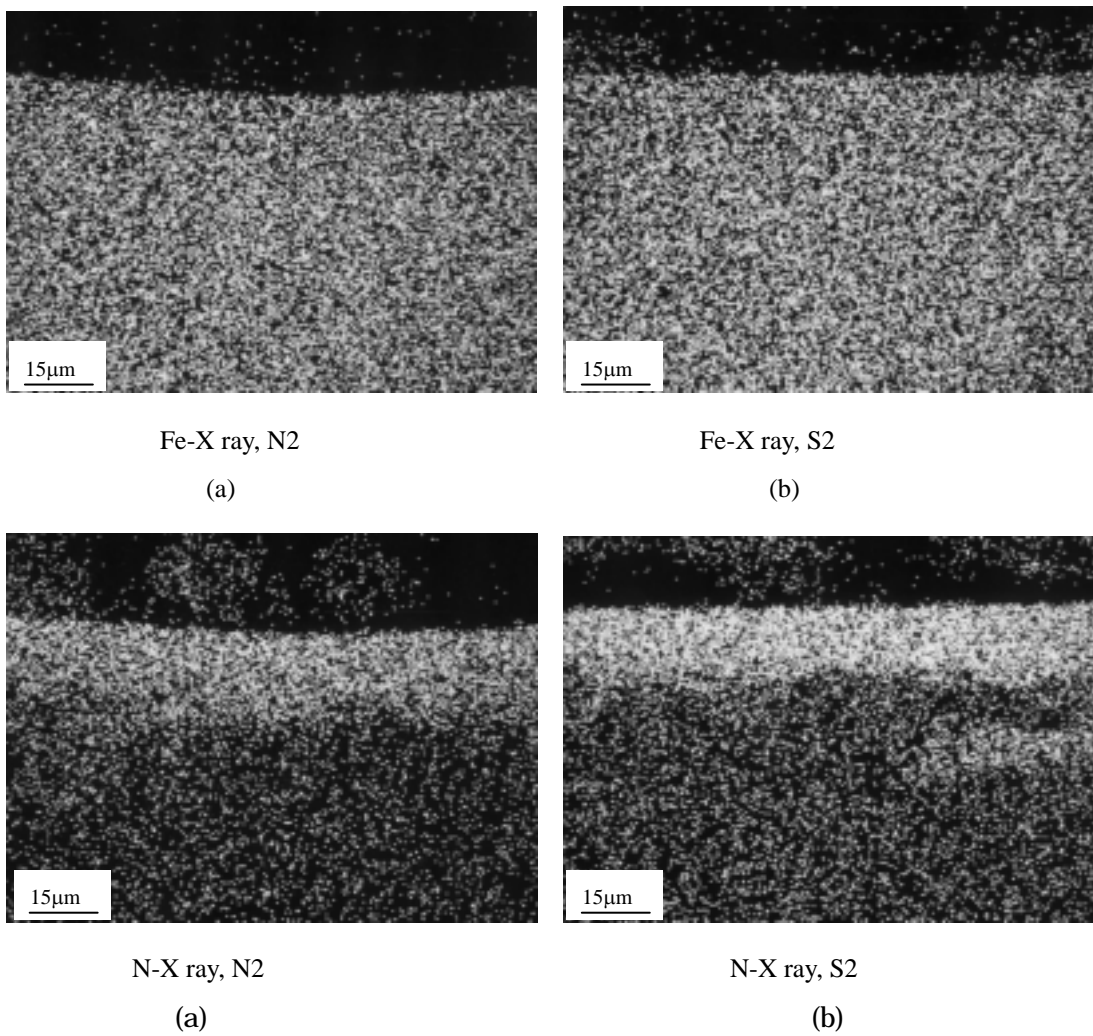
Figure 4.8   EMPA analysis result.

Test Results of EMPA

Material: Ion nitrided eutectoid steel   **Code: S2**

Stage: X= 24.0510 , Y=38.3085, Z= 10.7065

Acc. Voltage: 15.0(KV)   Probe Dia.: 5   Scan: off

Dated on Apr 28 01:41 2004

WPS only   No. of accumulation: 1

Curr.(A): 2.020E-08

Element	Peak, mm	Net, cps	Bg-, cps	Bg+, cps	S.D., %
1 Fe	191.071	320.1	0.0	0.0	12.50
2 N	146.937	267.9	0.0	0.0	13.74
3 Mn	145.684	144.5	5.0	5.0	19.61

ZAF Metal

Element	Wt.%	Atom, %	K, %	ZAF	Z	A	F
Fe	91.503	74.5969	97.353	1.1008	1.0175	1.0819	1.0000
N	7.583	24.6449	5.037	1.7634	0.8411	2.0966	1.0000
Mn	0.914	0.7581	1.031	1.0397	1.0383	1.0014	1.0000
Total	100.000	100.0000	103.420	Iteration =6			

Material: Ion nitrided eutectoid steel   **Code: N2**

Stage No.1   Position mm   X= 64.7515 , Y=36.2230, Z= 10.7065

Acc. Voltage: 15.0(KV)   Probe Dia.: 5   Scan: off

Dated on Apr 28 00:07   2004

A- Rank: C   N   Si   Mn   Fe   Cu

B- Rank: O Cr

Measurement Condition

WDS elements

Element	X-ray	Crystal	CH	Acc.v	Peak Pos	(Angstrom)	Bg_L	BG_U ,mm
1 N	Ka	LDE1H	(1)	15.0	146.587	31.60000	11.850	23.600
2 Si	Ka	TAP	(2)	15.0	77.321	7.12542	3.300	1.450
3 Mn	Ka	LIFH	(3)	15.0	146.084	2.10182	3.250	2.950
4 Fe	Ka	LIFH	(3)	15.0	134.334	1.93604	2.450	3.850
5 Cu	Ka	LIFH	(3)	15.0	106.484	1.54056	2.750	2.150

Curr. (A): 2.00E-08

Element	Peak, mm	Net, cps	Bg-, cps	Bg+, cps	S.D. ,%
1 N	146.587	241.7	5.0	0.0	14.55
2 Si	77.321	143.5	15.0	10.0	19.79
3 Mn	146.084	165.3	10.0	0.0	17.76
4 Fe	134.334	13758.7	35.0	15.0	1.91
5 Cu	106.484	207.9	45.0	40.0	17.72

ZAF Metal

Element	Wt.,%	Atom, %	K, %	ZAF	Z	A	F
N	8.710	25.059	4.587	1.7810	0.8415	2.1165	1.0000
Si	0.408	0.6246	0.276	1.4788	0.9075	1.6328	1.0000
Mn	1.237	0.9676	1.190	1.0396	1.0388	1.0015	0.9993
Fe	93.842	72.1932	92.214	1.0175	1.0193	0.9993	0.9988
Cu	1.708	1.1550	1.552	1.1002	1.0546	1.0433	1.0000

Total   105.347   100.0000   99.819   Iteration = 4

4.3.3 Hardness

The distribution of hardness from the surface of the specimen to its interior is shown in Fig. 4.9-10. The surface parts were obtained by stepwise removing the material by careful electro polishing. At the same time, the cross sections of the specimen were used to measure the hardness distribution from the surface to the interior region. The depth of compound layer is about 20μm for all of the nitrided specimens. However, the case depth (base hardness +30HV) of the smooth specimen is greater than that of the notched one. For smooth specimen, the case depth is about 500μm, whereas the corresponding value of notched specimens is about 400μm, indicating that the smooth ion-nitrided specimens have a more extended diffusion zone than the notched ones. The detailed information can be seen from the Fig.4.9 (a) and (b). The increase in hardness may be explained by the formation of iron nitrided precipitates in the nitrided layer. At the same time, two specimens in the interior region were tested. The results showed that the specimen under 550°C nitrided was softened in the middle. And the value in hardness is bout 250HV corresponding to 270HV, the average hardness of the non-treatment ones. The reason for this phenomenon may be attributed to the fact that the material became soft and tempered at a high temperature and time [18].

According to the test results, surface hardness of S2 (813HV) is higher than that of S1 (724HV). In other words, the surface hardness of the specimen treated at 500°C is higher than that at 550°C.   This can be explained by the temperature dependence of the dispersion hardening of the nitrided precipitates within the matrix. Precipitate with a certain size and number is the most effective in obstructing the movement of dislocation and producing the maximum strengthening and hardness. At a higher nitriding temperature (550°C), the precipitate particles are larger in size and more prone to coarsening, leading to a lower precipitate density and hence lower hardness [18].
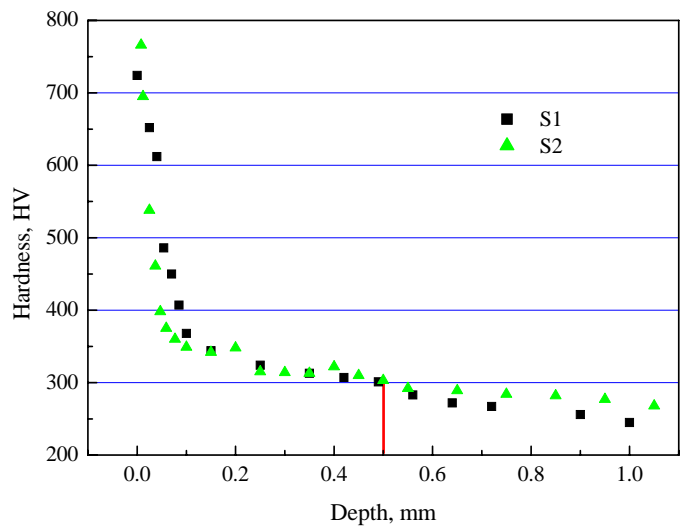
(a)   Smooth specimens.
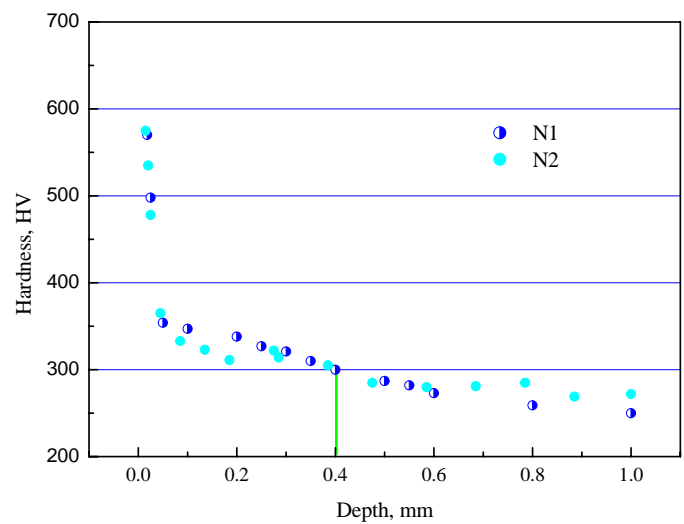
(b)   Notched specimens.

Figure 4.9   Hardness distribution patterns from specimen's surface
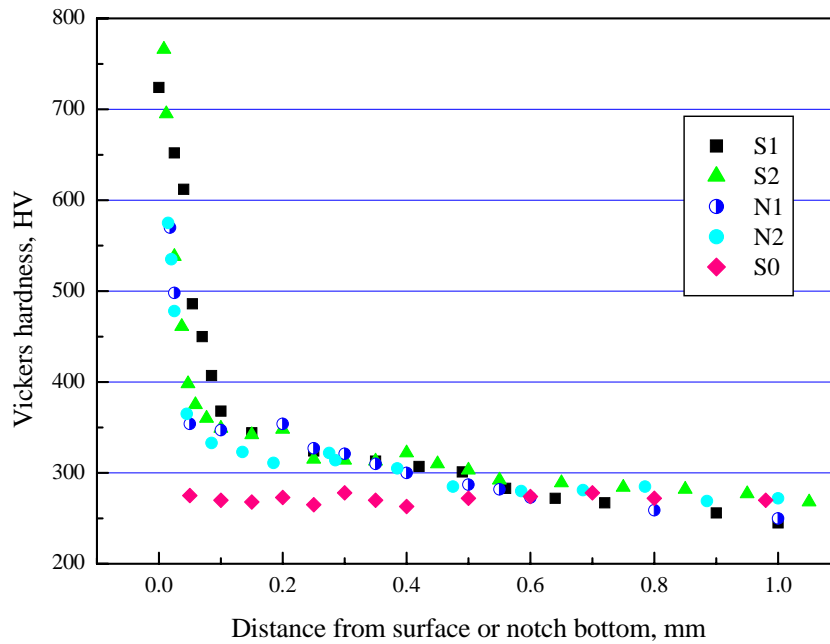
Figure 4.10   Hardness distribution of eutectoid steel.

Table 4.5 Residual stresses after ion nitriding

	S0	S1[*]	S1	S2	N0	N1	N2
$\sigma_{RS,}$ MPa	-	-472	-460	-412	-	-459	-417

4.3.4 Residual Stress

The major changes produced by ion nitriding occurred in the vicinity of the outer surface as the compound layer and diffusion layer are formed. These changes result in an increase of strength and generation of high compressive residual stress in the nitrided layer and balancing tensile stresses in the core. The increased strength is related to the formation of iron nitrided precipitates in the nitrided layer. Residual stresses originate from a nitrogen concentration gradient, formation of nitrided precipitates in the diffusion zone during the nitriding and cooling process, and also from the interaction between the compound layer and the metal matrix [19]. Kreft et al. [20] conducted in-situ measurements of residual stresses during nitriding and

cooling and found that due to a thermal misfit by different thermal expansion coefficient between compound layer and steel substrate, compressive residual stresses in the compound layer increased during cooling and the compressive residual stresses in the diffusion zone decreased. The test results of the residual stress are listed in Table 4.5.

4.3.5 Fatigue Strength

Ion nitriding Ι (550°C)

It is reported that fatigue limits increase with increasing case depth and the thickness of compound layer has no dominant influence on the fatigue characteristics. In order to verify the effect of compound layer, one half of it (about 7-10μm) is removed by electronic polishing, and this specimen is labeled as S1*. Figure 4.11 shows the S-N curves of the eutectoid steel after ion-nitriding treatment at 550°C. According to the figure, the fatigue strengths of all specimens are enhanced significantly after cold rolling. For N0, N1, S0, S1 and S1*, the fatigue limits are 200MPa, 320MPa, 285MPa, 490MPa and 460MPa, respectively. Compared to the smooth specimen with the same size (S0), the fatigue strength of S1 improved by 72%. Compared to the non-nitrided notched specimen, the fatigue limit of nitrided notched specimen (N1) is increased to 320Mpa, an increase in fatigue limit ratio by 60%. Also, its stress amplitude is higher than that of the smooth specimen (S0). The fatigue strength of S1* is affected little by the thickness of compound layer and decreases with decreasing the layer depth.

Ion-nitriding Π (500°C)

The S-N curves of the test material after nitriding at 500°C are showed in Figure4.12. Like the ion-nitriding at 550°C, the fatigue limit of the smooth and notched ones had significant improvement. The fatigue limit of S2, N2, S0 and N0 is 535, 330, 285 and 200 MPa. For the ion-nitrided specimen, the fatigue strength of the smooth and notched one increased to 188% and 165%. The net increase in fatigue strength is higher than that ion-nitrided at 550°C. Ion nitriding treatment at 500°C is more effective in improving the fatigue strength than a higher temperature.
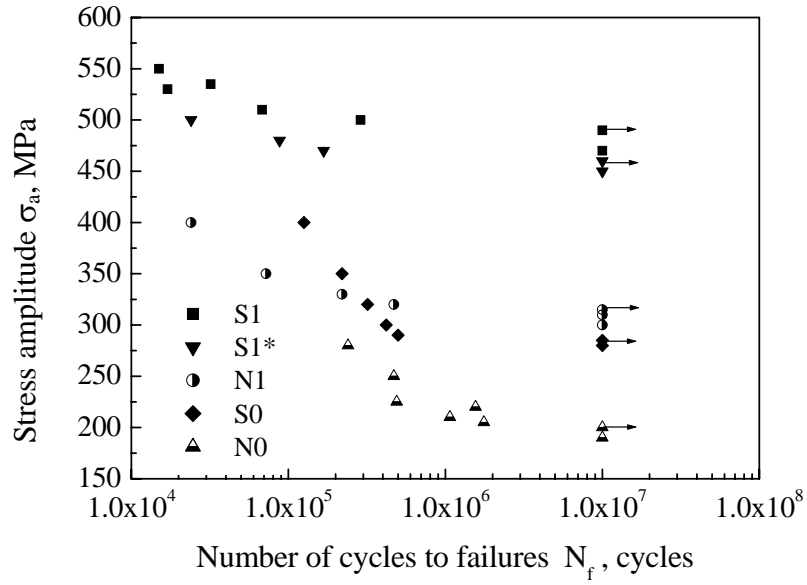
Figure 4.11   S-N curve of eutectoid steel after ion nitriding (550°C).
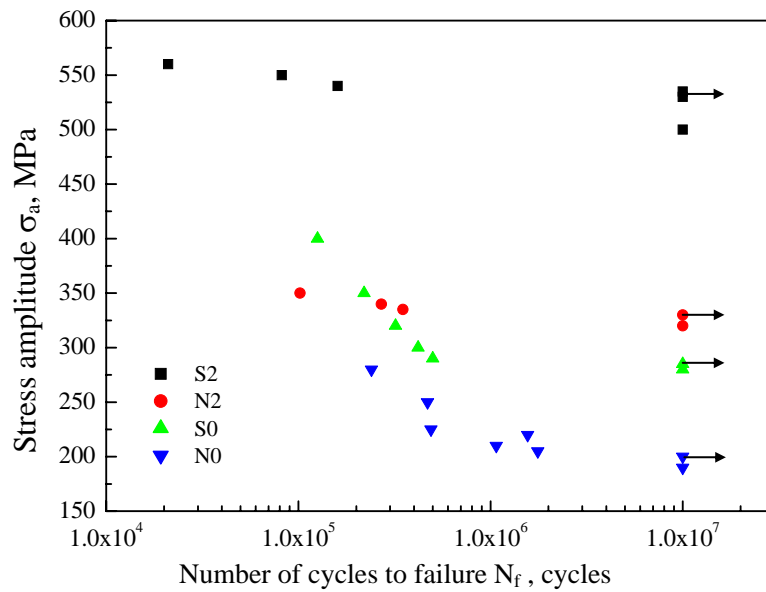
Figure 4.12   S-N curves of eutectoid steel after ion-nitriding treatment (500°C).

Figure 4.13 shows the S-N curves of eutectoid steels under two ion-nitriding conditions. In general, the fatigue strength of nitrided specimens is much higher than that of non-nitrided one. Comparing the fatigue limit of the two pairs (S2 and S1, N2 and N1), the fatigue strength of the latter is a little higher than that of the former. That is, nitrided at 500°C is more suitable than that at 550°C in improving the fatigue limit. The detail reason for this appearance will be discussed in the following paragraphs.

4.3.6 Mechanisms of Fatigue Strength Improvement.

The mechanism for the improvement in fatigue strength after ion nitriding is related to the alteration of surface properties and case depth that produces compressive residual stress at surface. Table 4.6 summarizes the results from the hardness, residual stress, fatigue limit and ratio of fatigue strength. Fig.4.14 shows the relationship of fatigue limit and the ion nitriding temperature. The mechanism for the modification of fatigue strength can be explained in refined microstructure, surface hardening and deformation of case depth, and residual stress field induced by ion nitriding process.

Refined microstructure: Figure 4.7 shows the refined microstructure at the surface of the specimens. The refined structure may have prevented the crack initiation and resisted the propagation of fatigue crack into the interior region during the fatigue test. Consequently, fatigue strength is improved.

Surface hardening and deformation of case depth: After ion-nitriding, the hardness of S1 and S2 increased to HV724 and HV813. The surface hardness provides an improvement in the fatigue strength because the hard layer prevents plastic flow [21]. At the same time, the case depths of S1, S2, N1 and N2 were about 500μm, 500μm, 400μm and 400μm, respectively. In this region, the formation of precipitates can hinder dislocation motion and therefore slip band penetration through the nitrided layer. As a result, the fatigue strength is improved. The results showed the case depths in the two nitrided temperatures have no obvious difference. On the other hand, compared to the smooth specimen, the notched specimens have a small value in case depth. As it is well known, the increase in hardness directly improves the fatigue strength of the materials.

92

Residual Stress Field: The residual stress is another main factor that affects the fatigue strength. Under ion nitriding, a compressive residual stress is introduced to the substrate of the surface. In cyclic loading of machine components, the effective stress acting on the specimen is the main controlling parameter and it depends strongly on the applied and residual stress, which is extremely important for cyclic stressing in bending and /or torsion. In the fatigue test, parts of the applied stress may have been offset by the residual stress. Therefore, the fatigue strength is improved greatly. Fig.4.15 shows the relationship of residual stress and ion nitriding temperature. According to this figure, the absolute value of residual stress at a lower temperature is higher than that at a higher temperature.

Comparing the test results listed in Table 4.6 and the relationship shown in Figs. 4.14 and 4. 15, it is clear that the fatigue strength of the specimen treated at 500°C is higher than that treated at 550°C, both for smooth and notched specimen. Although the residual stress induced at higher temperature is a little higher than that at a lower one, the surface hardness of the former is much smaller than that in the latter. This may be a reason for a higher fatigue limit treated at 500°C than that at 550°C.
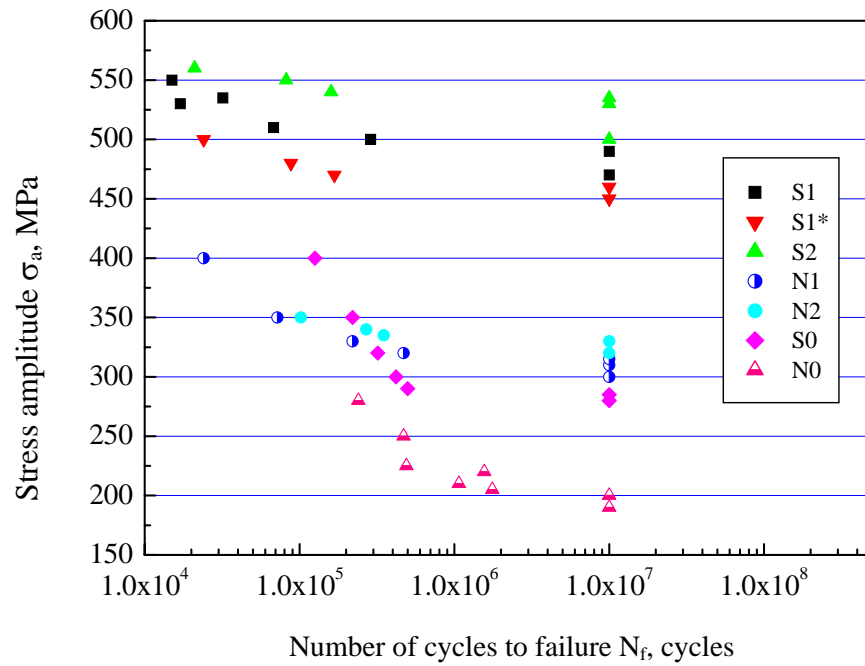
Figure 4.13　S-N curves of eutectoid steel after ion-nitriding treatment.

Table 4.7　Test results of eutectoid steel after ion nitriding treatment.

	S0	S1*	S1	S2	N0	N1	N2
σ_w, MPa	285	460	490	535	200	315	330
σ_w*	100	161	172	188	100	158	165
K_t	-	-	-		1.425	1.425	1.425
$\sigma_{RS,}$ MPa	-	-472	-460	-412	-	-459	-417
Surface Hardness, HV	271	652	724	813	-	-	-
Depth of Nitriding, μm	-	8-10	17-20	17-20		17-20	17-20
Case Depth, μm	-	500	500	500	-	400	400

σ_w*:　　Sx/ S$_0$ ×100% ;　　Nx/N$_0$ ×100%
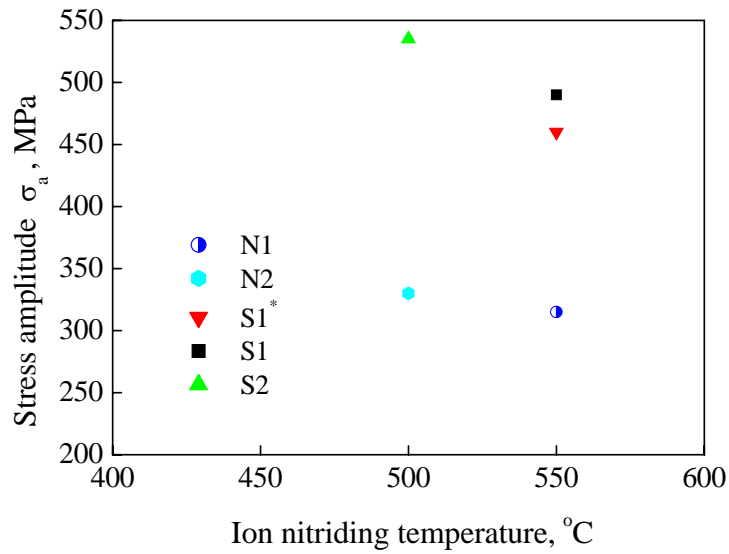
Figure 4.14   Relationship of fatigue limit and ion-nitriding temperature.
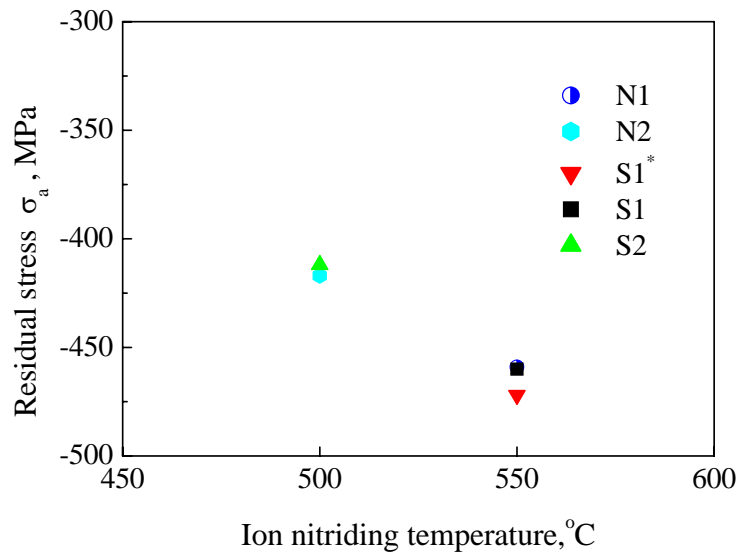
Figure 4.15   Relationship of residual stress and ion-nitriding temperature.

4.3.7 Fracture Surface

Figure 4.16 shows the fracture surfaces of S1*, S1and S2, respectively. It is clear that all of the fatigue cracks initiate in the surface of the specimen just like the non nitrided one. Fig.4.17 shows the fracture surfaces of the notched specimen after nitrided and cold rolling, respectively.

Comparing the fracture surface may shed some insight in better understanding the mechanisms for eutectoid steel under different surface treatments. For all of fracture surfaces, fatigue cracks initiated in the surfaces. The difference lies in the number of crack initiation and propagation behavior. The crack initiated at one or few points for non-treated and nitrided specimens and propagated into the opposite side of the surface; on the other hand, for cold rolled specimen, many cracks initiated around the circumference after cold rolling and propagated into the core of the specimen. This may suggest that different mechanisms were involved and resulted in the improvement of fatigue strength, though the result of the two methods were similar (The fatigue limits of eutectoid steel after nitriding and cold rolling are 490MPa and 510MPa). For cold rolled specimen, the net increase in hardness was no more than HV55. Residual stress plays the most important role in improving the fatigue strength among the residual stress, work hardening and variation of surface microstructure, though it has no strong influence to the crack initiation [22, 23]; since the applied stress was much higher than what triggers the crack initiation (the applied stress of cold rolled specimen was about 1.5 times higher than that of non-treated one), many crack generated in the specimen surface and propagated into the interior region. However, for ion nitrided specimen, the surface hardness increased about HV460, the hard and refined martensite phase strongly resisted the initiation of the crack and then improved the fatigue strength greatly. In other word, the relative significance of surface hardening in nitriding and cold rolling is much different. The surface hardening distributed more in the former than that in the latter and it greatly resisted the initiation of fatigue crack in the following test. Therefore, the crack initiated from only one or few points though the applied stress amplitude was similar to that of the cold rolled one.
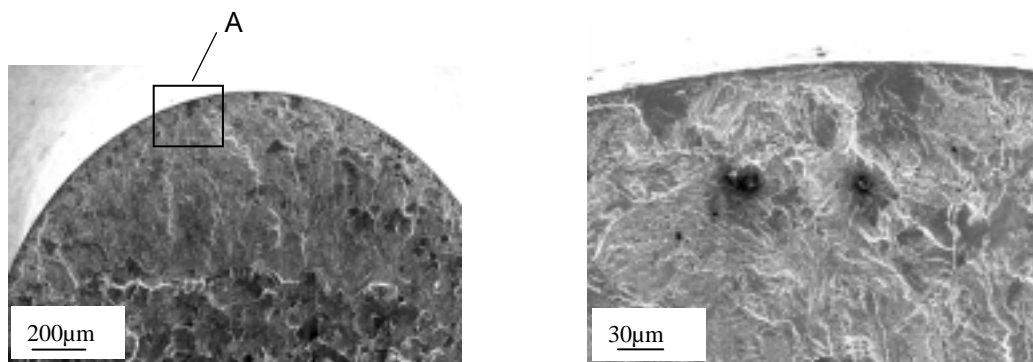
(a) Nitrided specimen (550°C) (b) Enlarged of A in (a)
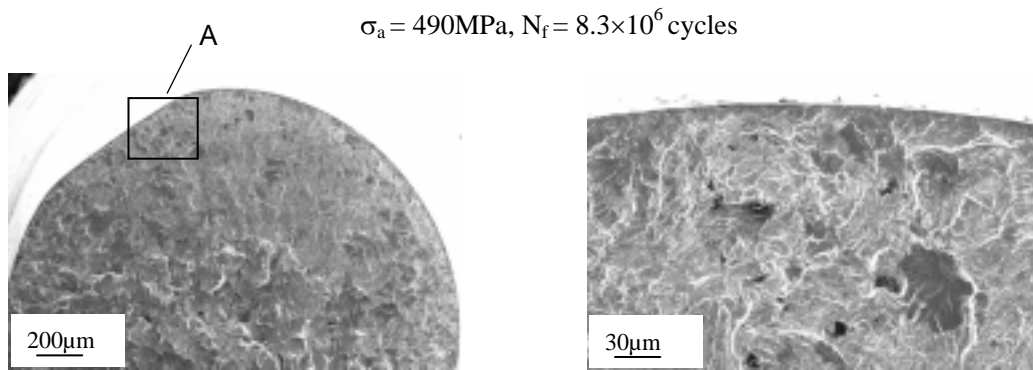
$\sigma_a = 490$MPa, $N_f = 8.3 \times 10^6$ cycles

(a) Nitrided specimen (550°C) (b) Enlarged of A in (a)

$\sigma_a = 540$MPa, $N_f = 1.0 \times 10^5$ cycles
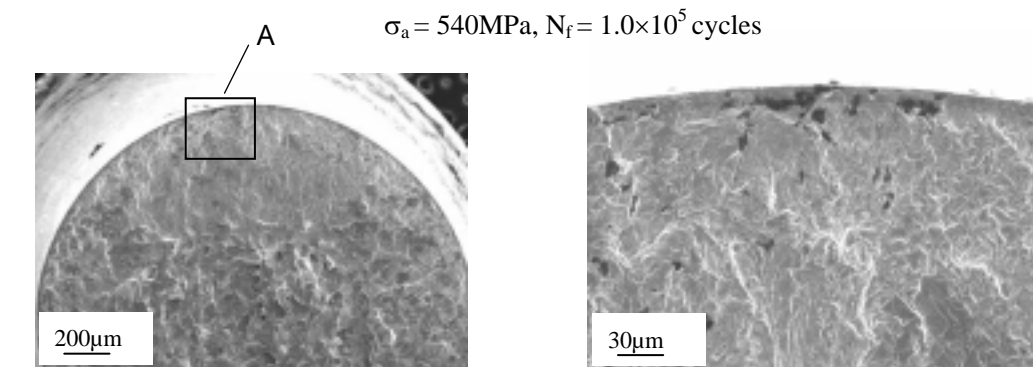
(a) Nitrided specimen (500°C) (b) Enlarged of A in (a)

$\sigma_a = 540$MPa, $N_f = 1.6 \times 10^5$ cycles

Figure 4.16 Fracture surfaces of smooth specimen after nitriding
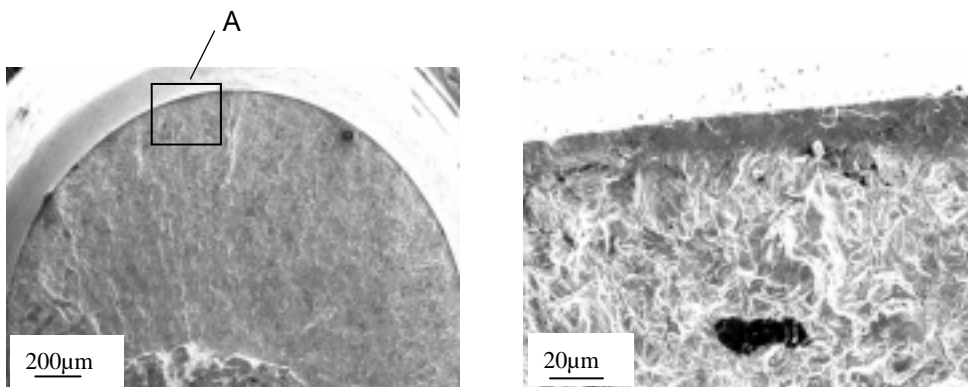
(a) Notched Nitrided specimen (550°C)   (b) Enlarged of A in (a)

$\sigma_a = 320$MPa, $N_f = 4.7 \times 10^5$ cycles
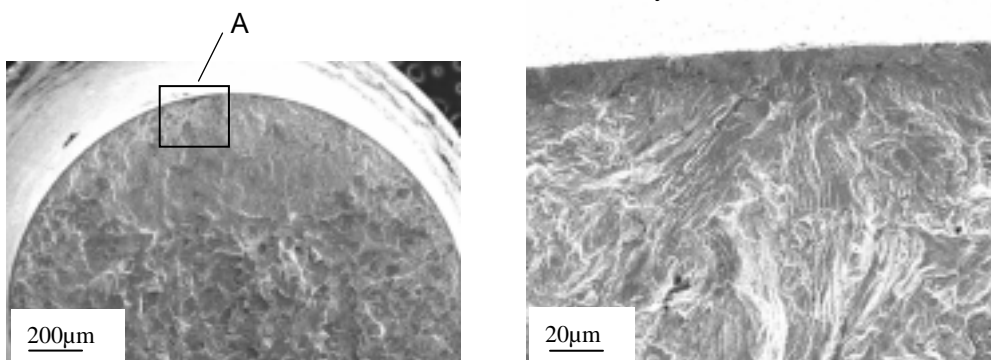
(a) Notched nitrided specimen (500°C)   (b) Enlarged of A in (a)

$\sigma_a = 335$MPa, $N_f = 3.5 \times 10^5$ cycles
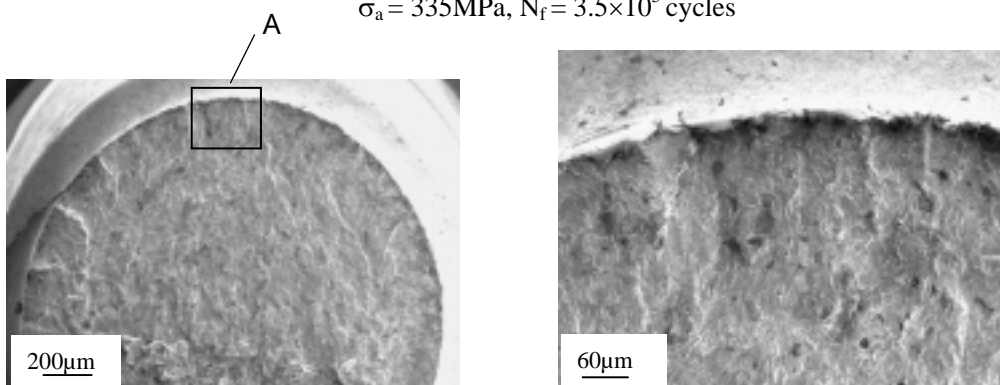
(a) Cold specimen   (b) Enlarged of A in (a)

$\sigma_a = 520$MPa, $N_f = 27 \times 10^4$cycles

Figure 4.17   Fracture surfaces of specimen after nitriding or cold rolling.

4.4 Conclusions

The following conclusion can be derived from the results of this study:

1. Ion nitriding treatment confirmed its efficiency in improving the fatigue properties of eutectoid steel. In the present study, the fatigue strength of eutectoid steel after ion nitriding at 550°C and 500°C increased by 72% and 88% for smooth specimen; by 58% and 65% for notched specimens.

2. Surface hardening, refined microstructure and compressive stress are the three main factors for the modification of fatigue properties.

3. The depth of compound layer is approximately 20μm and it is consisted mainly of Fe_3N. The case depth in this test is about 500μm for smooth specimen and 400μm for notched specimen.

4. The reduction in core hardness (softening) of eutectoid steel treated at 550°C was observed, making this steel less suitable for nitriding at high temperature.

References

[1] Metals Handbook, Vol.4, Heat Treating, 9th edition, American Society for Metals, Metals Park, OH, 1991, pp.387.

[2] B. Edenhoffer, Engineering Bookshelf, Source Book on Nitriding, American Society for Metals, Metals Park OH, 1997, pp.181.

[3] C.K. Jones, S. W. Martin, D.J. Sturges, M. Hudis, Ion nitriding, in Heat Treatment, Vol.73, The Metal Society, London,1973, pp.71-77.

[4] B. Edenhofer, J.J. Bewley, Low-temperature ion nitriding: nitriding at temperatures below 500°C for tools and precision machine parts, *Heat Treatment,* vol.76, The Metal Society, London, 1976, pp.7-14.

[5] B. Edenhofer, Production and structure of highly ductile plasma nitrided layer without a white layer, *Heat Treatment,* Vol. 79, The Metal Society, London, 1979, pp.52-59.

[6] M. Hudis, Study of ion nitriding, *J. Appl. Phys*. 44(4)(1973), pp.1489-1496.

[7] G.G. Tibbetts, Role of nitrogen atoms in "ion nitriding", *J. Appl. Phys.* 45(11)(1974), pp.5072-5073.

[8] H. Michel, T. Czerwiec, M.Gantois, D. Ablitzer, A. Richard, Progress in the analysis of the mechanisms of ion nitriding, *Surf. Coat. Technol.*72(1995), pp.103-111.

[9] Y. Sun, T. Bell, Plasma surface engineering of low alloy steel, *Mater. Sci. Eng*. A140(1991), pp.419.

[10] A. Alsaran, M. Karakan, A. Celik, The investigation of mechanical properties of ion-nitrided AISI 5140 low-alloy steel*, Materials Chracteristics,* 48(2002), pp.323-327.

[11] K.Genel, M. Demirkol, M. Capa, Effect of ion nitriding on fatigue behavior of AISI 4140 steel, *Material Science and Engineering,* A279(2000), pp.207-216.

[12] M. Guagliano and L. Vergani, Effect of nitriding on low-cycle fatigue properties, *Internaional journal of Fatigue,* Vol.19(1997), No.1, pp.67-73.

[13] J. Erler, Engineering Bookshelf, Source Book on Nitriding, American Society for Metals, Metals Park OH, 1997, pp.232.

[14] A. Celik, S. Karadeniz, Improvement of the fatigue strength of AISI 4140 steel by an ion nitriding process, *Surface Coat. Tech.*72(1995), pp.15.

[15] J.Wan, A. Fatemi, Cyclic deformation and fatigue behavior of ion nitrided steel,

*Int. J. Fatigue***17**(1995), pp.15.

[16] P. De. La Cruz. M. Oden. T. Ericsson, Influence of plasma nitriding of fatigue strength and fracture of a B-Mn Steel, *Mater. Sci. Eng*. A242(1998), pp.181.

[17] P. De la Cruz, M. Oden, T. Ericsson, Influence of plasma nitriding on fatigue strength and fracture of a B-Mn steel*, Materials science and Engineering* **A242**(1998), pp.181-194.

[18] F. Mahboubi, M. Samandi, D. Dunne, A. Bloyce, T.Bell, Plasma nitriding of micro alloyed steel, *Surface and Coating Technology* 71(1985), pp.135-141.

[19] T. Ericsson, *Residual stress caused by thermal and thermal chemical surface treatment, V*ol.4, Pergamon Press, Oxford, 1987, pp.87-113.

[10] U. Kreft, F. Hoffmann, T. Hirsch, P. Mayr, Investigation of the formation of residual stress in the compound layer during the gas nitriding*,* V. Hauk, H.P. Hougardy, S. Macherauch , H.D.Tietz(Eds), *European Conference on Residual stress,* DGM Informations gesellschaft, Frankfurt a. M., Germany, 1992, pp.123-127.

[21] A. Celik, S. Karadeniz , Improvement of the fatigue strength of AISI 4140 steel by an ion nitriding process, *Surface Coating Technology,* 72(1995),pp.169-173.

[22] X. Peng, A. Kharlov, V. Bystritski, E. Garate, E. Lavernia, Characteristics of material surface modified using plasma-enhanced ion beams, *Mater. Sci. Eng*. A251 (1998), pp.142-149.

[23] P. J. Haagensen, Residual stress techniques for fatigue life improvement, *Fatigue 2002*, Proc. Int. Conf.   Stockmolm, Sweden (2002), pp.1-10.

Chapter 5

Summary and Recommendations

for Future Research

5.1 Summary

The present research consists of several studies that assess the effect of pre-strain on fatigue properties of eutectoid steel and to evaluate ways to improve the practical performance of eutectoid steel by cold rolling and ion-nitriding methods. The ultimate goal in the entire study is to better understand the fatigue mechanism of eutectoid steel, and to improve the practical performance of the test material. The objectives of these studies are to evaluate and ascertain the above method on effect of fatigue strength, crack initiation and propagation behavior, the most effective and suitable method to improve the test material with the smooth and specimen with stress concentrations.

In Chapter 1, a brief history of fatigue research was reviewed. The importance of fatigue study in industry and engineering was discussed and the background for the fatigue study was introduced. The central topic was the various mechanisms involved in fatigue crack initiation and propagation in material and the subsequent behavior of fatigue strength.

In chapter 2, the static and cyclic properties of New Head Hard (NHH) rail, a kind of eutectoid steel treated with induction hardening was studied. This kind of rail is usually used in tunnel or mine areas where the environment is harsh and showed excellent wear resistance. In this study, the influence of pre-strain on fatigue strength, crack initiation and propagation behavior were investigated. The main results obtained from this test are as follows:

(1) Induction hardening is a very effective method for improving the practical properties including fatigue strength, wear resistance and mechanical properties.

(2) Plastic pre-strain decreases the fatigue limit of eutectoid steel. All fatigue limits of specimens with different pre-strain ratio are lower than that of specimens

without pre-strain (ε_p=0%).

(3) The fatigue limits of pre-strained eutectoid steel become deteriorated and do not exhibit significant change in the range of ε_p=2% to ε_p=6%.

(4) For non-pre-strained specimen, fatigue cracks preferentially initiate from boundary of the pearlite blocks or inter-lamellar of the pearlite; but for pre-strained specimens, fatigue cracks occur in slip lines, or micro cracks that were generated in the process of plastic pre-strain. The fatigue cracks initiate by crossing or along the inter-lamellar of the pearlite and their direction are at about 20° to 45° with the loading axis in the early stage. As it grows, however, the cracks change their direction and propagate perpendicularly to the stress axis by crossing the lamellar or along the boundary or the inter-lamellar.

Chapter 3 focused on the effect of cold rolling on practical properties of eutectoid steel with stress concentration, especially fatigue strength, crack initiation and propagation behavior. The mechanisms for the modification were explained by residual stress, fiberized microstructure and work hardening. The relationship of residual stress and deformation values can be expressed by an equation in this test. The optimum deformation value for improving the cold rolling was discussed. Non-propagating cracks were found on the surfaces of all four cold-rolled specimens used in the test and the depths of the cracks increase with increasing the degree of plastic deformation.

The main results obtained in the present study are as follows:

1). Cold rolling is an effective method for improving the fatigue strength of notched eutectoid steel. After cold rolling, the fatigue limits of specimens increased from 175% to 265%.

2). Compressive residual stress, work hardening and fiberized microstructure are the three main factors for the improvement of fatigue properties. The residual stress is the most effective factor in improving the fatigue limit.

3). Non-propagating cracks are found at the notch bottom surfaces of all three cold rolled specimens, and the depths of these cracks increase with the increasing of plastic deformation value.

Chapter 4 studied the effect of typical thermal chemical method, ion nitriding on fatigue properties of eutectoid steel. Two different temperatures (550°C and 500°C) and two different types of specimens (smooth and notched one) were used in this study to ascertain the mechanism of modification. Residual stress, EMPA analysis

were used to derive the quantity relationship among case depth, residual stress and fatigue strength. The following conclusion can be derived from the results of this study:

1. Ion nitriding treatment confirmed its efficiency in improving the fatigue properties of eutectoid steel. In the present study, the fatigue strength of eutectoid steel after ion nitriding increased about 88% for smooth specimen and 65% for notched specimens.

2. Surface hardening, refined microstructure and compressive stress are the three main factors for the modification of fatigue properties.

3. The depth of compound layer is approximately 20μm and it is consisted mainly of Fe_3N. The case depth in this test is about 500μm for smooth specimen and 400μm for notched specimen.

4. The reduction in core hardness (softening) of eutectoid steel treated at 550°C was observed, making this steel less suitable for nitriding at high temperature.

5.2 Recommendations for Future Research

There are many ways in which the work in this thesis can be extended. For the fatigue properties of notched eutectoid specimens, more systematic studies are recommended to obtain a comprehensive understanding of the mechanism of cold rolling or other plastic deformation method, and their effect on fatigue behavior of components.

Studying the residual stress distribution on the cross section is very useful on understanding the fatigue mechanism after cold rolling. Due to the limitation of experiment condition, only the surface residual stress after cold rolling was measured. However, in order to understand the crack growth behavior, the residual stress distribution into the bulk is particularly important. It is very useful to test the residual stress profile on the cross section, i.e. into the bulk, by gradual surface removal of the notch root by electro polishing or non–destructive method like synchrotron or neutron method. These methods will allow a more acute quantitative relationship between the applied stress and the residual stress distribution to be developed.

In the present study, the relationship of fatigue crack length in the surface and

number of cycles to failure were derived. It will be very useful to determine the aspect ratio and get the relationship of crack depth and number of cycles because the crack propagation behavior into the depth direction is more important.

It is worth reminding that fatigue research is very costly (in terms of time and cost). In recent years, finite element method (FEM) has been well used in fatigue research to perform some quantitative analysis. The method can also be used to the present study to predict the value and variation of residual stress after cold rolling.

Challenge the other surface modification methods in improving the fatigue property of eutectoid steel. Beside plastic deformation, there are still many choices to complete surface modification of components, such as treat the specimen with shot peening or develop nanoscale microstructure on the surface.

The research on the effect of ion-nitriding is just in its beginning stage. Although the ion nitriding has proved its efficiency in improving the fatigue properties of eutectoid steel, there is still a lot of work that should be done to obtain a comprehensive understanding of the fatigue mechanism. It is shown that fatigue strength has direct correlation to temperature and time. There should exist an optimum time and temperature through which the fatigue properties of eutectoid steel can be improved the most by ion nitriding. The relationship of case depth and fatigue strength, the detail mechanism is also recommended.

List of Figures

List of Tables